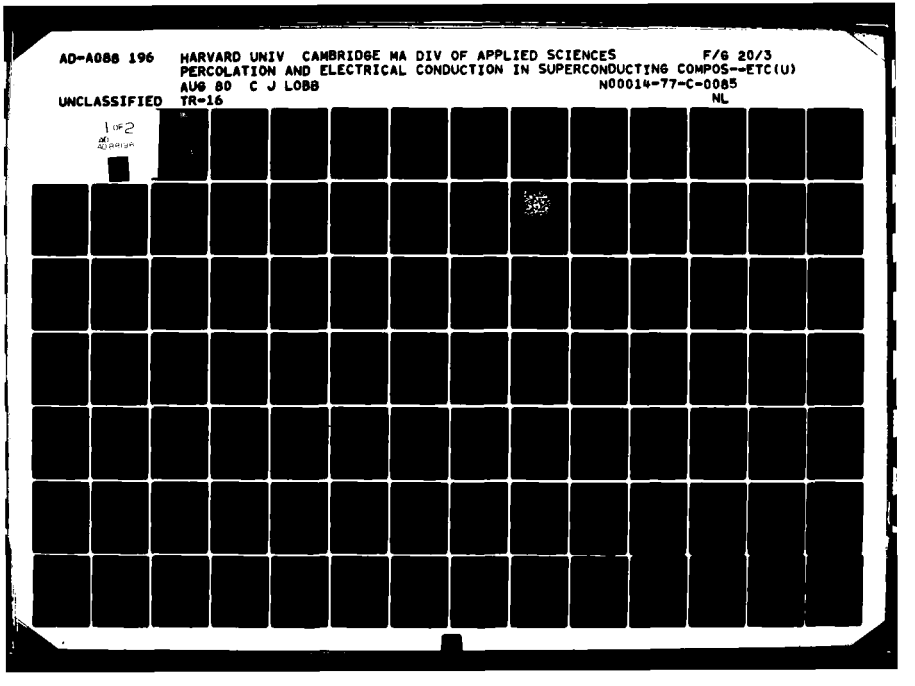
AD-A088 196
HARVARD UNIV CAMBRIDGE MA DIV OF APPLIED SCIENCES F/G 20/3
PERCOLATION AND ELECTRICAL CONDUCTION IN SUPERCONDUCTING COMPOS--ETC(U)
AUG 80 C J LOBB N00014-77-C-0085
UNCLASSIFIED TR-16 NL
1 OF 2
AD A088196

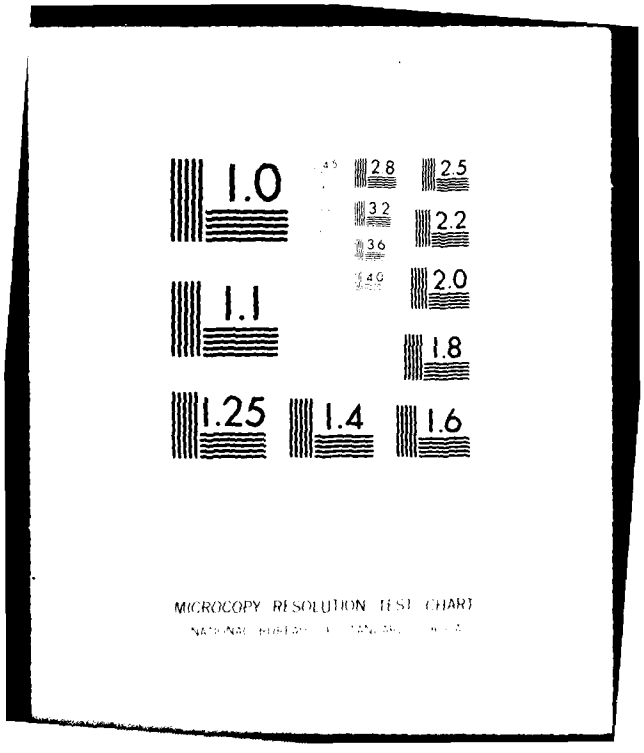
1.0
2.8
2.5
3.2
2.2
3.6
4.0
2.0
1.1
1.8
1.25
1.4
1.6
MICROCOPY RESOLUTION TEST CHART

LEVEL II

12 B.S.

Office of Naval Research
Contract N00014-77-C-0085 NR-318-083
Contract N00014-75-C-0648 NR-372-012
National Science Foundation Grant DMR77-24295
National Science Foundation Grant DMR79-04155
National Science Foundation Grant DMR79-09011

PERCOLATION AND ELECTRICAL CONDUCTION IN SUPERCONDUCTING COMPOSITES

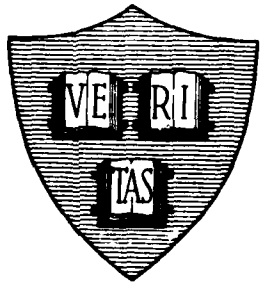

By

Christopher J. Lobb

August 1980

Technical Report No. 16

Division of Applied Sciences
Harvard University Cambridge, Massachusetts

Unclassified

SECURITY CLASSIFICATION OF THIS PAGE (When Data Entered)

REPORT DOCUMENTATION PAGE	READ INSTRUCTIONS BEFORE COMPLETING FORM
1. REPORT NUMBER: Technical Report No. 16	2. GOVT ACCESSION NO.: AD-A088196	3. RECIPIENT'S CATALOG NUMBER
4. TITLE (and Subtitle): PERCOLATION AND ELECTRICAL CONDUCTION IN SUPERCONDUCTING COMPOSITES	5. TYPE OF REPORT & PERIOD COVERED: Interim Report
	6. PERFORMING ORG. REPORT NUMBER
7. AUTHOR(s): Christopher J. Lobb	8. CONTRACT OR GRANT NUMBER(s): N00014-77-C-0085, N00014-75-C-0648, NSF DMR77-24295, NSF DMR79-04155, NSF DMR79-09011
9. PERFORMING ORGANIZATION NAME AND ADDRESS: Division of Applied Sciences, Harvard University, Cambridge, Mass. 02138	10. PROGRAM ELEMENT, PROJECT, TASK AREA & WORK UNIT NUMBERS
11. CONTROLLING OFFICE NAME AND ADDRESS	12. REPORT DATE: Aug 80 — 129
	13. NUMBER OF PAGES: 128
14. MONITORING AGENCY NAME & ADDRESS (if different from Controlling Office)	15. SECURITY CLASS. (of this report): Unclassified
	15a. DECLASSIFICATION/DOWNGRADING SCHEDULE

16. DISTRIBUTION STATEMENT (of this Report)

Reproduction in whole or in part is permitted for any purpose of the United States Government. Approved for public release; distribution unlimited.

17. DISTRIBUTION STATEMENT (of the abstract entered in Block 20, if different from Report)

18. SUPPLEMENTARY NOTES

19. KEY WORDS (Continue on reverse side if necessary and identify by block number)

Superconducting Properties
Percolation
Anisotropic Networks
Numerical Simulations

20. ABSTRACT (Continue on reverse side if necessary and identify by block number)

We report the experimental properties of a number of random superconducting-normal metal composites. Theoretical interpretation is also presented, with emphasis on the effects of geometrical randomness.

The electrical properties of in situ multifilamentary Cu-V_3Ga wires are discussed, with emphasis on critical current and field properties which are relevant to applications. We found that these wires had upper critical fields as high as 22.4T at 4.2K with a transition temperature of 15.5K. Their overall critical current density ($2 \times 10^5 A/cm^2$ at 4T, $10^4 A/cm^2$ at 18T) compared favorably with

DD FORM 1 JAN 73 1473 EDITION OF 1 NOV 65 IS OBSOLETE S/N 0102-014-6601

Unclassified

SECURITY CLASSIFICATION OF THIS PAGE (When Data Entered)

410457

20. Abstract continued

commercial wires.

The results of electrical measurements on in situ Cu alloy-Nb composites are reported which elucidate the roles of percolation and the proximity effect in these materials. Our data show that the proximity effect is very important in clean, low superconducting concentration samples, with geometrical percolation being more important as the matrix becomes dirtier. In addition, we discuss models for the superconducting to normal transition in these materials which include the effects of randomness and thermal fluctuations.

A two-dimensional thin film system based on Cu-Pb is discussed and shown to be qualitatively similar to the three-dimensional in situ composites. The critical c3rrent of these films is proportional to $(T_c-T)^{1.8}$, a result which is not well understood theoretically.

Finally, we report calculations on square random resistor lattices. Large lattice numerical simulations, effective medium theory and a renormalization group method are used to study the bulk conductance of anisotropic networks as a function of concentration. The last technique is used to provide highly accurate estimates of the percolation transport exponents t and ν. In two dimensions, our calculations indicate that they equal the coherence length exponent ν to within a few percent. We have also calculated ν by the same technique, obtaining a result which supports the notion of site-bond universality.

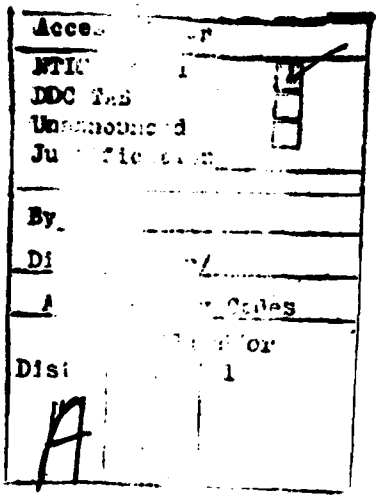

Office of Naval Research

Contract N00014-77-C-0085 NR-318-003
Contract N00014-75-C-0648 NR-372-012
National Science Foundation Grant DMR77-24295
National Science Foundation Grant DMR79-04155
National Science Foundation Grant DMR79-09011

PERCOLATION AND ELECTRICAL CONDUCTION IN SUPERCONDUCTING COMPOSITES

By

Christopher John Lobb

Technical Report No. 16

August 1980

The research reported in this document was made possible through support extended the Division of Applied Sciences, Harvard University, by the Office of Naval Research, under Contract N00014-77-C-0085, Contract N00014-75-C-0648 and by the National Science Foundation under Grants DMR77-24295, DMR79-04155 and DMR79-09011.

Division of Applied Sciences

Harvard University · Cambridge, Massachusetts

ABSTRACT

We report the experimental properties of a number of random superconducting-normal metal composites. Theoretical interpretation is also presented, with emphasis on the effects of geometrical randomness.

The electrical properties of in situ multifilamentary Cu-V_3Ga wires are discussed, with emphasis on critical current and field properties which are relevant to applications. We found that these wires had upper critical fields as high as 22.4T at 4.2K with a transition temperature of 15.5K. Their overall critical current density ~~(2×10^5 A/cm^2 at 4T, 10^4 A/cm^2 at 18 T)~~ compared favorably with commercial wires.

The results of electrical measurements on in situ Cu alloy-Nb composites are reported which elucidate the roles of percolation and the proximity effect in these materials. Our data show that the proximity effect is very important in clean, low superconducting concentration samples, with geometrical percolation being more important as the matrix becomes dirtier. In addition, we discuss models for the superconducting to normal transition in these materials which include the effects of randomness and thermal fluctuations.

A two-dimensional thin film system based on Cu-Pb is discussed and shown to be qualitatively similar to the three-dimensional in situ composites. The critical current of these films is proportional to $(T_c-T)^{1.8}$, a result which is not well understood theoretically.

Finally, we report calculations on square random resistor lattices. Large lattice numerical simulations, effective medium theory and a renormalization group method are used to study the bulk

conductance of anisotropic networks as a function of concentration. The last technique is used to provide highly accurate estimates of the percolation transport exponents t and v. In two dimensions, our calculations indicate that they equal the coherence length exponent ν to within a few percent. We have also calculated ν by the same technique, obtaining a result which supports the notion of site-bond universality.

TABLE OF CONTENTS

LIST OF FIGURES

LIST OF TABLES

PREFACE

During my graduate studies I have benefited extensively from the assistance of a number of people. It is a pleasure to acknowledge their help here.

I am grateful to my advisor, Michael Tinkham, who provided overall guidance and critical insight for my work. Teun Klapwijk and Bill Skocpol were both generous with their knowledge of superconductivity and low temperature techniques, and Joze Bevk provided guidance in metallurgical matters. I am thankful to David Nelson and Bertrand Halperin, who were always willing to help me understand critical phenomena and the renormalization group.

Much of my work on percolation theory would have been impossible without David Frank's knowledge of circuit theory and his clever circuit reduction algorithms. In addition to working with me on everything from percolation theory to sample preparation, Keith Karasek has been an excellent friend. Andy Smith and Fawwaz Habbal have always been generous with their time, helping me to solve innumerable experimental difficulties.

Finally, I am grateful to Louis Defeo, who constructed most of my experimental equipment, and Joe Bell, who always helped with sample preparation problems. Their knowledge and craftsmanship were indispensible assets.

CHAPTER ONE: INTRODUCTION

The problem of the resistivity of metallic mixtures has attracted scattered attention for more than a century. As early as 1860, resistivity measurements were made on a wide variety of binary alloys (Matthiessen 1860). On the theoretical side, Maxwell (1892) developed a simple theory for the effective resistivity of a mixture.

The literature of the next fifty years was not extensive. Landauer (1952) reviewed the experimental and theoretical literature up to 1952, comparing the existing theories and deriving an expression (originally due to Bruggeman (1935)) for the effective resistivity by assuming that each crystallite acts as if it were surrounded by a homogeneous medium whose properties are those of the mixture. A recent comprehensive review of electrical conduction in inhomogeneous media has been written by Landauer (1978).

An extensive early study of superconductivity in alloys was done by Allen (1933). Many of his results anticipate later work, but he was hampered (as were early researchers working on normal metal mixtures) by inadequate theoretical understanding.

Three theoretical developments have encouraged the wide current interest in inhomogeneous media. First, the electronic properties of substitutional alloys received considerable theoretical attention. This led to interest in the classical mixture problem, and to the application of alloy theory techniques to the classical problem (Kirkpatrick 1973, Stroud 1974). The recognition that random resistor lattices were a good model for inhomogeneous media put the classical problem into a more tractable form (Kirkpatrick 1973). Finally, the

application of modern phase transition theory to the classical resistor lattice (Stinchcombe and Watson 1976) and quantum mechanical Josephson junction array (Giovannini and Weiss 1978) provided deeper understanding of experimental phenomena.

The work reviewed in the following chapters covers a number of areas in the general field of inhomogeneous superconductors. We first discuss our work on practical properties of *in situ* Cu-V_3Ga. This material is a random mixture of normal Cu and superconducting V_3Ga. Our measurements indicated that the material is potentially useful. We then review our work on *in situ* composites which helped to clarify their physics, emphasizing the roles of various mechanisms that contribute to their superconductivity. In response to the considerable current interest in phase transitions in lower dimensions, we have studied a two-dimensional thin film composite system and report our initial results here. Finally, we review our theoretical work on random resistor lattices. This work elucidated the effects of conductance anisotropy, introduced the idea of non-ohmic percolating networks, and led to greatly improved estimates of two-dimensional transport critical exponents in the percolation problem.

CHAPTER TWO: HIGH FIELD V_3GA *IN SITU* COMPOSITES

The ability to carry very large, essentially lossless currents in high magnetic fields makes type II superconductors attractive for applications. We begin this chapter with a brief discussion of the practical shortcomings of type II superconductors and how standard composite wires overcome these problems. The *in situ* technique, an alternative approach to composites, is discussed, and some of the results in the literature are summarized. We outline the process developed at Harvard for producing *in situ* composites, and then discuss the superconducting properties of a specific system, Cu-V_3Ga. Finally, we mention some aging properties of CuNi-Nb composites which may have some practical implications.

2.1 Standard Composite Wire

The development of practical high-field superconducting wires did not immediately follow the discovery of high H_{C2} compounds. As discussed in chapter 5 of Tinkham (1975), the short electronic mean free paths of type II superconductors place severe design constraints on practical wires. A fluctuation into the normal state, with its resulting dissipation, will grow unless the heat generated can be carried away from the superconductor. In order to increase heat flow away from the wire, practical wires are multifilamentary (to increase the surface to volume ratio) and clad in copper. Filaments less than 100 μm in diameter are generally small enough to ensure stability.

Commercial composite superconductors achieve this filament size by

starting with large billets of copper into which a number of holes have been drilled. (Alternatively, the Cu can be extruded with holes.) A ductile superconducting rod is placed in each hole, and the material is extruded, swaged and drawn until the desired diameter is reached. After a certain amount of reduction, pieces can be bundled to increase the number of filaments in a cross section, and the wire may be annealed to relieve work hardening. When the final wire size is reached, other elements are often plated on and diffused into the composite. For example, if the original rods were Nb (which is ductile), Sn can be added and reacted to form Nb_3Sn. Nb_3Sn is a better superconductor than Nb but is not ductile.

This process works well, although it does have some drawbacks. Machine-shop-size rods of superconductor must be reduced to less than 100 μm, and this takes a considerable number of steps. In addition, the number of filaments in a wire is limited by how much initial stacking and bundling can be done economically, so that commercial wires often have from a few hundred to a few thousand filaments.

2.2 Tsuei Wire

An alternative way to make composites is the *in situ* technique. Metals which are immiscible in the solid state, such as copper and niobium, are melted together and cooled at a controlled rate. The superconductor precipitates out, giving small superconducting inclusions in a normal metal matrix (see figure 2.1). The material is then drawn, elongating the inclusions into filaments (see figure 2.2).

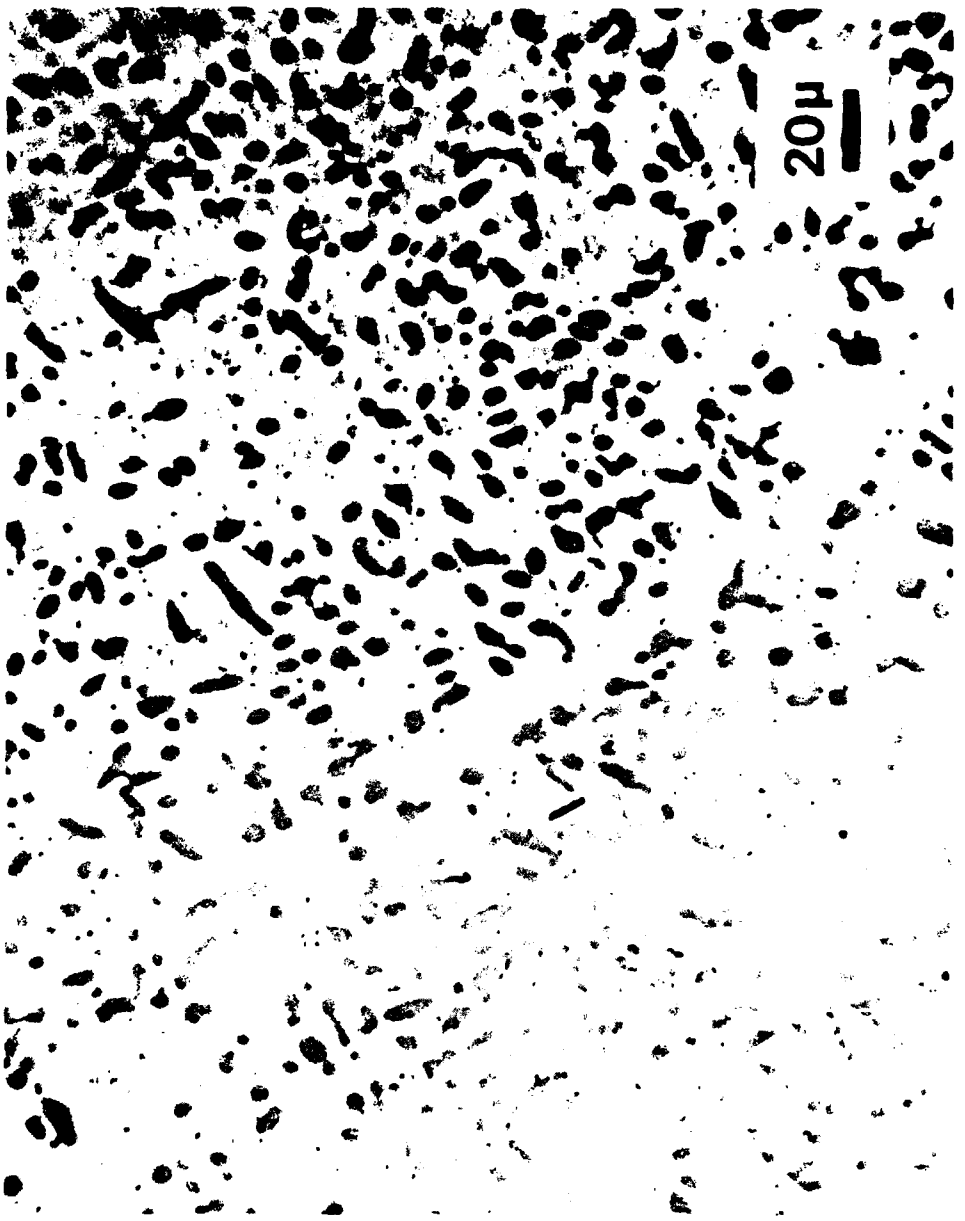

Figure 2.1 Nb in a Cu-Sn matrix, as cast.
From Harbison 1977.

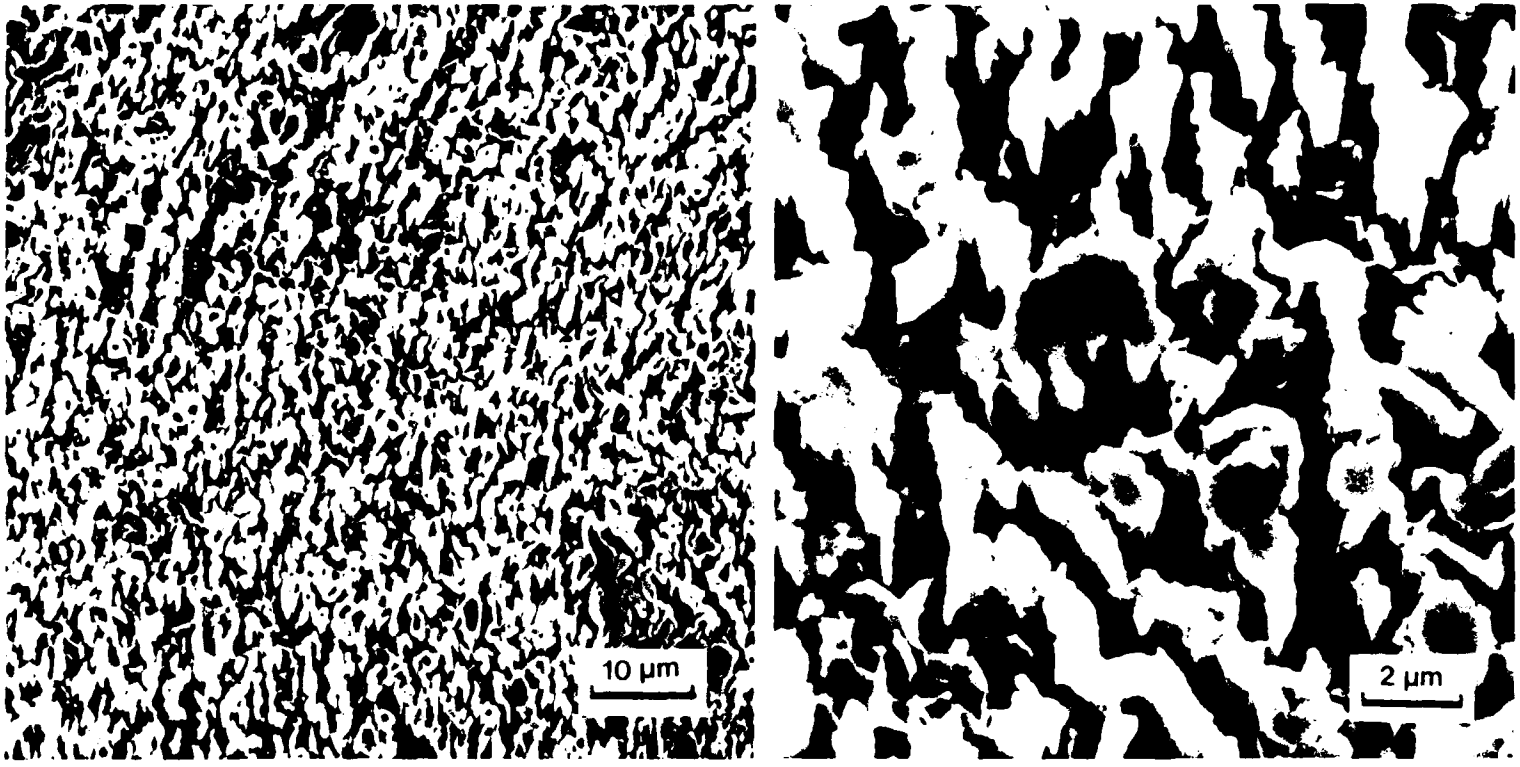

Figure 2.2 End of drawn Cu-Nb_3Sn wire with the Cu matrix etched away. The ribbon-like structure results from texture formation in the Nb during drawing, as discussed in Bevk et al. (1978). Figure from Harbison 1977.

This technique was first used to make superconducting wire by Tsuei (Tsuei 1973, 1974, Tsuei and Newkirk 1974).

There are a number of differences between in situ and conventionally produced composites. The filaments in the former are randomly placed and possibly discontinuous. Some of the consequences of this will be discussed in the next chapter. The in situ approach has the advantage of starting with smaller superconducting inclusions so that less mechanical reduction is needed to reach a given final size. In addition, the smaller initial size makes it possible to have 10^4 or more filaments in a cross section without having to bundle the wire.

It remains to be seen whether the in situ approach will prove commercially competitive. Some of the experimental results to date are reviewed below.

A. Some Previous Work on In Situ Composites

Much of the practical effort in superconducting materials has been to produce wires with high critical temperature, current and field. A number of groups have produced Nb_3Sn in Cu in situ composites using similar techniques. (Bevk et al. 1980, Fihey et al. 1979, Finnemore et al. 1979).

Figure 2.3 shows the critical current density as a function of field for a number of Cu-Nb_3Sn in situ composites prepared at Harvard (Bevk et al. 1980). These composites are approximately 23% Nb_3Sn by volume, and have critical current densities comparable to conventional

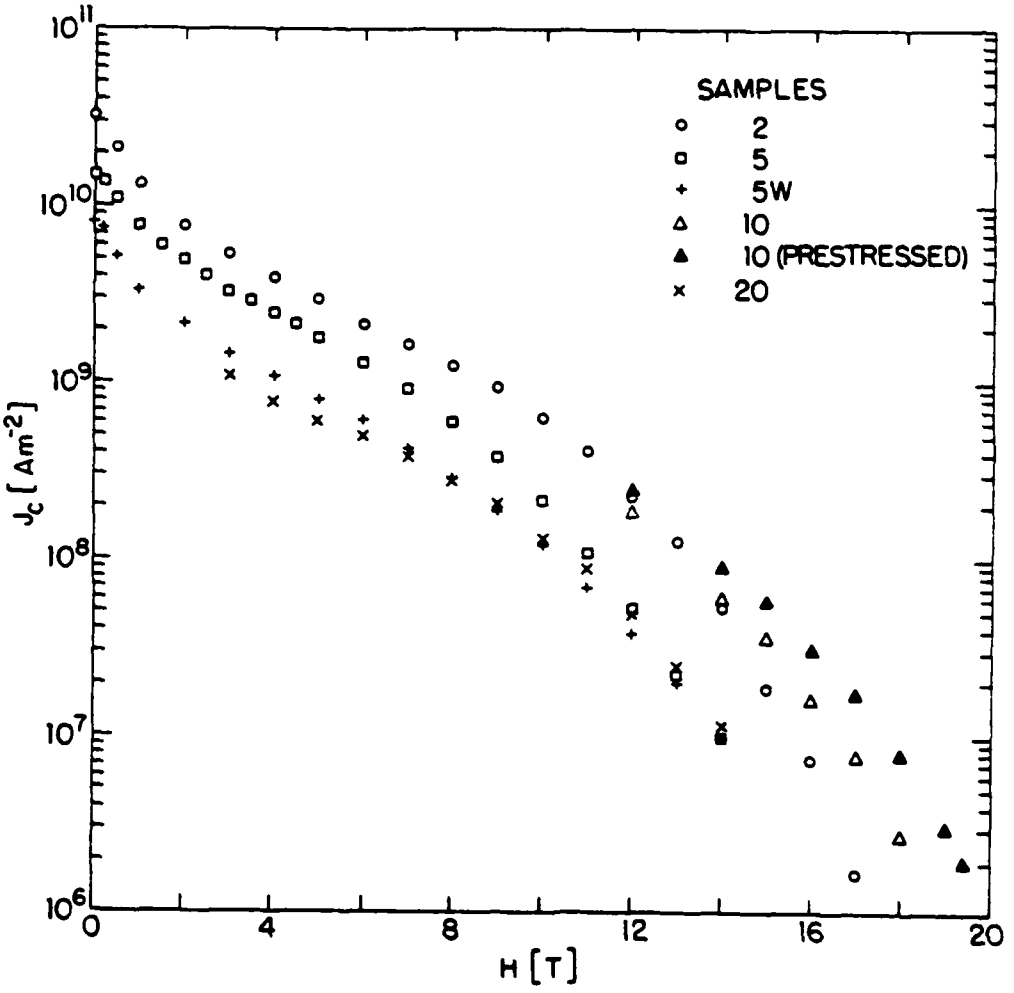

Figure 2.3 J_c fs. H for various Cu-Nb_3Sn samples, from Bevk et al. 1978.

composites. These results are typical of those obtained by other groups. AC loss measurements are encouraging, although improvement will be needed before Tsuei wire can compete with conventional composites in this area (Bevk et al. 1980). The mechanical strength of in situ composites is very high (Karasek and Bevk 1979, Bevk and Harbison 1978), which is very important in high field and rotating machinary applications.

Initial attempts at producing in situ V_3Ga, which should have a higher critical field, were not as successful. Chen and Tsuei (1976) produced a number of compositions by combining all of the constituents in the initial melt, deforming the resulting ingots into wires and tapes, and heat treating. They were unable to obtain a transition temperature above 13 , which is 2 -3K lower than the bulk value (Das et al. 1977). In addition, their J_c values were quite low (see figure 2.4). There are at least two factors that contribute to these effects. Some off-stoichiometric V_3Ga probably forms during the initial melt, since the superconducting transition begins as high as 9 for some of the unannealed samples. This is significantly higher than the 5.3K value of T_c for bulk V (Roberts 1969). The early formation of a brittle compound could lead to breaking of the filaments during reduction, which would lower the critical current density. The decrease in T_c is more difficult to explain. All of the Ga will not react with Va, but in these samples there was as much as four times the amount of Ga necessary to form stoichiometric V_3Ga , and X-ray analysis indicated that the A-15 structure was present. It is possible that their annealing temperatures, which varied from 600 to 850 , were too

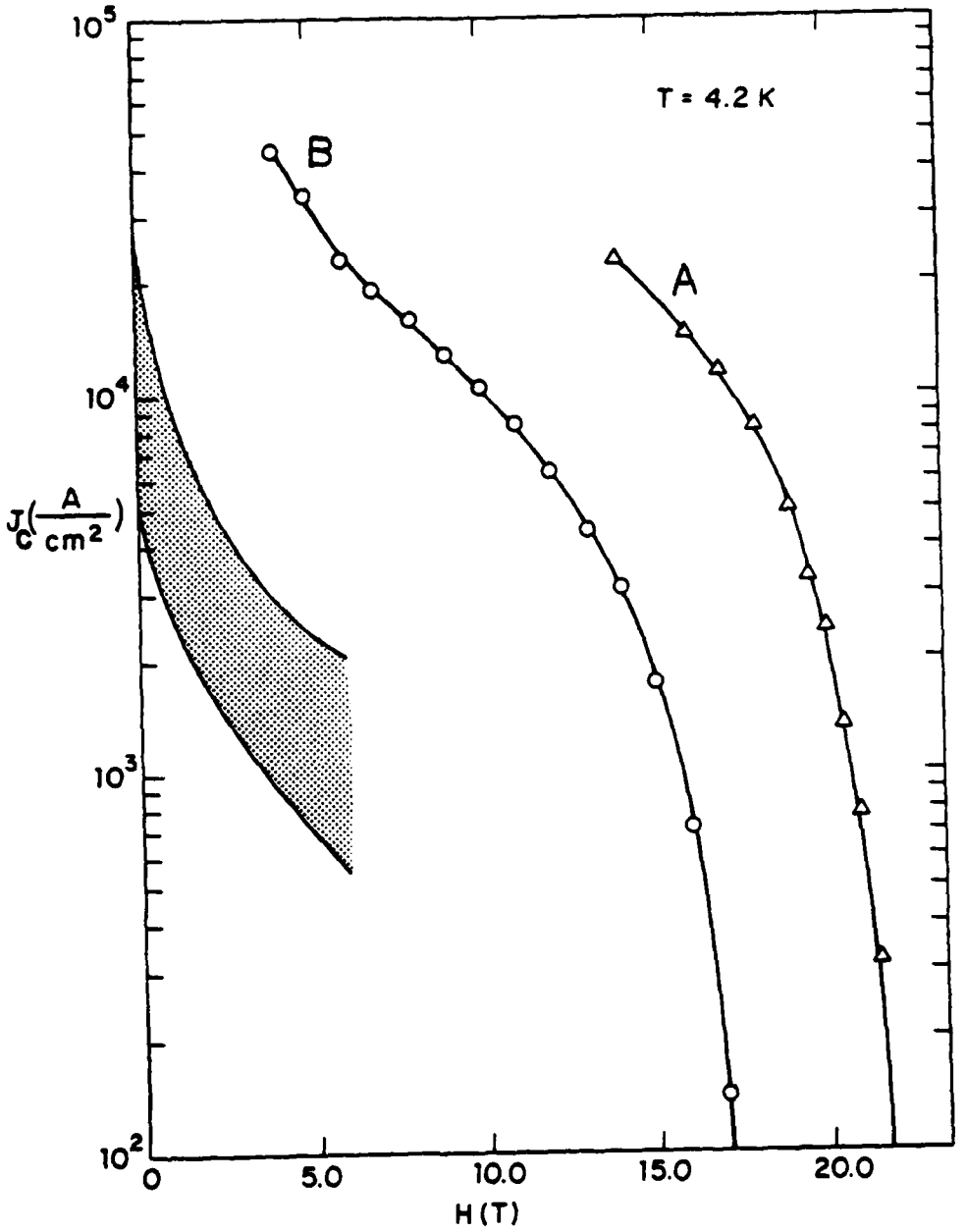

Figure 2.4 J_c vs. H for the two Cu-V_3Ga samples. Sample B has roughly the amount of Ga required to form stoichiometric V_3Ga, sample A about twice as much as is necessary. The shaded area encompasses the data of Chen and Tsuei (1976).

high. This can destroy the long-range order of the V chains in V_3Ga, causing Ga and V atoms to interchange on the lattice. Experiments and theory indicate that this lowers T_c (Dew-Hughes 1975, Labbé and Friedel 1966). In the next section we describe our more recent work on Cu-V_3Ga which has been more successful.

B. Preparation of In Situ V_3Ga

All of the composites discussed in the remainder of this chapter and in the next chapter were produced by radio frequency levitation melting. This method was first used to make in situ superconducting composites by Harbison and Bevk (1977).

Cu and V were melted together in an RF coil which provided the energy both to melt the materials and levitate the sample. Levitation allows very high temperatures to be reached, avoids crucible contamination, and mixes the components through convection. Samples were melted a number of times this way in an argon atmosphere to insure good mixing and dropped into a water cooled copper mold after each melting. The samples were subsequently placed in a slotted water cooled vertical boat and RF melted, with the RF also keeping the molten metal away from the sides. When the RF power was lowered, the molten samples spread onto the walls of the boat. This provided more uniform cooling than was possible by dropping into a mold. Samples were next swaged and drawn down to the desired size, and Ga was vapor deposited onto them. The Ga was reacted in a two-step process by annealing at 450°C for five days and at 590°C for one day. These low reaction

temperatures were adequate at least partly because of the very fine ribbon-like structure of the V filaments. Diffusion times scale as the shortest dimension squared, and these filaments were typically 1000Å to 2000Å thick by 1 μm to 2 μm wide.

C. Superconducting Properties of In Situ V_3Ga

We have studied two series of V_3Ga samples (Bevk et al. 1979a,b). Both started with 20 volume percent V in a Cu matrix. The first set was coated with 12.4 weight percent Ga, about twice as much as was necessary to transform all of the V into V_3Ga. The second set was coated with slightly less Ga than was needed to form stoichiometric V_3Ga.

The superconducting transition temperature T_c was measured for one sample from each set. T_c was measured resistively using the standard four-probe technique. Both of the samples reached one-half of their normal state resistance at 15.5 K in zero field. The high Ga concentration sample had a narrower transition, going from one-quarter to three-quarters of its normal state resistance in 0.13 K, compared to 0.3 K for the low Ga sample. The high T_c and narrow transitions indicate that stoichiometric V_3Ga can be formed in situ at fairly low annealing temperatures.

The critical current density was measured as a function of field at 4.2 K. The critical current was taken to be that current which produced a 1 μV drop across 5 mm of wire. Critical current density as a function of field is plotted in figure 2.4, along with the values

obtained by Chen and Tsuei (1976).

The upper critical field was obtained in two ways. One way was to extrapolate the data in figure 2.4 to J_c=0. The other was to apply a small measuring current (about 1amp/cm^2) and measure voltage as a function of applied field. Both methods gave essentially the same answer. The high Ga content sample had H_{C2}= 22.4±0.1 T, a very good value. The lower Ga content sample had H_{C2}=18.3±0.1 T, which indicates incomplete formation of V_3Ga. This is consistent with earlier data on conventional composites (Yoshida et al. 1975) which indicated that significant amounts of Ga remain in the Cu matrix even after heat treatment.

The properties of our V_3Ga are significantly better than those of the material produced by Chen and Tsuei (1976). We attribute the high J_c to the relatively low annealing temperature, which causes less recrystaliztion and thus allows better pinning. The high T_c and H_{C2} were also the result of the low annealing temperature, which would introduce a minimum of lattice disorder into the V chains.

We note that the properties of these materials have not been optimized. Improvement will probably result from varying concentrations and heat treatment, and by adding third elements.

D. Aging

Composite wires intended for applications in time-varying fields have requirements in addition to those mentioned in the beginning of this chapter. For example, losses due to eddy currents induced in the

normal metal matrix by the alternating field must be minimized (Tinkham 1975, chapter 5). One approach is to decrease the induced currents by increasing the matrix resistivity. This can be done by adding a third element such as Ni.

Some of the Cu-Nb samples which will be discussed in the next chapter had 3 atomic percent Ni added to the matrix. We found that these samples were superconducting when measured within months of being made, but that samples that were re-measured two years later were not superconducting. One sample <u>without</u> Ni did not lose its superconducting properties in the same time. This difference could be the result of Ni diffusing into the Nb, although it is difficult to understand such effects occuring at room temperature, even with the short diffusion distances necessary because of the fine filament sizes. Since Ni is an excellent material for increasing the resistivity of Cu, this effect clearly deserves further study.

CHAPTER THREE: ELECTRICAL CONDUCTION IN *IN SITU* COMPOSITES

In the last chapter, we discussed high current and high field properties of some *in situ* composites. It was noted that these materials can carry large supercurrents which are comparable to those obtained in conventional continuous-filament composites. This is interesting, since the filaments in *in situ* composites are random and possibly discontinuous.

Three explanations have been given for the large supercurrents of these materials. One is that the filaments percolate, that is, that they form a continuous network through random contacts (Davidson and Tinkham 1976). A second explanation is that the proximity effect carries a supercurrent between filaments which do not actually touch (Tsuei and Newkirk 1973). Finally, it has been shown that highly reduced wire can have a very low resistance even when the filaments do not touch and the matrix is fully normal (Davidson *et al.* 1975, Davidson and Tinkham 1976).

These explanations are not mutually exclusive, of course. In this chapter, we will outline earlier work which compared the different explanations, and review our own work on the subject (Lobb *et al.* 1978). We will then present a heuristic model of the superconducting to normal transition which is based on percolation theory (Tinkham 1977, Lobb *et al.* 1978), and discuss a more rigorous theory which is isomorphic to the ferromagnetic XY model (Giovannini and Weiss 1978, Patton *et al.* 1980, Imry 1980).

3.1 Early Experiments and Interpretations

Tsuei and Newkirk (1973) investigated samples of $Cu_{1-x}Nb_x$ with x varying between 0.005 and 0.05. Their specimens were cast and then rolled down to 3/4 of their initial cross sectional area. They explored the superconducting transition resistively and inductively, using the latter technique to estimate the volume fraction of the samples from which the flux was excluded. They found that this effective superconducting volume fraction was up to an order of magnitude larger than the Nb volume fraction. In addition, many of the samples had a resistivity of less than 10^{-11} ohm-cm at 2K, in spite of the lack of metallographic evidence for continuous Nb paths. These two facts led Tsuei and Newkirk to suggest proximity effect coupling as the important conduction mechanism in these low Nb concentration materials.

Higher concentration materials were later studied, usually with greater elongation and with Sn present to form Nb_3Sn. Two important plots are shown in figures 3.1 and 3.2. These data were taken with a SQUID voltmeter which allowed subpicovolt signals to be detected (Davidson and Tinkham 1976).

Figure 3.1 shows a sample with roughly 8 volume percent Nb_3Sn. The wire was drawn until its cross sectional area had been reduced by a factor of 200. As the figure shows, there is a four order of magnitude drop in the resistance between 16K and 17K. The resistance then levels off, staying roughly constant between 7K and 16K. Finally, below 7K, a second transition occurs, and the resistance drops below the range of the voltmeter.

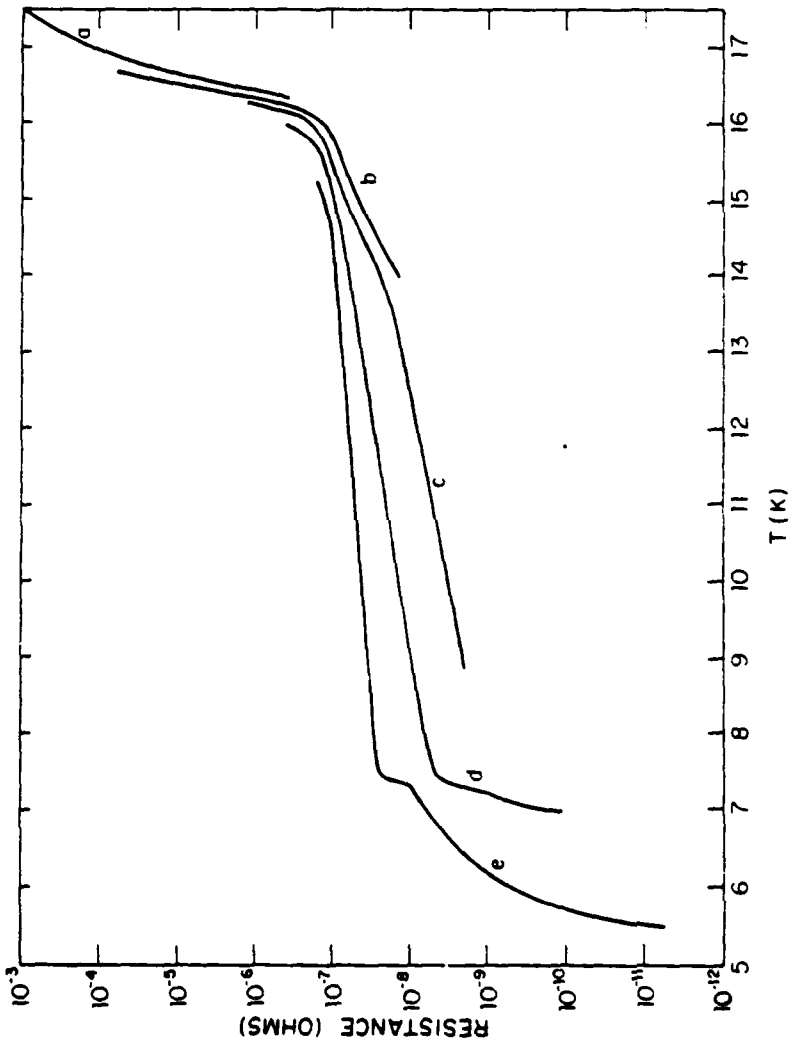

Figure 3.1 Resistive transition in a Cu-8 volume percent Nb_3Sn sample. From Davidson and Tinkham (1976).

The data plotted in figure 3.2 are for a 15 volume percent sample with a cross sectional area reduction of 300. These curves have no pronounced resistance plateau. This sample appears to be completely superconducting at fairly high temperatures.

These results inspired a number of important ideas. First, it was shown that non-connected superconducting filaments in a fully normal matrix should lead to an effective resistivity ρ_{eff} given by

$$\rho_{eff} \propto \rho / f A^3 \qquad (3.1)$$

where ρ is the resistivity of the matrix, f is the superconducting volume fraction, and A is the cross sectional area reduction (Davidson et al. 1975). This formula explains the level of the plateau in figure 3.1, and agrees reasonably well with data obtained over a wide range of reductions (Davidson et al. 1975, Callaghan and Toth 1975, Roberge et al. 1978).

The behavior of the sample of figure 3.2 was explained by noting that if enough superconductor is present, the filaments will form a continous network through random contacts (Davidson and Tinkham 1976). Above the critical volume fraction f_c at which this occurs samples are expected to be resistanceless, while below f_c, a resistance of the order predicted by (3.1) should appear. We note that (3.1) can be modified by multiplying the right hand side by $(f-f_c)$ to take this into account (Tinkham 1977). Various theoretical values of f_c exist,

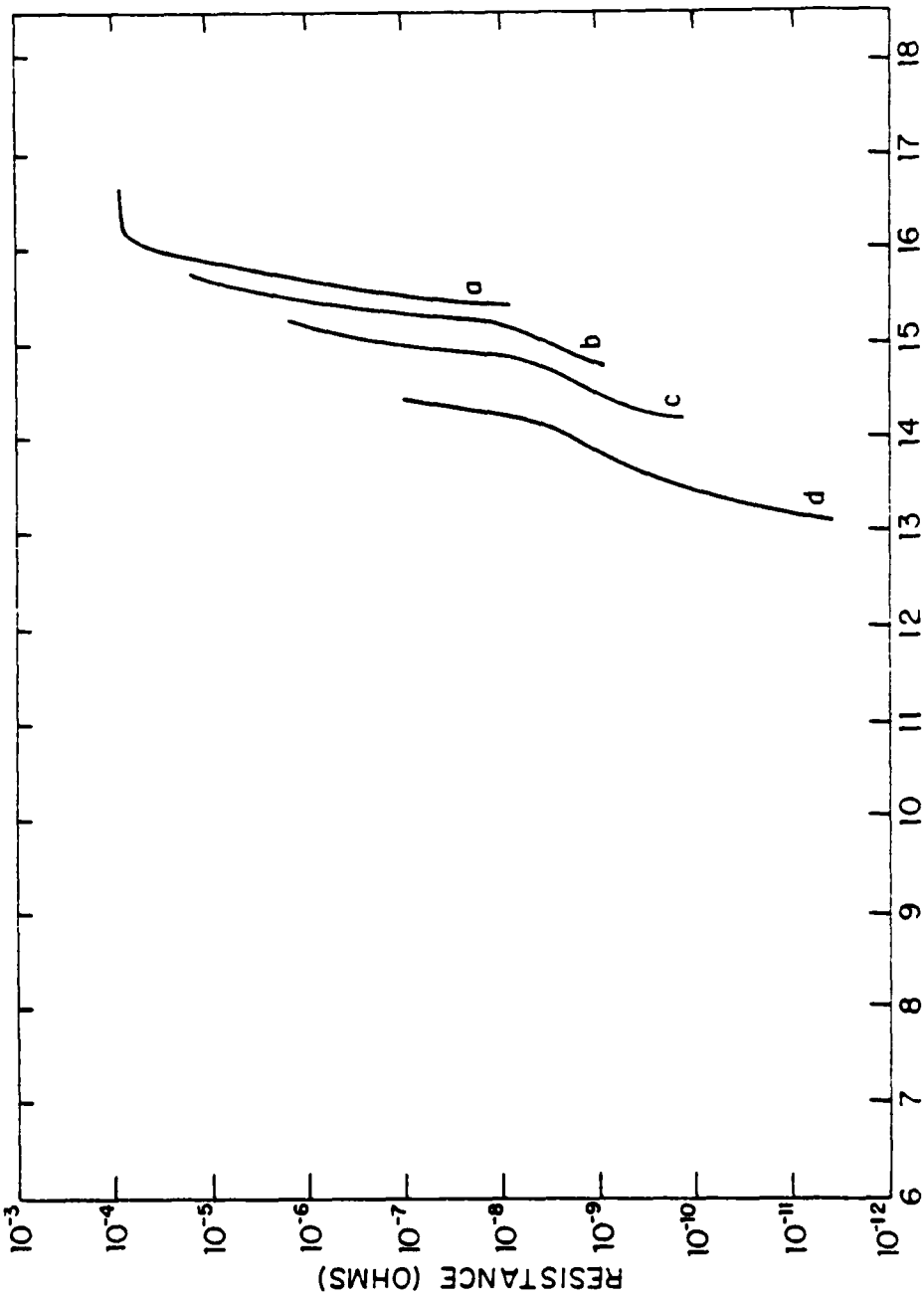

Figure 3.2 Resistive transition in a Cu-15 volume percent Nb_3Sn sample. From Davidson and Tinkham (1976).

ranging from 0.15 for randomly packed hard spheres (Sher and Zallen 1970) to 0.25 for grains which have, on the average, similar shapes (Kirkpatrick 1973) to 0.29 for randomly placed overlapping spheres (Shante and Kirkpatrick 1971) to 1/3 from the mean field theory. These theoretical values are of the same order as the amount of Nb_3Sn in the second sample.

3.2 Reduced Cu(Ni,Zn)-Nb Samples

To help distinguish between the explanations offered in the last section, we studied a number of samples with a variety of concentrations of Nb (to test for percolation) and different amounts of impurities (to vary the strength of the proximity effect). The samples studied were Cu-Nb alloys without Sn. (We left out the Sn because Cu-Nb-Sn alloys have more than two phases present since it is difficult to get all of the Nb to form stoichiometric Nb_3Sn.) All samples were made by the process outlined in the previous chapter.

Measurements were made with SQUID voltmeters. Initially, the SQUID voltmeter built by Davidson (1975) was used, but it was eventually replaced by a more reliable instrument using a cryostat built around a SHE SQUID and electronics.

A. Cu-Nb Samples

The first series of samples studied consisted of Cu-Nb, with the Nb occupying from 0.1 to 0.2 of the total volume (Lobb et al. 1978).

The cross sectional area reduction was 24 for all of these samples. These samples all had a single transition, with no distinct plateau in the R vs. T curves, in spite of current densities as high as 600 A/cm^2 which were intended to suppress the proximity effect.

Resistance is plotted against temperature for an f=0.1 sample in figure 3.3. We note that (3.1) predicts a plateau at about 6×10^{-6} ohm, well within the sensitivity of the voltmeter. Thus, these samples are either percolating, or else the proximity effect is very strong in them.

At an NS interface, the pair amplitude decays in the normal metal over a characteristic distance

$$\xi_N = \hbar v_F/2\pi k_B T = 1.91\times10^{-6}\ (m\text{-}K)/T \qquad \text{(clean)} \quad (3.2a)$$

$$\xi_N = \left(\frac{\hbar v_F \ell}{6\pi k_B T}\right)^{1/2} = 7.98\times10^{-4}\left(\frac{\ell}{T}\right)^{1/2} (m\text{-}K)^{1/2} \qquad \text{(dirty)} \quad (3.2b)$$

where v_F is the Fermi velocity, T is temperature and ℓ is the electron mean free path (Deutscher and deGennes 1969). We have used the free electron value for the Fermi velocity $v_F=1.57\times10^6$m/s for Cu here.

We estimated ℓ for these samples using the experimentally determined value $(\rho\ell)^{-1}=15.4\times10^6$ ohm-m^2 (Chambers 1952).

Using $\ell=2.6\times10^{-7}$m for the 10% sample of figure 3.3, we get a ξ_N of 2.39×10^{-7}m from the clean formula (3.2a) and 1.44×10^{-7}m from the

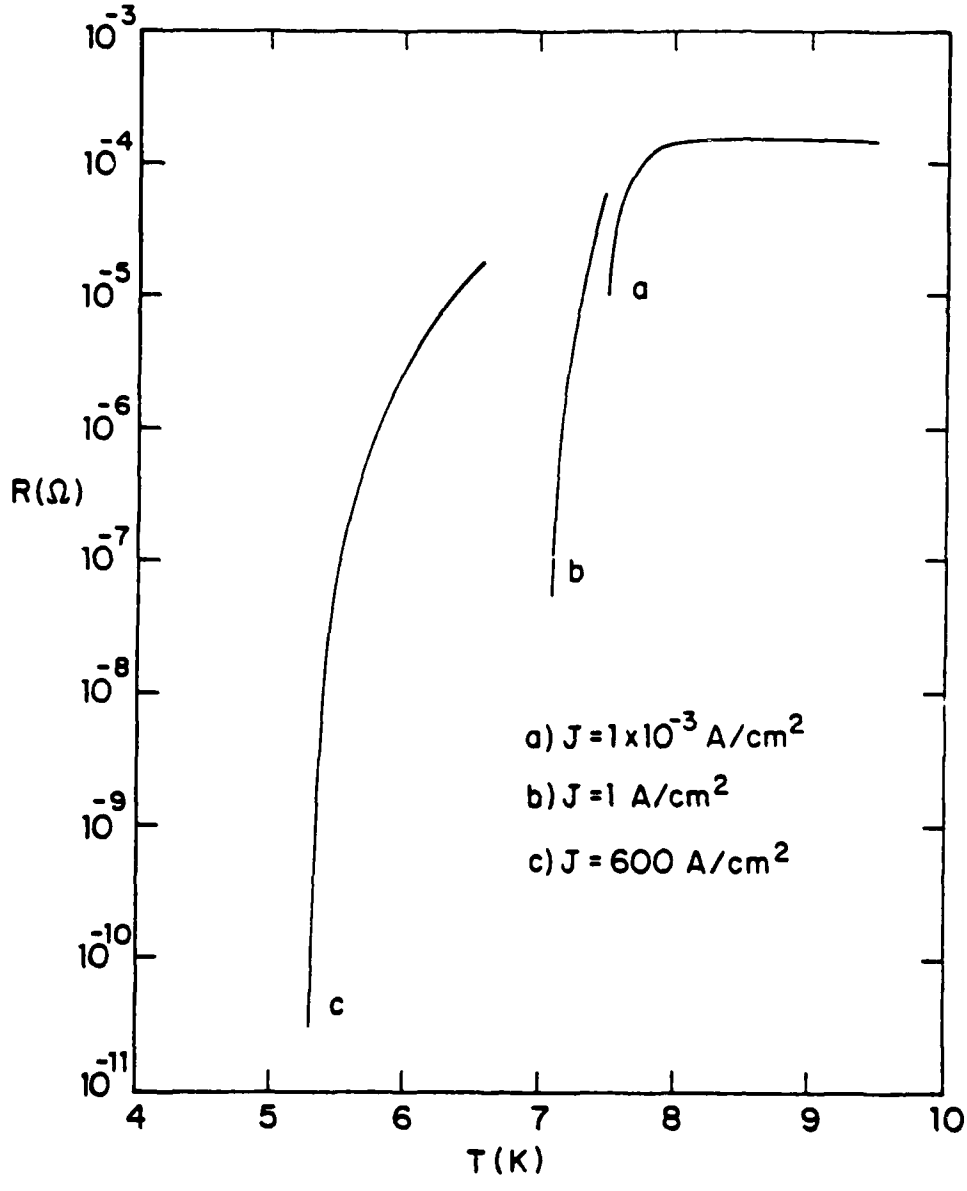

Figure 3.3 Resistive transition for a Cu-10 volume percent Nb sample.

dirty formula (8.2b) at 8K. Since the filaments are typically 10^{-6}m or less in cross section in these samples, we see that a significant volume of Cu will be influenced by the proximity effect. Defining an effective volume fraction as

$$f^* = f(1+ \xi_N/a)(1+ \xi_N/b)(1+ \xi_N/c) \qquad (3.3)$$

where a, b, and c are measured average values for the axes of the Nb filaments and using the conservative dirty limit formula for ξ_N, the 10% sample has f*=0.16. It was clearly desirable to shorten the mean free path if we wished to see a plateau.

B. A CuZn-Nb Sample

To see the effect of shortening ℓ, the 10% sample discussed in the last section was sealed in an evacuated quartz tube. At the other end of the tube was a small pellet of Zn. Zn was chosen because of its low boiling point and solubility in Cu. The tube was placed in a 900°C oven, which vaporized the Zn. The oven was turned down to 800°C and the sample was annealed at this temperature for five hours. At the end of this time, the sample was weighed, indicating that all but 0.8% of the Zn (by mass) was in the wire.

Resistivity measurements indicated that ℓ had shortened from 2.6×10^{-7}m to 1.2×10^{-7}m. Resistance vs. temperature curves showed a

small plateau, as can be seen in figure 3.4.

These experiments showed the importance of proximity effect in these composites. Clean Cu-Nb samples with f as low as 0.1 had no plateau, while the addition of an impurity quenched the proximity effect enough to cause a plateau.

C. CuNi-Nb Samples

Adding Zn to samples after they are produced has some drawbacks. The heat treatment causes changes which are not desirable. For example, figure 3.4 shows evidence for superconductivity above 12K, indicating that phases other than pure Nb are present.

Zn could be added to the initial ingot, but its low boiling point would cause much of it to evaporate during the high-temperature processing. Another impurity was needed.

After checking phase diagrams (Hansen and Anderka 1958), we decided to add Ni to the Cu matrix. Ni is soluble in Cu in all concentrations, which is desirable to avoid having two different normal phases present. In addition, the solubilities of Ni in Nb and Nb in Ni are small. Finally, Ni has a higher melting point than Cu, so material loss was not a problem.

We made samples with f ranging from 0.07 to 0.18, where the matrix consisted of Cu with 3 atomic percent Ni added. All of the samples were swaged until the cross sectional area was reduced by a factor of 16.

Typical resistance vs. temperature curves are shown in figure

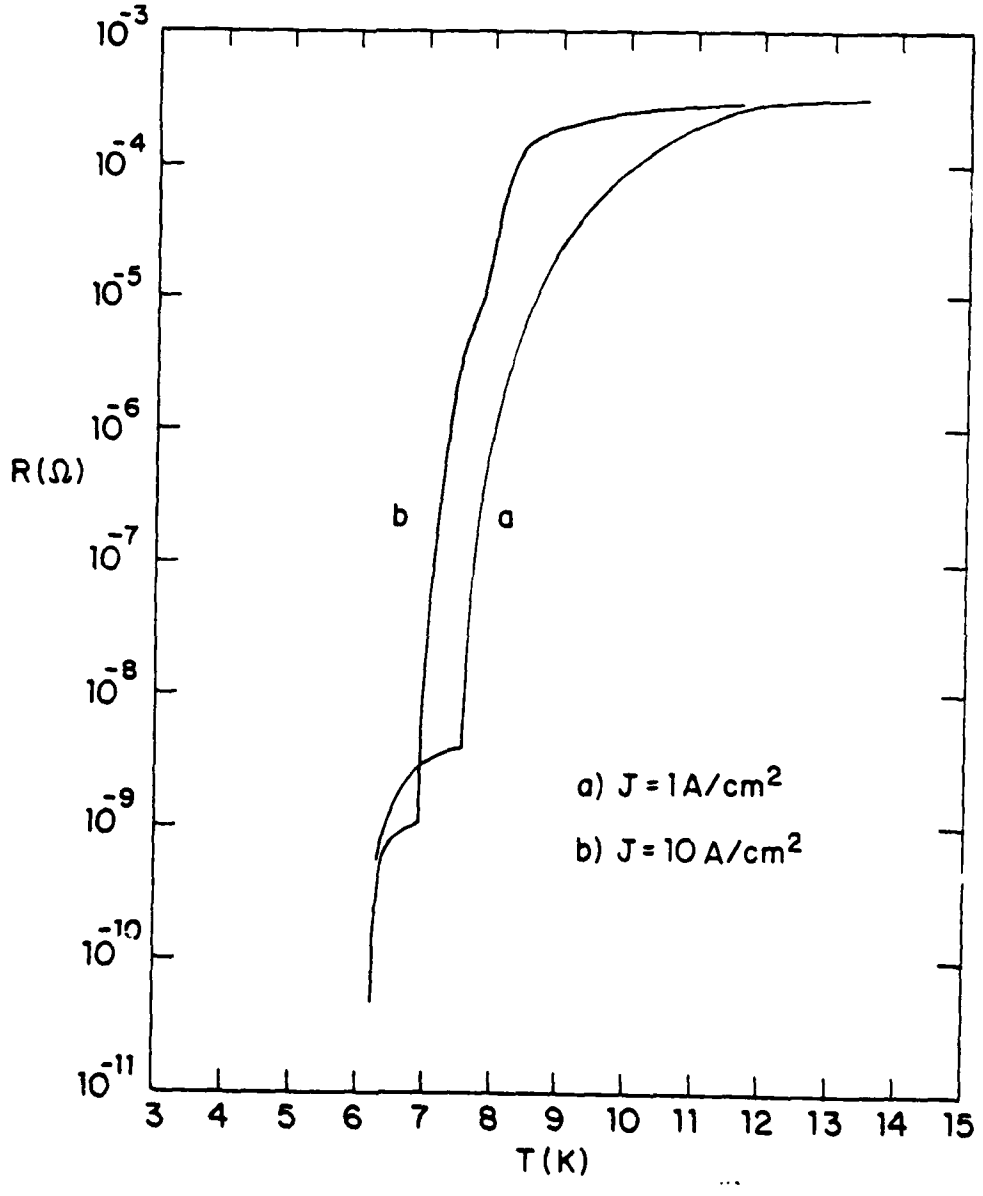

Figure 3.4 Resistive transition for the sample shown in figure 3.3 after Zn was added to the matrix to shorten the mean free path.

3.5. The sharp drop in resistance as the temperature is reduced between 7K and 8K results from the Nb becoming superconducting. The slower falloff in resistance with temperature, which begins at around 10^{-7}ohms, is attributed to the gradual strengthening of the proximity effect coupling between filaments until a current-dependent temperature T_{C1} is reached where R=0. This interpretation is supported by the maximum magnitude of the resistance in the slow falloff region of the curves, which is in reasonable agreement with that predicted for a fully normal matrix in (3.1). All of the CuNi matrix samples had the characteristic two-part transition, indicating that the filaments probably do not form a geometrically connected network in the range of concentrations studied. We conclude from this that f_c is greater than 0.18 in these samples. We emphasize that samples with the same amount of superconductor, but with different amounts of impurity in the matrix, can have quite different electrical behavior.

The smooth variation below the first sharp drop in resistance in figure 3.5 is interesting. We found that at higher currents, the resistance went to zero as a power law, $R=R_o(T/T_{C1}-1)^{\mu}$. The experimental points were fit using a least-squares procedure with $\log(R)$ and $\log(T/T_{C1}-1)$ as the variables and μ, R_o and T_{C1} as fitting parameters. We obtained good agreement with a power law over two orders of magnitude for the 7% sample for constant currents ranging from 50 to 142 amps/cm^2 (see figure 3.6). For lower current densities, for which the transition occurs at higher temperatures, spurious signals due to the transition of the soldered voltage lead connections and thermal EMF's prevent quantitative interpretation of the data.

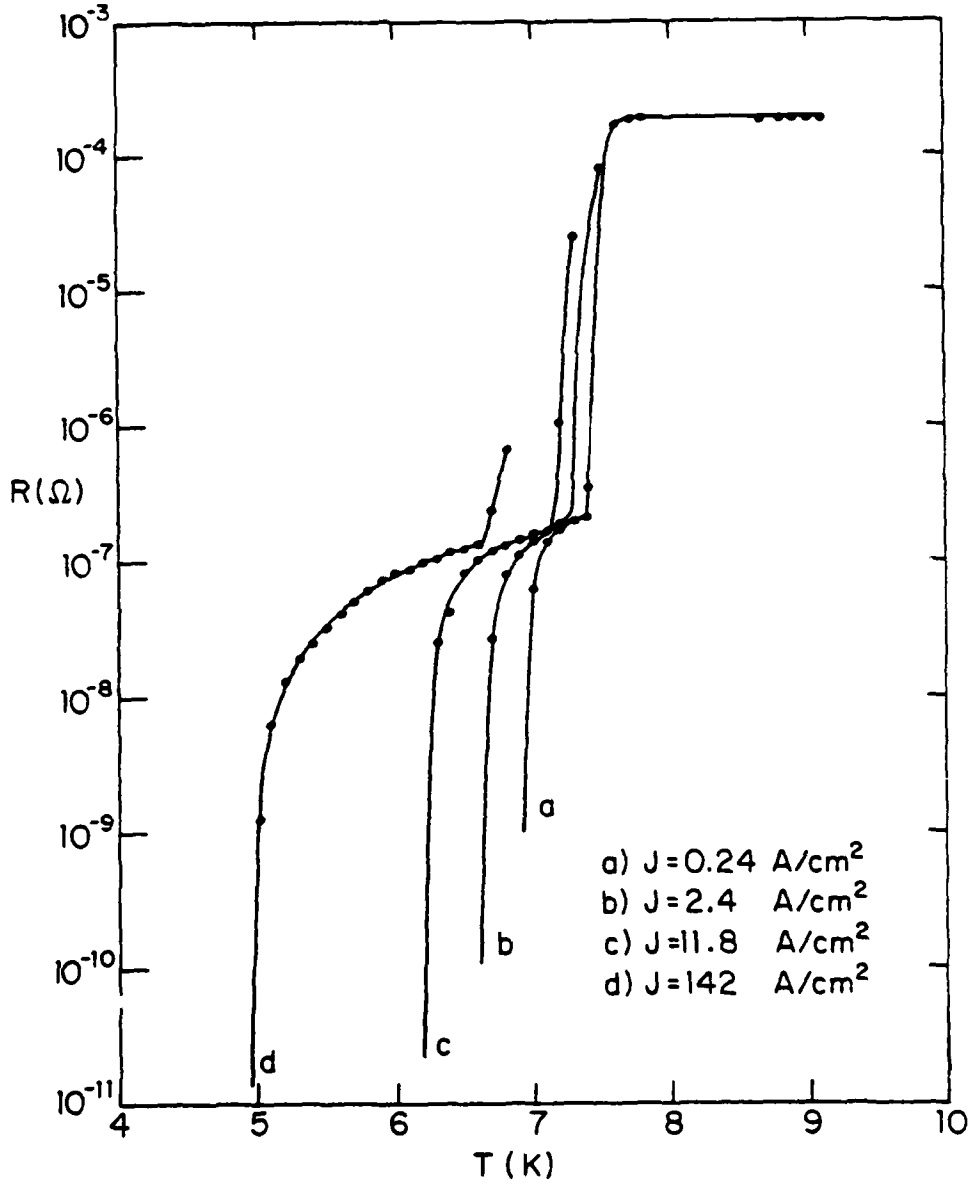

Figure 3.5 Resistive transition for CuNi-7 volume percent Nb sample.

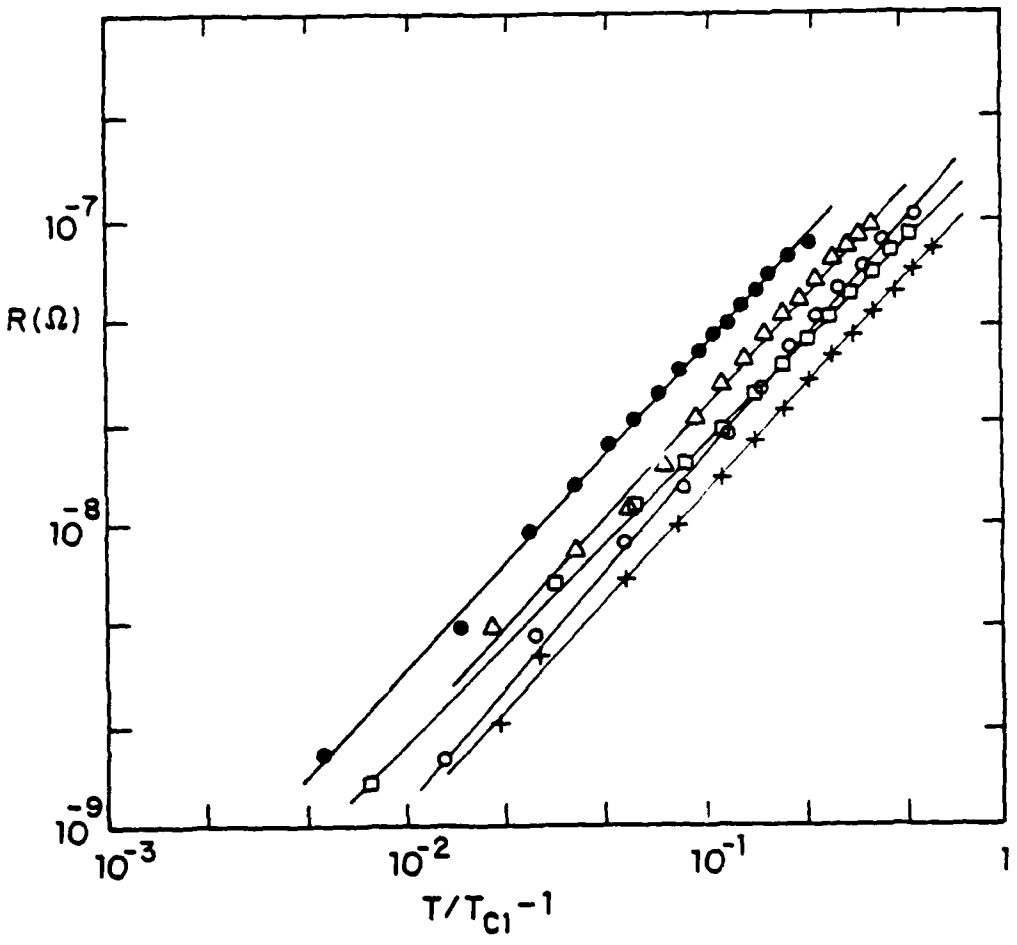

Figure 3.6 Log-log plot of plateau resistance vs. $(T/T_{G1}-1)$ of data from figure 3.5. Current density ranges from 47A/cm^2 to 142 A/cm^2 (left to right). The solid lines are least-squares fits to the data.

Samples with 13% Nb showed more variation from one current to the next, probably because of bad mixing or finite sample size effects, both of which are aggravated by having more Nb. A single dirty sample prepared by hot extrusion from powders which contained 5% Nb and no Ni also gave data in good agreement with a power law. For the 5% and 7% samples, fitted values of μ ranged from 1.0 to 1.15 for the currents used, with a mean of 1.06 and an rms deviation of 0.04.

D. Undrawn CuNi-Nb Samples

In order to remove any effects caused by the filament elongation, we prepared a series of samples with Cu-3 atomic percent Ni matrices where the volume fraction of Nb varied between 0.07 and 0.3. These samples were not reduced, but were spark cut into wires which were roughly 2.5cm by 0.1cm by 0.1cm.

A serious problem hampered this work. Between f=0.1 and f=0.18, samples did not mix well, as macroscopic clumps of Nb were present. Some conclusions can be extracted from the remaining data, however.

The f=0.2 sample had a small plateau about 0.1K wide with R_o/R_N of order $5x10^{-3}$ and the f=0.3 sample had just a single transition. From this we concluded that f_c is between 0.2 and 0.3, and is probably between 0.2 and 0.25, in these samples. This agrees with our results on the reduced wire.

3.3 Theoretical Models for the Plateau Resistance

The transistion of a composite superconductor is drawn schematically in figure 3.7. At T_c, the resistance drops from the normal state value to R_o. The variation of resistance with temperature becomes slower below T_c, with resistance eventually dropping to zero at T_{C1}. We would like to understand how R_o and T_{C1} depend on material parameters, as well as how the resistance depends on temperature. We note that some articles in the literature follow a different convention, calling the upper transition temperature T_{co} and the lower one T_c.

A. Percolation Near T_c

Just below T_c, where the Nb inclusions have just become superconducting, the coupling between filaments will be weak if the normal metal coherence length is short. This is true because the critical current I_c between two filaments approaches zero as T approaches T_c and the coupling energy between filaments is proportional to I_c (Tinkham 1975, chapter 6). In the case of a dirty matrix the resistance near this temperature is thus essentially the resistance of a classical mixture of two materials.

Percolation theory describes the bulk properties of classical inhomogeneous media. We will discuss percolation at some length in chapter 5. For now, a summary of results is all that is necessary.

A number of important ideas have emerged from considering large

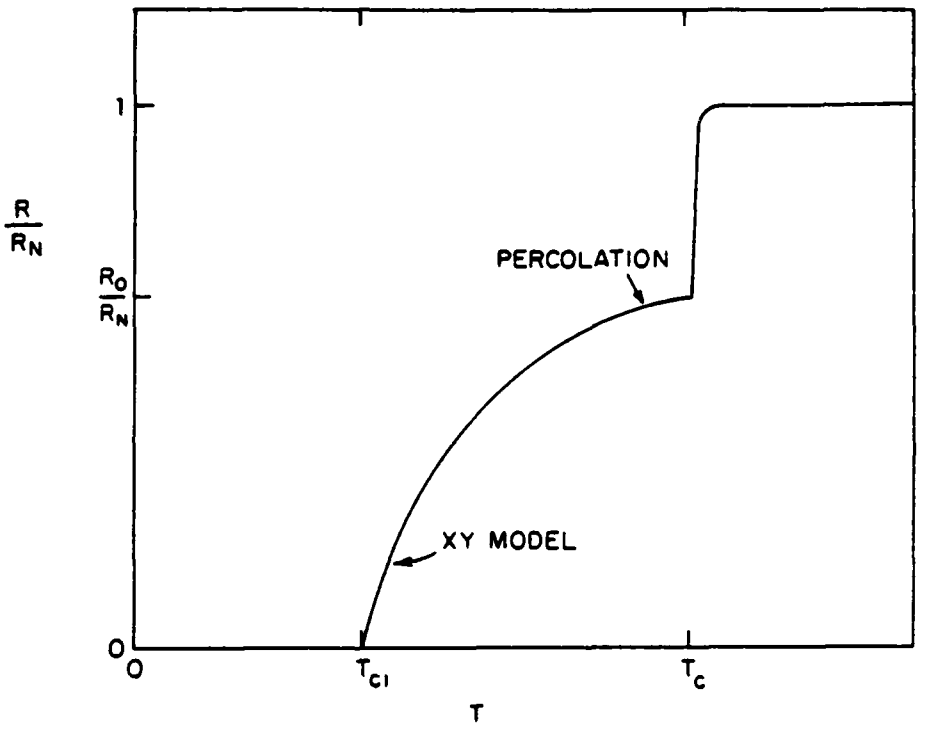

Figure 3.7 Schematic drawing of the two-part resistive transition in a composite superconductor.

two-component lattices of resistors r_1 and r_2 (Straley 1977a, Kirkpatrick 1973, 1979). If one of the resistances, r_1, occurs with probability p, then there is a critical probability p_c above which the r_1's form an infinite cluster. This p_c is different for different lattices. Furthermore, when $1/r_2=g_2=0$, for a small range above p_c, the bulk conductance G varies as

$$G \propto (p-p_c)^t \qquad (p>p_c) \tag{3.4}$$

where t seems to depend at most only weakly on everything but the dimensionality of the lattice. For a lattice consisting of shorts (with probability p) and resistors, the bulk resistance varies as

$$R \propto (p_c-p)^s \qquad (p<p_c) \tag{3.5}$$

For three dimensional systems, numerical simulations indicate that s is between 0.6 and 0.8 and that t is between 1.5 and 1.7 (Straley 1977a). In two dimensions, $s=t=1.35\pm0.02$ (Lobb and Frank 1979,1980).

In real materials, occupation probabilities p in (3.4) and (3.5) are replaced by component volume fractions f. In general, the critical volume fraction f_c will depend on the system studied. The critical

exponents s and t are again expected to depend only on the dimensionality of the system. Aggregate films (Liang et al. 1976) and cermets (Abeles et al. 1975) have been shown to give experimental values for t in two and three dimensions which are comparable to the values cited above.

The general shape of the R_0 vs. f curve is concave downward for the isotropic samples, indicating that s is less than one. This qualitative result is in agreement with the percolation model. The scatter due to sample inhomogeneity prevented us from obtaining any quantitative estimate for the critical exponent s.

We can phenomenologically combine (3.1) and (3.5) to obtain (Tinkham 1977)

$$R_0/R_N \propto (f_c-f)^s/fA^3 \qquad (3.6)$$

which we expect to hold for (f_c-f) small and A large.

Equation (3.6) is qualitatively consistent with the data available on Tsuei wire (Callaghan and Toth 1975, Davidson et al. 1975, Tinkham 1977, Lobb et al. 1978). Increasing A and f decreases R_0/R_N. Unfortunately, quantitative comparison is difficult because of sample inhomogeneities and sample-to-sample variations. The important conclusion to be drawn from (3.6) is that R_0 approaches zero as f approaches f_c so that we expect a two-part transition only for f less

than f_c. The dependence of R_0 on f is indicated schematically in figure 3.8.

B. A Percolative Model of the Temperature Dependence

When the superconducting phases of the filaments are strongly coupled, the classical model of the last section may break down. Nonetheless, it is instructive to ignore this problem to construct a simple theory of the temperature dependence of the resistance.

The results outlined earlier in this chapter showed the importance of the proximity effect in these wires. The presence of Ni in the matrix changed the electrical characteristics greatly. This suggests that an effective volume fraction f* and not the nominal volume fraction f is important. In the clean samples, $f^*(T_c)>f_c$ so that no plateau appears. In the samples containing Ni, $f^*(T_c)<f_c$ so that the temperature must be lowered to T_{C1} for an infinite superconducting cluster to form. We would expect f* to depend on the normal metal coherence length (3.2a,b), which varies smoothly with temperature. Expanding f*(T) around T_{C1}, we obtain (Tinkham 1977, Lobb et al. 1978)

$$f^*(T) = f^*(T_{C1}) + \left(\partial f^*/\partial T\right)_{T_{C1}}(T-T_{C1}) + \ldots \qquad (3.7)$$

Combining (3.6) and (3.7) gives (Tinkham 1977, Lobb et al. 1978)

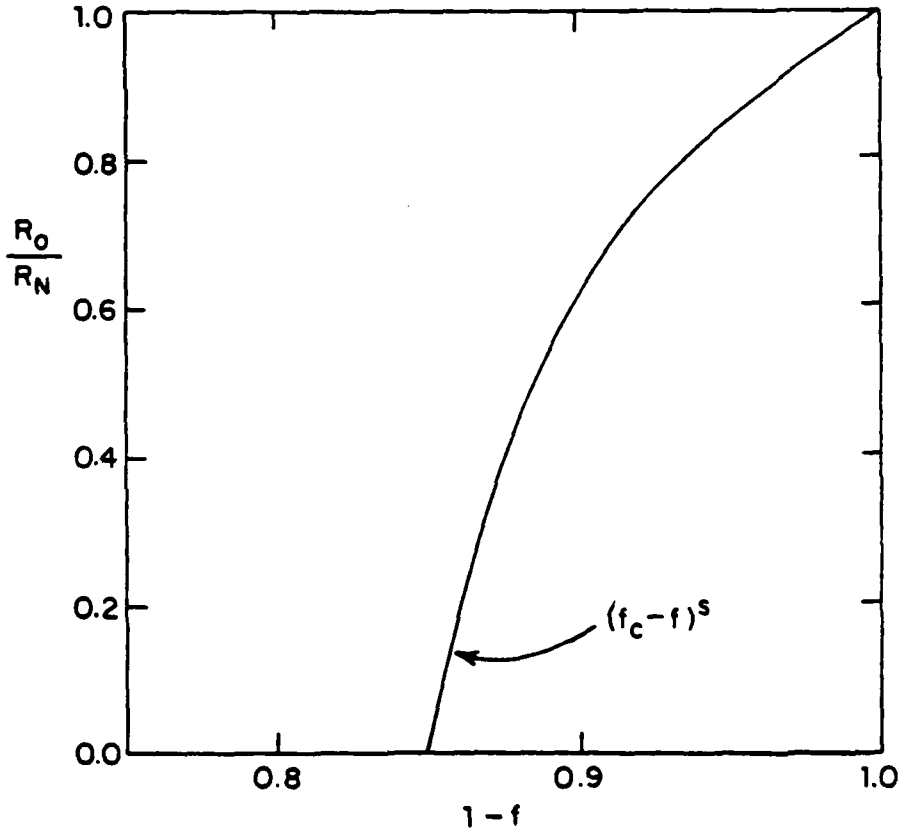

Figure 3.8 Plateau resistance near T_c (see figure 3.7) as a function of superconducting volume fraction f.

$$R(T) \propto (T/T_{C1}-1)^{s}/A^{3} \qquad (\text{for } T_{C1}<T<T_{c}) \qquad (3.8)$$

where R(T) is the temperature-dependent resistance of the composite.

This model predicts T_{C1} through $f^*(T_{C1})=f_c$. Assuming f_c is between 0.1 and 0.3 and using (3.3) with parameters for the 7% Nb in CuNi wire, T_{C1} is of the order of a few degrees, in reasonable agreement with the data in figure 3.5.

The model also predicts that the resistance should go to zero as $(T-T_{C1})^{\mu}$, and that $\mu=s$. Experimentally, we found that $\mu=1.06\pm0.04$ (figure 3.6), which does not agree well with either the two-dimensional (1.35 ± 0.02) or three-dimensional (0.6-0.8) values for s. It is possible that this disagreement is the result of the anisotropy of the samples, a point which we will discuss in chapter 5. Unfortunately, the isotropic samples with $f<f_c$ which would have yielded an experimental value of μ were the ones which were badly mixed. Thus, it was impossible to measure μ for undrawn samples. More fundamentally, the model used in this section is an oversimplification. We discuss a more rigorous model in the next section.

C. The XY Model

Two superconductors separated by an insulator or a normal metal have a coupling energy given by $-(\hbar I_c/2e)\cos\Delta\varphi$, where I_c is the critical current of the junction and $\Delta\varphi$ is the phase difference between the superconductors. For an array of superconductors which are

assumed to interact only with their nearest neighbors, we can add up these energies to write a Hamiltonian

$$H = H_0 - (\hbar/2e) \sum_{<i,j>} I_{c_{ij}} \cos(\varphi_i - \varphi_j) \qquad (3.9)$$

where H_0 represents terms for the individual islands, and the sum is due to the coupling energies.

This is seen to be equivalent to the standard model Hamiltonian for magnetic systems

$$H = H_0 - \sum_{<i,j>} J_{ij} \vec{S}_i \cdot \vec{S}_j \qquad (3.10)$$

if the spins $\vec{S}_i$ are confined to a plane so that $\vec{S}_i \cdot \vec{S}_j = S_i S_j \cos(\varphi_i - \varphi_j)$. Thus, an array of weakly coupled superconductors is isomorphic to a ferromagnet whose spins have two components. This is the n=2 (where n is the number of components) or XY model (Giovannini and Weiss 1978, Patton et al. 1980, Imry 1980). The number of components in the XY model falls between the more familiar Ising (n=1) and Heisenberg (n=3) models (Ma 1976).

We expect the phases to become coupled when kT is lower than the coupling energy between grains. We thus estimate T_{C1} by saying

$$k_B T_c = (\hbar/2e) z I_c(T) \qquad (3.11)$$

where $I_c(T)$ is the average intergrain critical current, z is the coordination number, and we are ignoring factors of order unity.

To get a more explicit estimate for T_{C1}, we can calculate the limiting form of (3.10) for an array of BCS superconductors connected by tunnel junctions (Klapwijk 1980). In this case

$$I_c(T) = (\pi\Delta(T)/R)\tanh(\Delta(T)/2k_B T) \qquad (3.12)$$

where R is the resistance of a junction and $\Delta(T)$ is the energy gap (Tinkham 1975, chapter 6). Combining (3.11) and (3.12) near T_c, we obtain

$$T_c/T_{C1} \simeq 1+Re^2/3.7\hbar z = 1+R/(z\cdot 15{,}222\text{ohm}) \qquad (3.13)$$

so that T_{C1} depends on the single junction resistance R and the

coordination number z.

Near T_{C1} the resistance as calculated by the XY model varies as $(T-T_{C1})^{\mu}$. It has been suggested that $\mu=(4-d)\nu$, where the coherence length exponent $\nu=.670\pm0.006$ in three dimensions (Ma 1976). This implies that $\mu=0.67$ in three dimensions, which agrees with the percolation model of section 3.3B but does not agree with our experimental value of 1.06.

In two dimensions, ν is infinite (Kosterlitz 1974), which suggests that μ is infinite. This agrees with the result of Halperin and Nelson (1979), who found that R went to zero exponentially as T approaches T_{C1}. This disagrees markedly with the percolation model prediction, which says that $\mu=1.35$ (Lobb et al 1978). (Some two dimensional samples will be discussed in the next chapter.)

CHAPTER FOUR: SUPERCONDUCTING COMPOSITE FILMS

In this chapter we report preliminary work on a thin film composite system. The films are analogous to the materials discussed in the last two chapters in that they consist of superconducting islands in a normal metal matrix. The difference is that these samples are two-dimensional, that is, the films are only one island thick.

This work was motivated by the fact that many of the properties (such as the critical behavior) of inhomogeneous superconductors depend only weakly on parameters other than the dimensionality. In addition, many interesting effects are expected to occur in systems with reduced dimensionality (Halperin and Nelson 1979).

4.1 Discontinuous Normal Metal Films

When a metal is deposited on a substrate, there is generally a measurable lag between the beginning of deposition and the onset of electrical conduction. This effect occurs because metals tend to diffuse on the substrate and bead up to minimize the surface energy. In general, lower melting point materials have a higher conduction onset thickness because they diffuse more readily. A general review of electrical conduction in discontinuous films has been written by Morris and Coutts (1977).

Liang et al. (1976) studied resistivity as a function of thickness for Bi films deposited at room temperature. Their films were deposited onto an evaporated, and therefore rough, SiO layer, which would tend to discourage diffusion. They found a sharp five order of

magnitude drop in the resistivity in a narrow range of thickness around 100Å.

4.2 Composite Superconductor-Normal Metal Films

A. Pb-Cu Films

Our original choice for a superconducting material was Pb. We evaporated the Pb onto a room temperature glass substrate, and found that the resistance dropped from more than 10^8ohm to around 10^3ohm during additional deposition of a mass equivalent to less than 10Å thickness. Our onset occured at thicknesses between 500Å and 1000Å. We attribute the difference between our Pb and Liang et al.'s Bi to the substrate smoothness.

A number of films were made in which the Pb thickness spanned the aggregation thickness. The Pb films were overcoated with Cu without breaking vacuum. The resulting composite film was then removed from the evaporator and wired into a cryostat.

Measurements of resistance vs. temperature for these samples showed a depressed T_c and a broad transition. Transitions were typically a degree or more wide with the films remaining fully normal down to 4K. There was little evidence for the two-part transition seen in Tsuei wire (see figure 3.5).

The reason for this broad transition became apparent when the films were examined with a scanning electron microscope. The Pb islands were typically less than 1000Å in all dimensions, which is

comparable to the coherence length in Pb. In this limit of small islands, the electrons see an average electron-phonon coupling, so that the distinctions between the two materials become blurred as far as the superfluid is concerned (Deutscher and deGennes 1969). This is not a problem in superconductor-insulator composites because the order parameter in the superconductor is not depressed by an insulating boundary. Although the limit of small particle sizes (the Cooper limit) is interesting experimentally, it was not pursued because we wished to consider weakly coupled islands of strong superconductor. Further work in this area is warranted.

B. PbBi-CuAl Composite Films

We wished to make samples with weakly coupled islands of strong superconductor. This can be done by making the islands bigger (to reduce intraisland fluctuations) or by making the matrix mean free path shorter (to reduce the interisland phase coupling). In order to get large islands, we must have the island size large compared to the superconducting coherence length $\xi(T)$. In the dirty limit,

$$\xi(T)=0.855(\xi_0 \ell)^{1/2}/(1-T/T_c)^{1/2} \qquad (4.1)$$

where ξ_0 is the Pippard coherence length and ℓ the electron mean free path (Tinkham 1975, chapter 4). Thus, we can shorten $\xi(T)$ by shortening

ℓ. To this end, we prepared Pb-3 weight percent Bi alloys to use as the superconductor. We also increased the island size directly by tilting the substrate 60^{o} from the standard normal incidence (Holland 1958). To decrease strong interisland phase coupling through the proximity effect, we used Cu-4 weight percent Al for the the normal metal to decrease ξ_N, as suggested by (3.2b).

The samples were prepared on 2.5 cm square sapphire substrates vapor cleaned in ethanol followed by trichloroethylene. On a liquid nitrogen temperature substrate, 1000Å of Pb-30 weight percent Bi was evaporated through a mask to form strips on opposite sides of the sapphire to make high T_c leads (see figure 4.1). The sapphire was then removed from the evaporator, re-cleaned, and mounted on a rotatable stage in the evaporator. Next, PbBi (3%) was evaporated at a 60^{o} angle at 3Å/sec until the film's resistance dropped below 10^{8} ohm. At this point, evaporation was stopped by moving a shutter and turning off the heater current. After a minute or two, the film's resistance would be of the order of 1000 ohm and fairly stable. The stage was rotated back to normal incidence and CuAl (4%) was evaporated at 3Å/sec until the desired thickness was reached.

Three samples were made following the above prescription. All of them aggregated within 15Å of 765Å (this is an average thickness, assuming bulk density). Sample A had 1500Å of CuAl deposited on top, sample B had 750Å deposited on top, and sample C had 390Å deposited on top. All samples were 1.7cm long and 2.5cm wide.

C. Morphology of PbBi-CuAl Films

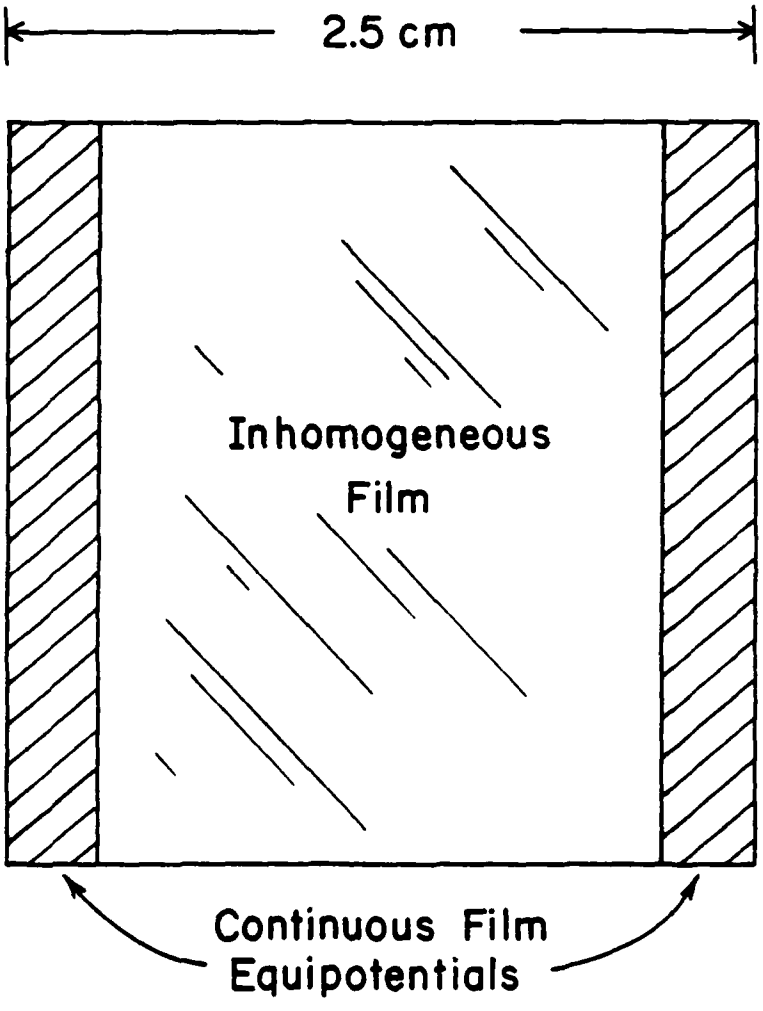

Figure 4.1 Diagram of the sample geometry.

A scanning electron micrograph of sample C is shown in figure 4.2. The morphology is typical of samples with this thickness of PbBi. The twisted, highly-connected network is the result of partial aggregation of the originally circular islands. This interpretation is supported by the fact that thinner Pb films have islands that are more nearly circular.

D. Electrical Properties of PbBi-CuAl Films

Samples were studied in a variable temperature cryostat by measuring voltage as a function of temperature at constant currents. A Keithly Nanovoltmeter was used to measure voltage. With care, noise could be reduced to below 60nV.

Resistance (V/I) vs. temperature is plotted in figure 4.3 for sample A. At low currents there is a single transition in a narrow temperature range. As the current is increased, a two-part transition develops. Our monitoring of resistance while the PbBi was being evaporated indicated that the PbBi was barely connected, that is $f \gtrsim f_c$. We would expect such a system to carry a small supercurrent as soon as the islands become superconducting, and this was the case for all three samples. When the current is increased, however, the interisland critical currents are exceeded fairly quickly, since the islands are only weakly connected.

Thus, the transition splits into two parts for higher currents. As temperature is lowered, the islands become superconducting,

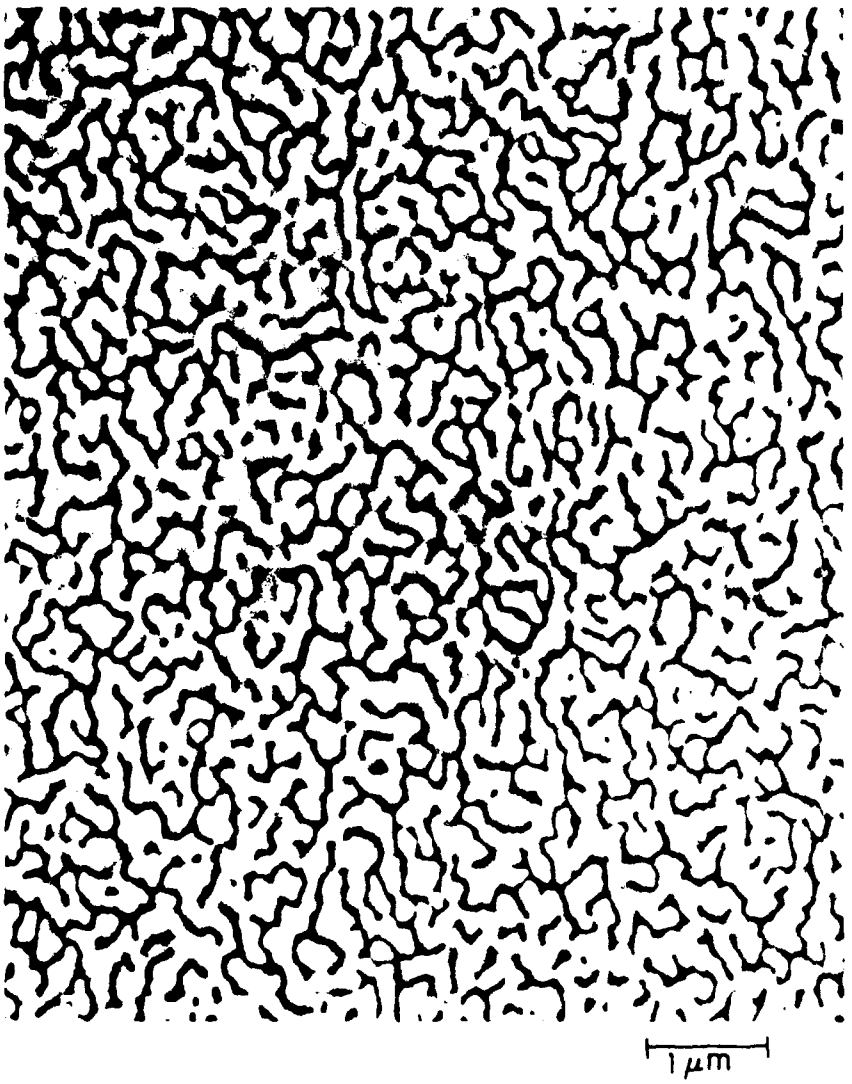

Figure 4.2 A scanning electron micrograph of film C.

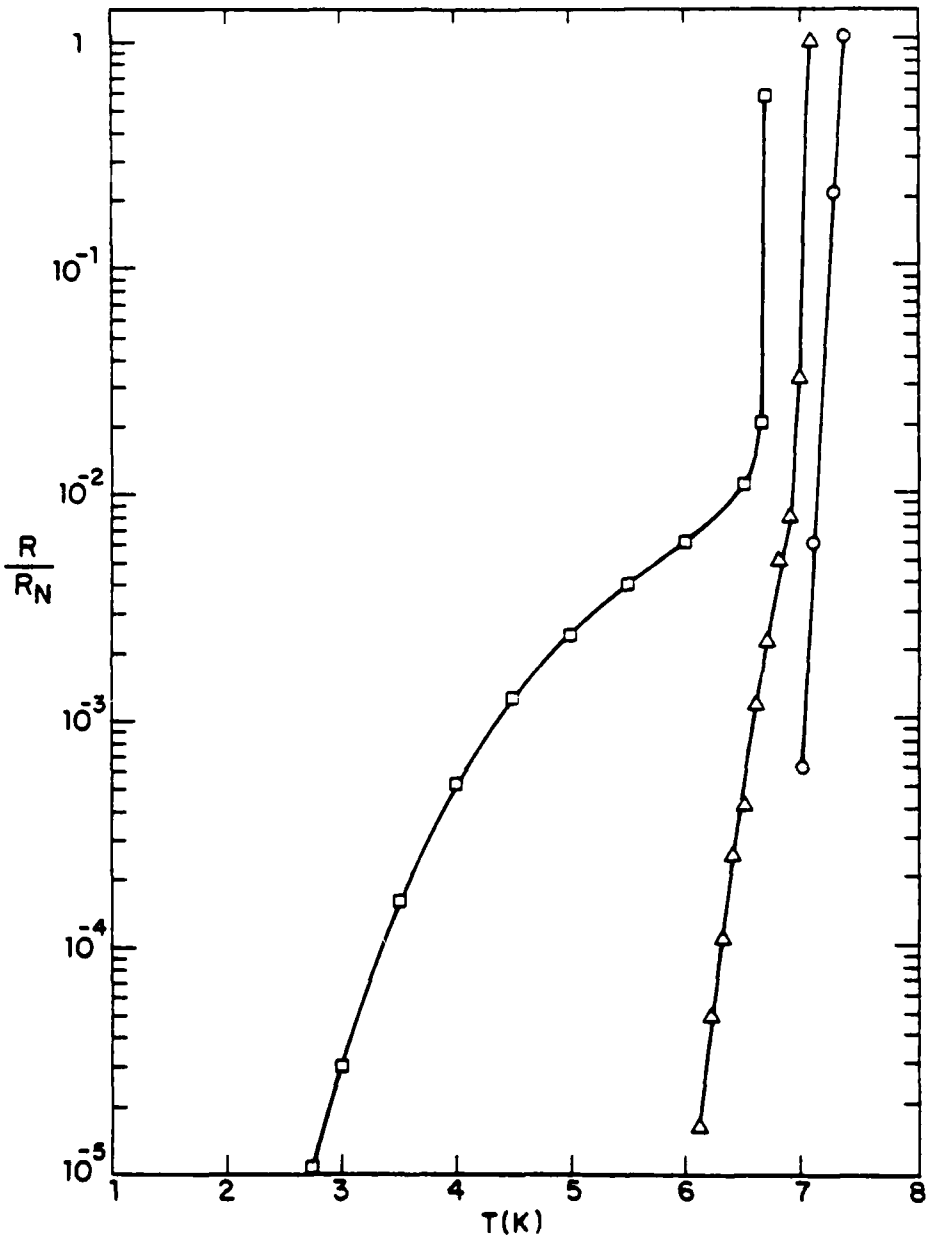

Figure 4.3 Semilogarithmic plot of resistance against temperature for sample A. The current ranges from 182mA to 10μA from left to right.

decreasing the resistance sharply. When the temperature is lowered further, the superconducting phase coupling increases in strength relative to kT until the composite resistance drops to zero.

The resistance of these samples is not a simple power of $(T-T_{C1})$. Qualitatively, the fitted exponent increases as the current is decreased. This is not surprising, in light of the fact that the power law dependence discussed in chapter 3 holds in the limit of small current. Since we have a single sharp transition for these samples as the current approaches zero, we cannot extract information about the value of the exponent μ.

We can study the critical current as a function of temperature in these samples, however. I_c was measured by increasing the temperature at constant current until 60nV appeared across the sample. Fitting to the form

$$I_c=I_o(1-T/T_c)^{\beta} \qquad (4.2)$$

where T_c is the small current transition temperature, we found that $\beta=1.8\pm0.2$ for these samples. A log-log plot of I_c against (T_c-T) for sample A is shown in figure 4.4. The straight line fit is quite good, extending over three decades in I_c.

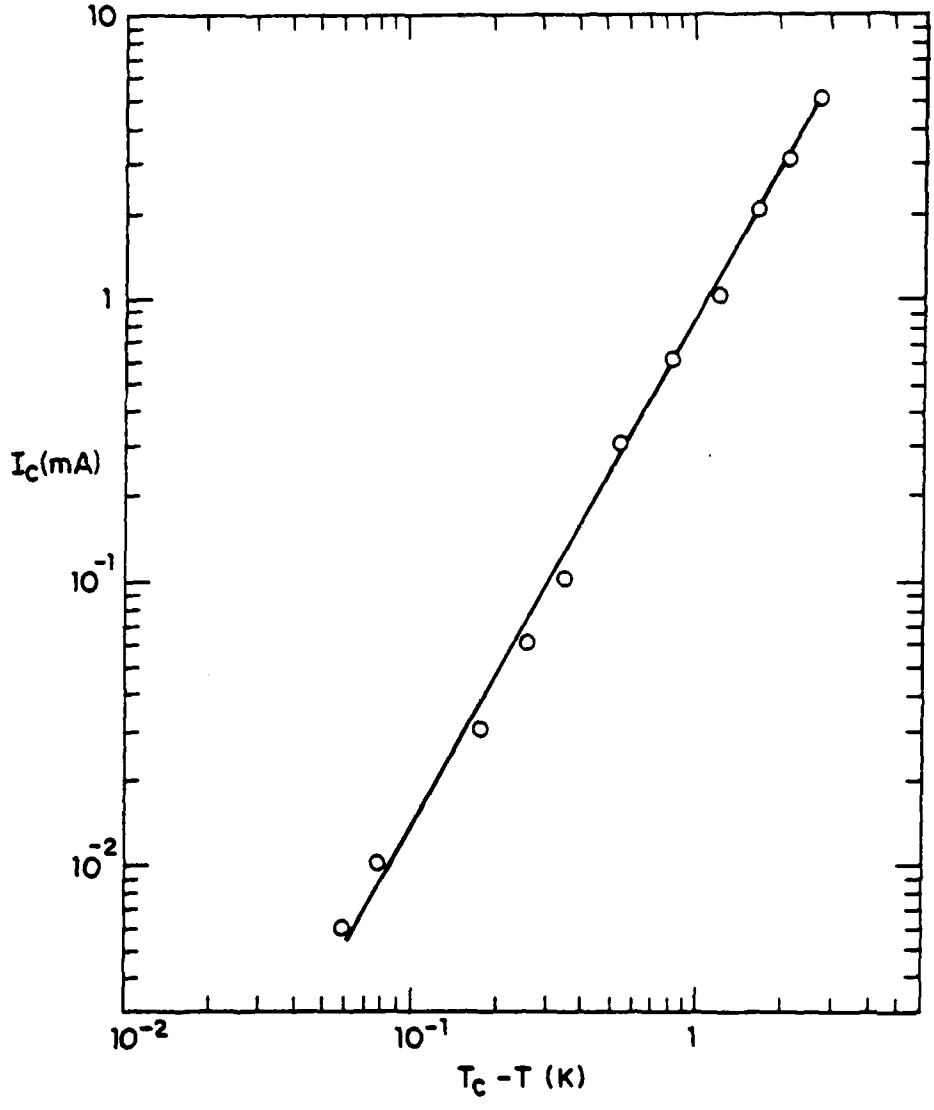

Figure 4.4 Log-log plot of I_c against (T_c-T). The slope gives the exponent β.

E. Discussion

Qualitively, the transition shown in figure 4.3 is similar to that of figure 3.5. The explanations for the two figures are the same. The transition splits into two parts for high currents because high currents destroy the phase coherence before they destroy the superconductivity of the individual islands. We expect the temperature variation of resistance to be more amenable to quantitative interpretation in thinner films where $f<f_c$. In this case, a current-independent resistance will probably develop in the limit of small current in the plateau (Patton et al. 1980).

The critical current behavior is strikingly similar to the data of Wolf et al. (1979) on a two-dimensional superconductor-insulator composite. They found a β of 1.7±0.2, essentially the same as our value.

Unfortunately, the theoretical prediction of the XY model is that $I_c=0$ (Halperin and Nelson 1979). It is possible that more sensitive measurements would agree with this result. Even if the data is a result of limited voltage sensitivity, there is presumably some explanation of the simple temperature dependence.

It is possible that these results are due to finite size effects. The requirement that the average size of fluctuations be less than the sample size is that $\xi_{xy}<<L$ where L is the sample size and ξ_{xy} is the coherence length appropriate to the phase transition. This leads to

$$|T/T_{ci}-1| >> (\log(L/\xi_{GL}(T)))^{-2} \qquad (4.3)$$

where we have used Halperin and Nelson's (1979) expression for ξ_{xy} and ξ_{GL} is the Ginzburg-Landau coherence length. If this requirement is not met, theoretical predictions based on assuming an infinite sample will not apply. Even if we use the zero temperature value of the Ginzburg-Landau coherence length, this implies that $|T/T_{ci}-1| >> 0.01$, which may be outside the critical region. It is worth noting in this connection that I_c varies as $(1-T/T_c)^2$ in a single SNS junction (deGennes 1966, chapter 7). Our data may indicate some sort of locking together of the different junctions in the sample.

Another possible explanation is that the I_c data represents a crossover from three dimensions to two dimensions. This may be true in Wolf et al's (1979) films because they may be more than one grain thick. Although our films are only one island thick, strong interisland coupling could make the film effectively homogeneous. In this case Ginzburg-Landau behavior (which predicts $\beta=3/2$, (Tinkham 1975, chapter 4)) would occur.

Further work is clearly called for, especially on thinner (and therefore more weakly coupled) films. Thinner films would also allow us to study resistance as a function of temperature in the limit of zero current, which would allow a determination of the exponent μ.

CHAPTER FIVE: PERCOLATION

Various aspects of percolation theory are discussed in this chapter in order to understand the effects of anisotropy on percolative conduction. We begin by outlining the connection between the random classical continuum, a model for composite materials, and random resistor networks, which are computationally more tractable. Approximate methods of solution are discussed, and then applied to anisotropic lattices in two dimensions. Finally, we apply one of the approximation techniques, the renormalization group, to isotropic two-dimensional lattices to obtain highly accurate estimates of critical exponents. This is necessary since critical exponents are often measured in real systems, while the uncertainties in earlier calculations make comparison between theory and experiment difficult.

5.1 The Classical Continuum and its Lattice Model

A. The General Problem

The materials discussed in the experimental sections of this thesis are properly described in quantum mechanical terms. Classical models are useful, however, since they often provide general insight and qualitatively correct results, and are easier to solve (Davidson *et al*. 1975, Davidson and Tinkham 1976).

The general problem is to understand the bulk transport properties of a two-component system where the components have isotropic conductivities $\sigma^{(1)}$ and $\sigma^{(2)}$ and occupy volume fractions f and 1-f.

We assume that the grains of both materials have average sizes L_i in the x_i direction, where these sizes are not necessarily equal in different directions but are the same for both materials. Current conservation requires that

$$\sum_i \frac{\partial}{\partial x_i}\left(\sigma(\vec{r})\frac{\partial}{\partial x_i}V(\vec{r})\right) = 0 \tag{5.1}$$

where $V(\vec{r})$ is the voltage at a point $\vec{r}$ and $\sigma(\vec{r})$ is isotropic. If we make the change of variables

$$x_i' = x_i L_1 / L_i \tag{5.2a}$$

$$\tilde{\sigma}_i'(\vec{r}') = \sigma_i(\vec{r}) \tag{5.2b}$$

$$V'(\vec{r}') = V(\vec{r}) \tag{5.2c}$$

the grains will be isotropic in the new coordinates, having an average size L_1 in all directions. Equation (5.1) becomes

$$\sum_i \frac{\partial}{\partial x_i}\left((L_1/L_i)^2 \tilde{\sigma}_i'(\vec{r}')\frac{\partial}{\partial x_i}V'(\vec{r}')\right) = 0 \tag{5.3}$$

where L_1 is the characteristic length in the x_1-direction.

This is equivalent to the continuity equation for a geometrically isotropic medium with anisotropic conductivity, where we identify $\sigma_i'(\vec{r}')=(L_1/L_i)^2\tilde{\sigma}_i'(\vec{r}')$. The problem of isotropically conductive prolate spheroid grains (Davidson and Tinkham 1976) is seen to be equivalent to the problem of spherical grains with $\vec{\sigma}'=(\sigma,(a/b)^2\sigma,(a/b)^2\sigma)$ where a and b are the semi-major and semi-minor axes of the ellipsoids.

The differential equation (5.3) can be changed to a finite difference equation on a cubic grid of size $\Delta r'$much smaller than the grain size L_1,

$$\sum_k g_{jk}(V_j-V_k)=0 \qquad (5.4)$$

where $g_{jk}\propto\sigma_i'(\vec{r}')$ in each direction and the sum is over the nearest neighbors of j on the grid.

Equation (5.4) is equivalent to Kirchoff's law for a cubic lattice of conductances g_{jk}. This result was derived for isotropic networks by Kirkpatrick(1973). We note that the g_{jk} are different in each medium, as are the σ_i'.

The resistors in this lattice are highly correlated by the condition $\Delta r<<L_1$. We can relax this constraint to simplify matters, while still maintaining the essential randomness and anisotropy of the

model, by removing correlations between the conductors. The problem then becomes a cubic lattice with conducting bonds between nearest neighbor vertices. These bonds have conductance $g_i^{(1)}$ with probability p and $g_i^{(2)}$ with probability 1-p, and

$$g_i^{(1)}/g_j^{(1)}=g_i^{(2)}/g_j^{(2)}=(L_j/L_i)^2 \qquad (5.5)$$

B. The Percolation Problem

The problem outlined in the previous section is especially interesting when the ratio of the two conductances becomes infinite. This can be done by letting one conductance go to zero, giving a metal-insulator mixture. Alternatively, one component can have infinite conductivity. This is a classical model for a normal metal-superconductor composite.

In these cases, connected clusters of the high-conductance component become very important. It is not possible, for example, for a metal-insulator composite to conduct at all until a cluster of metallic links becomes infinite (for an infinite sample). The geometrical properties of clusters, and the transport properties of the two limiting problems, are studied in percolation theory, which has been extensively reviewed (Shante and Kirkpatrick 1971, Kirkpatrick 1973, Straley 1977, Kirkpatrick 1979).

The probability at which a cluster first becomes infinite is the

percolation threshold, p_c. Near p_c, the mean cluster size S diverges as a simple power law

$$S \propto \ell |p-p_c|^{-\gamma} \tag{5.6}$$

where ℓ is the size of a single bond.

If p denotes the probability that conducting links g are present against an insulating background, the bulk conductance of a lattice of size $L>>\ell$ is given by

$$G \propto g(L/\ell)^{d-2}(p-p_c)^t \tag{5.7}$$

for a small region above p_c. Similarly, if superconducting links are present with probability p in a lattice of resistors r, the bulk resistance varies as

$$R \propto r(L/\ell)^{2-d}(p_c-p)^s \tag{5.8}$$

for a small region below p_c. In (5.7) and (5.8), d is the dimensionality of the system. Although p_c depends on the type of

lattice studied (Shante and Kirkpatrick 1971), the critical exponents ν, t and s seem to depend mostly on the dimensionality of the system. This is true because the structure of very large clusters is not strongly dependent on the type of lattice.

The voltages and currents in any network must satisfy Kirchoff's laws. The voltage drop around a loop must equal the applied EMF in the loop, and the net current into a node must equal zero. Two networks which satisfy the same set of equations, but with currents and voltages interchanged, are duals of each other. The duality transformation interchanges loops and nodes, resistances and conductances, and currents and voltages. Since square lattices are self-dual, it can be shown by duality that, for square lattices, the R vs. p and G vs. 1-p curves have the same shape, and thus that $p_c=1/2$ and that s=t (Straley 1977, Bernasconi et al. 1977, Bernasconi 1978). Most of the remainder of this chapter deals with two dimensional conductor-insulator problems, following the convention of the literature. The duality relationship allows any results obtained in this way to be related to the superconductor-conductor case by replacing conductances with resistances in graphs and equations. We also restrict ourselves to two dimensions, although many of the qualitative results are easily extended to three dimensions.

5.2 General Methods of Solution

We will outline various approximate methods for finding the conductance of random lattices in this section. For concreteness, we

consider a square isotropic lattice, where a fraction p of the bonds are conducting.

A. Effective Medium Theory

The effective medium theory (EMT) constructs a lattice from conductances G_e such that the average effect of replacing a single bond by a conductance g or 0 is zero (Kirkpatrick 1973). For a square lattice, the results are

$$G_e=0 \qquad p<1/2 \qquad (5.9a)$$

$$G_e=g(2p-1) \qquad p>1/2 \qquad (5.9b)$$

Comparing this result to (5.7), we see that the EMT predicts that $p_c=1/2$ (correctly, if coincidentally) and that s=t=1.

B. Numerical Methods

A brute force approach to the problem is to generate large random lattices on a computer and to solve the Kirchoff equation (5.4) at each vertex. This is difficult to do for large lattices, so an iterative scheme is usually employed (Kirkpatrick 1973). An initial guess is made for all of the voltages, then a computer is used to relax the

inverted form of (5.4):

$$V_i^{(n+1)} = \left(\sum_{j<i} g_{ij} V_j^{(n+1)} + \sum_{j>i} g_{ij} V_j^{(n)} \right) / \sum_j g_{ij} \qquad (5.10)$$

The superscripts refer to the iteration number and the sums use the most recent available value for V_i. Different weights can be given to the terms to speed up convergence (Webman et al. 1975).

C. Renormalization Group

A powerful technique, the renormalization group, has recently been borrowed from the theory of critical phenomenon and applied to the percolation problem (Young and Stinchcombe 1975, Stinchcombe and Watson 1976). This technique allows one to calculate R and G as well as the critical exponents and percolation threshold. Here we will discuss the real space renormalization procedure of Reynolds et al. (1978,1980) and Bernasconi (1978).

Consider a diluted lattice of unit conductors with $p \neq p_c$. The lattice is divided into cells of size $\ell' = b\ell$ (see figure 5.1). The conductance of each cell in a given direction is calculated by imposing equipotentials on the faces perpendicular to that direction. Each cell is then replaced by its conductances in the two directions.

We have thus changed the lattice constant from ℓ to $b\ell$, the conductance distribution from

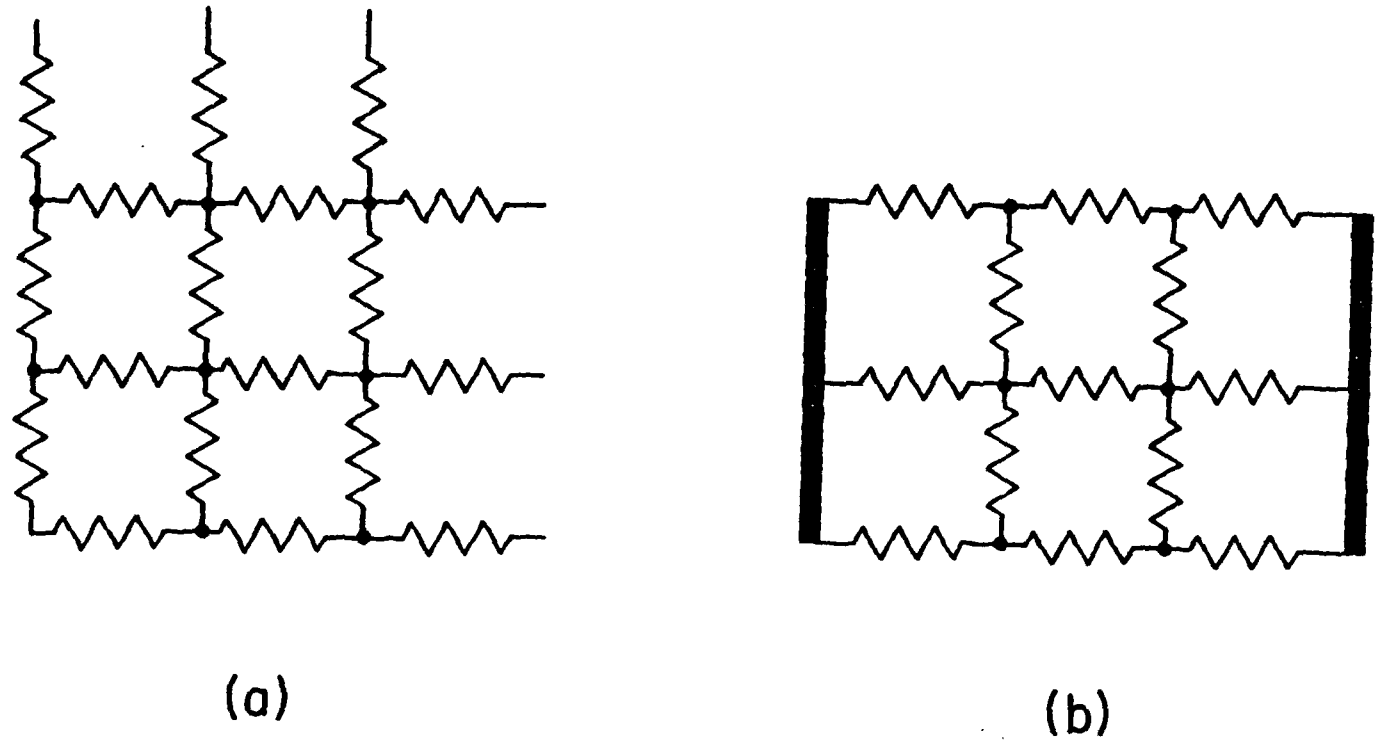

Figure 5.1 Cell used for the b=3 RG transformation (a). Rescaled probability is the probability of getting from left to right. For calculating rescaled conductance, equipotentials are imposed on the left and right, as in (b).

$$\tilde{P}(\ell,p) = (1-p)\,\delta(g)+p\,\delta(g-1) \tag{5.11}$$

to

$$\tilde{P}(\ell',p') = (1-p')\,\delta(g)+p'P(\ell',p',g) \tag{5.12}$$

and p to p'. The quantity p' is determined by counting the fraction of cells which conduct in a chosen direction. $P(\ell',p',g)$ is a sum of weighted delta functions corresponding to the possible conductances g of a cell of size $b\ell$. The basic approximation is that the new lattice is assumed to have the same bulk properties as the original lattice.

This decimation process is repeated, generating a sequence of lattices with spacing $b\ell$, $b^2\ell$, ...$b^n\ell$. Ultimately, the distribution of conductances approaches a single delta function centered at $\hat{G}$, and $p^{(n)}$ approaches either 0 or 1. When $p^{(n)}$ approaches 1, the original p is assumed to have been greater than p_c; when $p^{(n)}$ approaches 0, p is assumed to have been less than p_c. Since a lattice with all links equal to $\hat{G}$ has a conductance $\hat{G}$ in two dimensions, $\hat{G}$ is an approximation for G in two dimensions.

This procedure is accurate insofar as lines a distance $b\ell$ apart have a constant potential difference between them. This is true for

all b as p approaches 1 and for all p as b approaches infinity. Bernasconi's (1978) isotropic lattice results indicate that this procedure is a good approximation for all p with b equal to 2, indicating that compensating errors probably occur.

A further computational simplification results when $P(\ell',p',g)$ is replaced by a single delta function at the mean of $P(\ell',p',g)$ (Bernasconi 1978). This method is very accurate for isotropic lattices if the geometric mean is used (Bernasconi 1978).

The procedure is slightly different at the percolation threshold. At this point, $p=p'=p''=\ldots p^{(n)}$. For the cells used here, this is true at $p=1/2$ for all b, correctly predicting the value of p_c for the square lattice. Repeating the transformation at p_c eventually results in only a change of scale in $P(\ell^{(n)},p^{(n)},g)$. The relations (5.6) and (5.7) apply in a lattice both before and after a re-scaling, that is, $\xi=\xi'$ and $G=G'$ (renormalizing does not change bulk properties). For n large,

$$\xi \propto \ell^{(n)}(p^{(n)}-p_c)^{-\nu} = \ell^{(n+1)}(p^{(n+1)}-p_c)^{-\nu} \qquad (5.13a)$$

$$G \propto g^{(n)}(L/\ell^{(n)})^{d-2}(p^{(n)}-p_c)^{t} = g^{(n+1)}(L/\ell^{(n+1)})^{d-2}(p^{(n+1)}-p_c)^{t} \qquad (5.13b)$$

Using $b=\ell'/\ell$ and solving these equations for ν and t/ν gives

$$\nu = \log(b)/\log(\partial p'/\partial p)_{p_c} \qquad (5.13c)$$

$$t/\nu = \log(b^{d-2} g^{(n)}/g^{(n+1)})/\log(b) \qquad (5.13d)$$

where $g^{(n)}$ is any conductance characterizing $P(\ell^{(n)}, p_c, g)$ such as the mean conductance. We see that ν comes out of the RG directly, and t/ν can be estimated by extrapolating a sequence to $1/n=0$ (Bernasconi 1978).

The renormalization group approach is thus seen to give estimates of the critical parameters via (5.13), as well as giving bulk conductance as a function of p.

5.3 Anisotropic Networks

We will study anisotropic square resistor networks in this section, using the techniques outlined in the previous section. A solution for the perfect (p=1) anisotropic network is given, from which an effective medium theory is developed. (This work was done independently of Bernasconi (1974).) We also present numerical simulations and renormalization group calculations for this problem. The results of all three methods are discussed and compared, and they are also compared to experiments on an anisotropic conductor-insulator model system (Smith and Lobb 1979).

A. Effective Medium Theory

Consider a uniform square lattice of conductors, having conductance G if they are parallel to the x-axis and AG if they are parallel to the y-axis. G and AG are the (as yet) unknown bulk conductances as calculated by the EMT. If a current i_o is injected at the origin, Kirchoff's law requires the voltage at a site (m,n) to satisfy

$$G(V(m+1,n)+V(m-1,n)-2V(m,n))+$$
$$AG(V(m,n+1)+V(m,n-1)-2V(m,n)) = -i_o \delta_m \delta_n \qquad (5.14)$$

where δ_m is the Kronecker delta function. We have solved this problem by Laplace transforms. The isotropic lattice has been discussed in van der Pol and Bremmer (1950). We have generalized their approach to include anisotropy in the conductances. The inversion integral can be written in the form

$$V(m,n)=(4\pi)^{-2}\int_0^{\pi}\int_0^{\pi} ds_1 ds_2 \frac{\cos(s_1 m)\cos(s_2 n) - 1}{\sin^2(s_1/2)+A\sin^2(s_2/2)} \qquad (5.15)$$

where we have normalized so that the voltage at the origin is zero.

Equation (5.15) can be evaluated for (m,n)=(0,0), (0,1) and (1,0).

The results are

$$V(0,0)=0 \tag{5.16a}$$

$$V(1,0)=-(i_0/\pi G)\tan^{-1}(1/A)^{1/2} \tag{5.16b}$$

$$V(0,1)=-(i_0/\pi AG)\tan^{-1}(A)^{1/2} \tag{5.16c}$$

These results reduce to the proper limits $V(1,0)=V(0,1)= -i_0/4G$ for A=1 (the isotropic lattice) and $V(1,0)=-i_0/2G$ for A=0 (the one-dimensional limit).

Equation (5.16b) says that the current flowing between (0,0) and (0,1) is $(i_0/\pi)\tan^{-1}(1/A)^{1/2}$ when i_0 is injected at the origin. If we had extracted i_0 at (0,1) instead, the same current would have flowed between the two points.

If we superpose these two problems, the result is i_0 injected at the origin and removed at (0,1), with $(2i_0/\pi)\tan^{-1}(1/A)^{1/2}$ flowing through the conductance G. Thus, the voltage between (0,0) and (0,1) is $(2i_0/\pi G)\tan^{-1}(1/A)^{1/2}$. The total conductance between the two points is i_0 divided by this voltage. This conductance is a parallel combination of the direct link, G, and the conductance of all other paths, G'_x(see figure 5.2). Using the identity $\tan^{-1}(x)+\tan^{-1}(1/x)=\pi/2$, we obtain

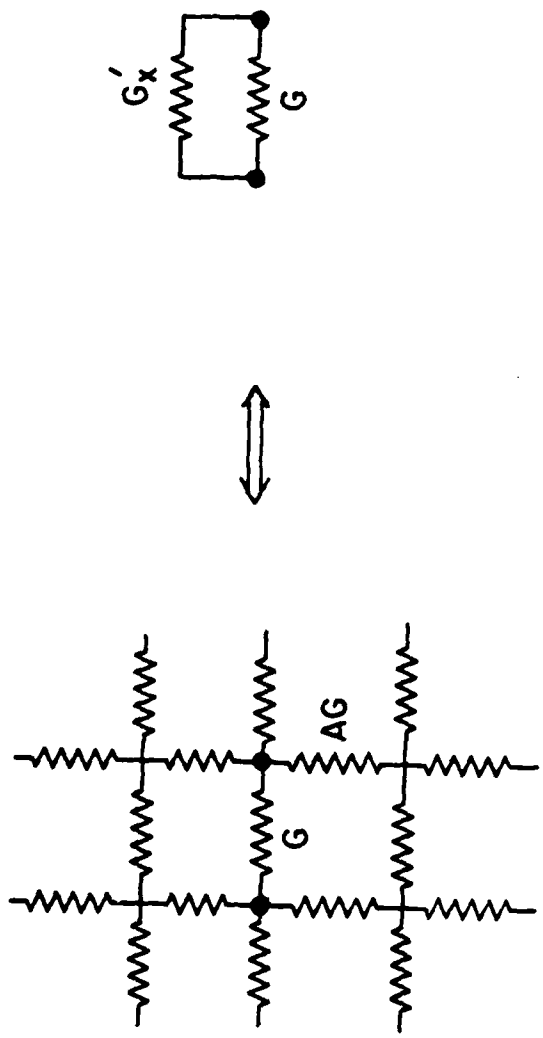

Figure 5.2 The conductance of the perfect (p=1) anisotropic lattice between the two points is equivalent to a parallel combination of G (representing the direct link) and G'_x (representing all other paths.)

$$G'_x = G\tan^{-1}(A)^{1/2}/\tan^{-1}(1/A)^{1/2} \equiv Gf(A) \quad . \quad (5.17a)$$

Similarly,

$$G'_y = AG\tan^{-1}(1/A)^{1/2}/\tan^{-1}(A)^{1/2} \equiv AG/f(A) \quad . \quad (5.17b)$$

To construct an effective medium theory, we consider a conductor g_i replacing one of the G's in an otherwise uniform lattice (see figure 5.3). We require the average voltage drop across the g_i's (which occur with probability p_i) to equal the voltage drop across a G in the uniform lattice. Thus

$$\sum_i p_i/(g_i+G'_x) = 1/(G+G'_x) \quad . \quad (5.18a)$$

The same argument in the y-direction gives

$$\sum_i p_i/(\alpha g_i+G'_y) = 1/(AG+G'_y) \quad . \quad (5.18b)$$

For the conductor-insulator case which we discuss here, (5.17) and

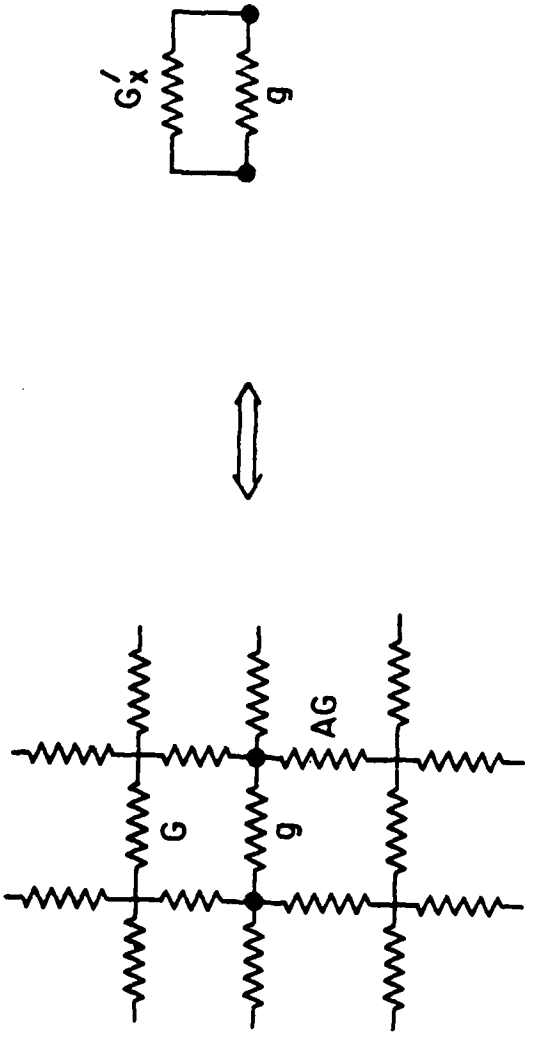

Figure 5.3 Circuit used to construct the EMT

(5.18) combine to give

$$(p+(p-1)/f(A))g = G \tag{5.19a}$$

$$(p+(p-1)f(A))\alpha g = AG \tag{5.19b}$$

where conductors $g_x=g$ and $g_y=\alpha g$ are present with probability p, and the lattice has bulk conductances G and AG in the x and y directions. When $\alpha=A=1$, these equations reduce to the familiar isotropic EMT of (5.9a) and (5.9b) (Kirkpatrick 1973).

Combining (5.19a) and (5.19b) to eliminate G gives the following equation for the dependence of A on α and p

$$\tan^{-1}(A)^{1/2}/\tan^{-1}(1/A)^{1/2} = \left\{(\alpha-A)p+\left[(\alpha-A)^2p^2+4(1-p)^2\alpha A\right]^{1/2}\right\}/2(1-p)\alpha \tag{5.20}$$

A is thus implicitly determined for a given p and α and can be substituted back into (5.19) to give G.

A number of interesting limits can be solved explicitly. When p approaches 1, (5.19) imply that A approaches α. The slope of the G vs. p curve at p=1 is thus given by

$$(\partial G(\alpha,p)/\partial p)_{p=1} = (1+1/f(a))g \qquad (5.21)$$

a result similar to that obtained in the continuum EMT (Davidson and Tinkham 1976).

The probability for which G=0 can also be obtained explicitly. Equations (5.19) imply that G=0 and A=1 when p=1/2, independently of α. This can also be seen by substituting p=1/2 into (5.20), which gives A=1. This effective medium theory predicts that p_c=1/2 regardless of the "microscopic" anisotropy α, and that the bulk conductance becomes isotropic (A approaches 1) as p approaches 1/2. This is in contrast to the continuum EMT, which gives the unphysical result that the critical area fraction f_c depends on the degree of anisotropy (Davidson and Tinkham 1976).

The results of solving (5.19) numerically are shown in figure 5.4. As expected, decreasing the y-direction conductance decreases G, making the network look increasingly 1-dimensional, that is G=0 unless p=1.

B. Numerical Simulations

We have done relaxation calculations on random fifty by fifty site arrays for a number of anisotropies. These arrays had equipotentials imposed on the left and right, and periodic boundary conditions on the top and bottom. Overrelaxation of (5.10) was used, as advocated by Webman et al. (1975). Lattices were solved by removing a few resistors, relaxing the voltages, and repeating the process until the

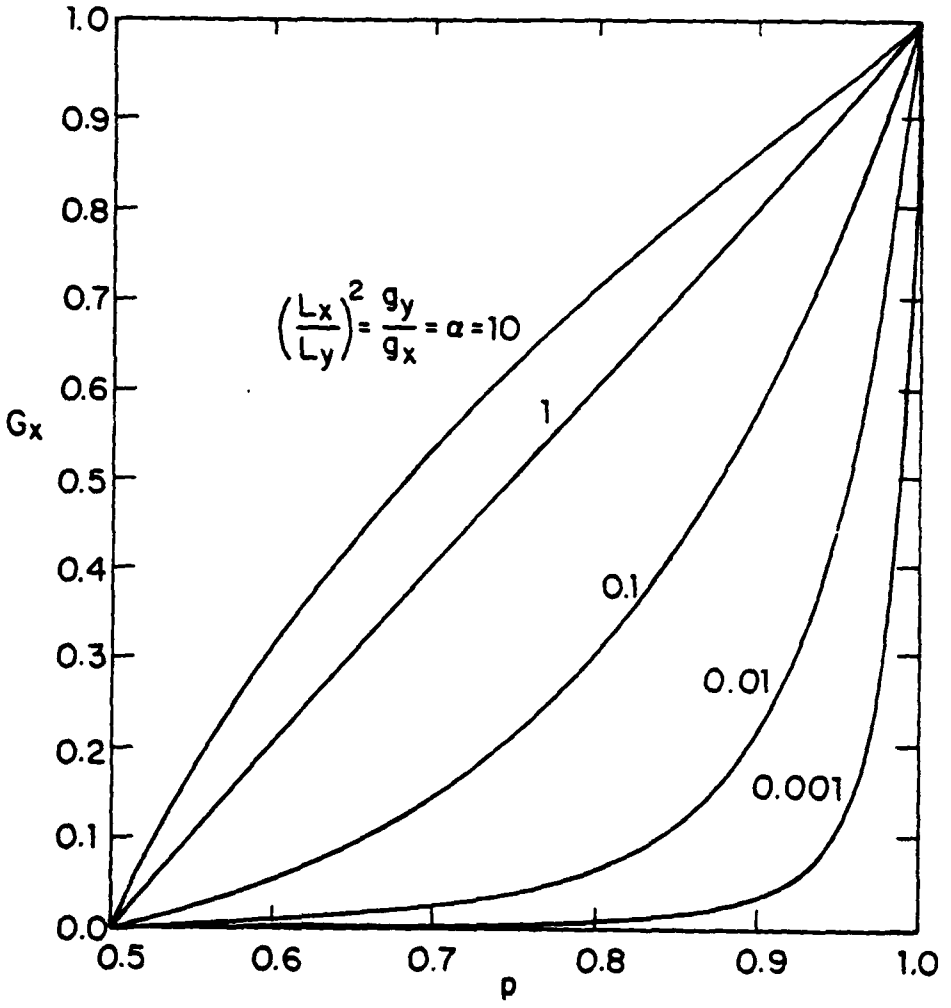

Figure 5.4 EMT conductance vs. concentration for various values of the anisotropy α.

desired value of p was reached. Close to the percolation threshold, the "insulating" elements were started out with a conductivity equal to that of the conducting elements. The network was solved in steps by gradually decreasing the conductance of the "insulating" elements. Convergence was slow near the percolation threshold, even using a fairly large computer, a DEC-10. The results of these calculations are compared to the EMT and RG in figures (5.5)-(5.7) for α=1,10, and 0.1. These results will be discussed in the next section.

C. Renormalization Group

Consider an infinite square lattice of lattice spacing ℓ, where the conductances between nearest neighbor sites are chosen at random, such that

$$\begin{aligned} g_x &= 1 \qquad \text{with probability } p \\ g_x &= 0 \qquad \text{with probability } 1-p \end{aligned} \tag{5.22a}$$

$$\begin{aligned} g_y &= \alpha \qquad \text{with probability } p \\ g_y &= 0 \qquad \text{with probability } 1-p \end{aligned} \tag{5.22b}$$

The microscopic anisotropy α ranges between 0 and ∞. The bond probability p is taken to be the same in both directions, so that the percolation threshold and coherence length are independent of α (Redner

and Stanley 1979).

Following the scheme outlined in section 5.2C, we rescale by partitioning the lattice into cells of size bℓ and replacing each cell by a single conductance in each direction. In principle, this transformation is repeatedly applied to the lattice, giving a sequence of conductance distributions which eventually converges to a single delta function for each direction (provided $p \neq p_c$ initially). These delta functions are centered at conductances $\hat{G}_x$ and $\hat{G}_y$. These conductances are only approximations to the lattice conductivity in the two directions because b is finite. In practice, we use an approximation to $\hat{G}$ which replaces each intermediate distribution of conductances by a simple double valued distribution. All of the non-zero conductances in the distribution are replaced by a single conductance which is the geometric mean of the non-zero conductances. This process eventually converges to conductances which are labeled $\hat{G}_{xapprox}$ and $\hat{G}_{yapprox}$.

Data for a number of anisotropies are presented in figures 5.5, 5.6 and 5.7 using G_{approx} for the b=3 transformation. (We compared $\hat{G}_{approx}$ to $\hat{G}$ for a number of these points and concluded that they are essentially equal for the range of anisotropies considered here.) The data are plotted with the EMT and our numerical results.

For the isotropic case, it has been noted that the EMT, numerical simulations and the renormalization transformations give essentially the same results near p=1 (Bernasconi 1978). In the region where the EMT breaks down, the b=2 transformation has been studied and agrees well with numerical simulations (Bernasconi 1978).

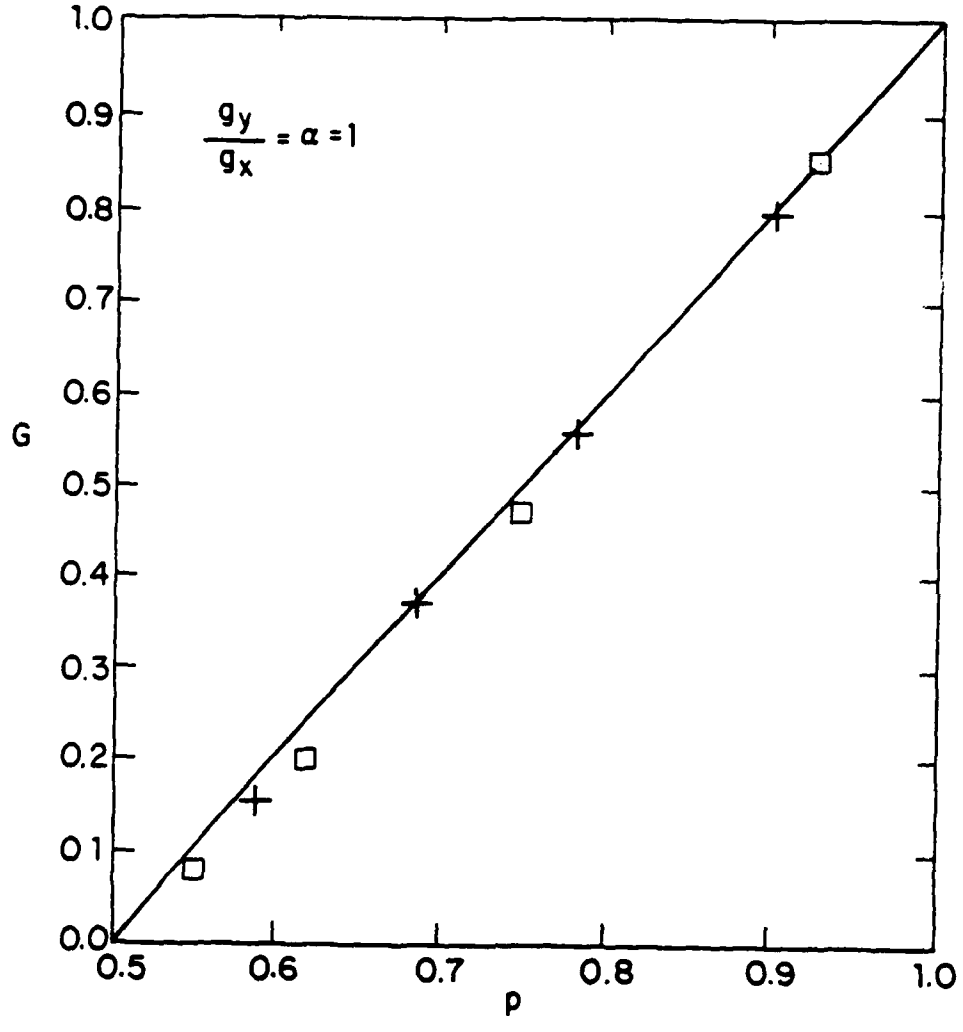

Figure 5.5 Conductance vs. concentration for $\alpha=1$ from the EMT (solid curve), numerical simulation (+) and the RG (□).

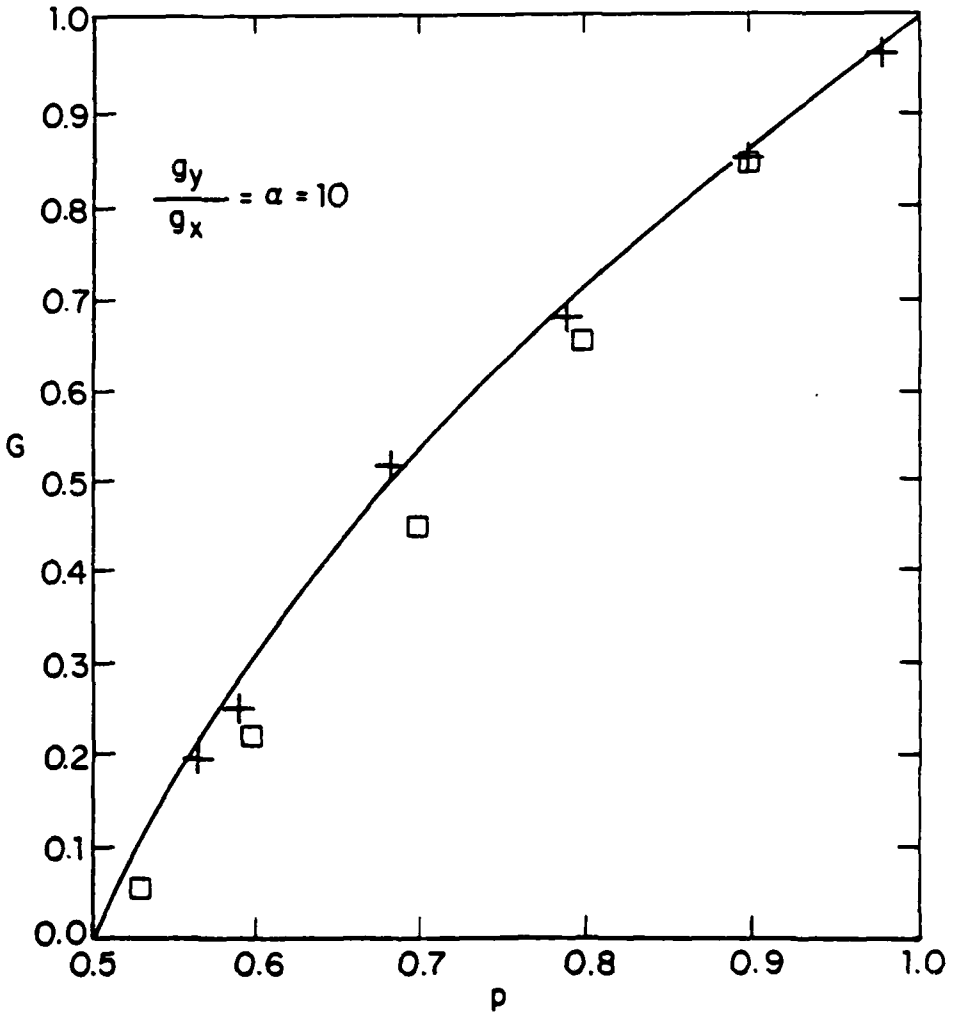

Figure 5.6 Conductance vs. concentration for α=10 from the EMT (solid curve), numerical simulation (+) and the RG (□).

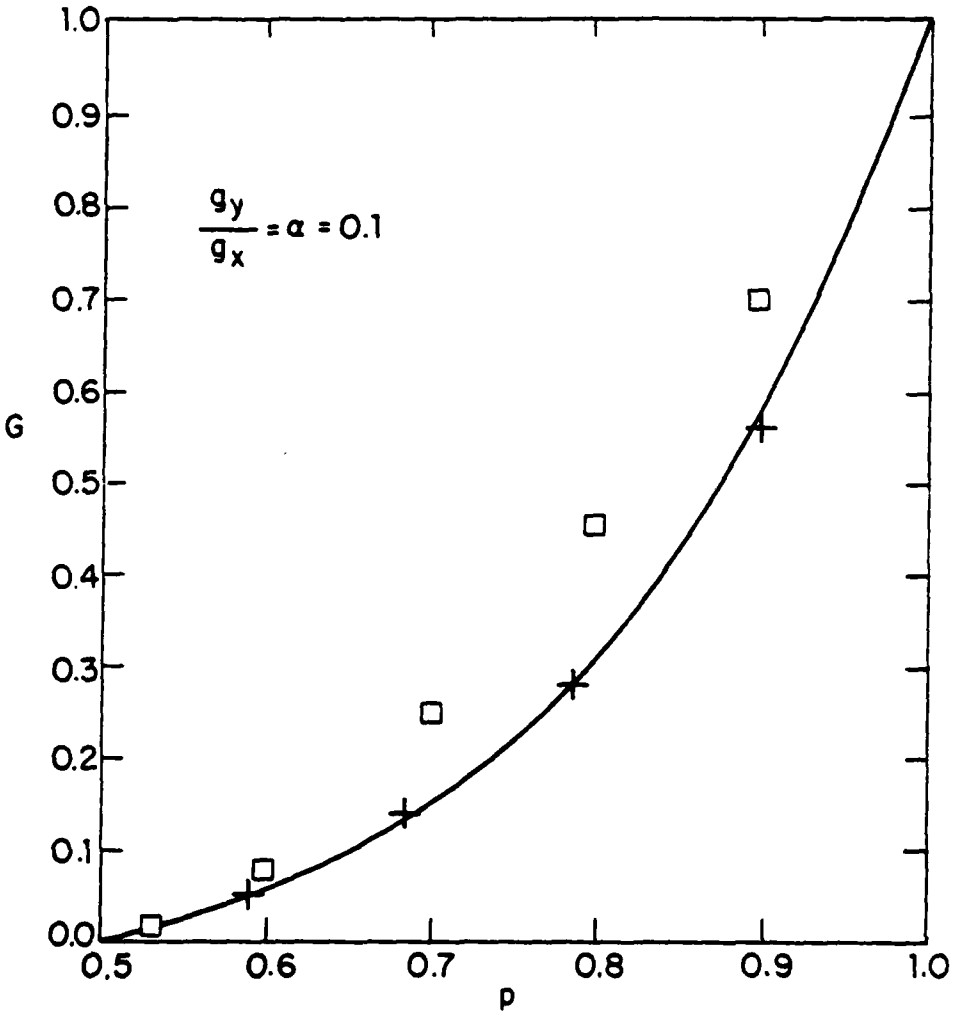

Figure 5.7 Conductance vs. concentration for α=0.1 from the EMT (solid curve), numerical simulation (+) and the RG (□).

For α=10 (figure 5.6), the EMT and numerical simulations agree well for p near 1. (The standard convergence problems and finite size effects make comparison difficult for p near p_c.) It is seen that the b=3 transformation underestimates the bulk conductance in this case.

When α=0.1 (figure 5.7), the EMT and numerical simulations agree outside the critical region. The disagrement with the RG, however, is quite pronounced (see figure 5.7). For this case, the RG overestimates the bulk conductance.

These discrepencies are easy to understand. For the b=3 transformation, only 4 of the 13 conductors in an x-direction cell have value αg, as compared to half of the conductors in the lattice itself (see figure 5.1). Thus, any effects due to varying α will be underestimated for a finite size cell transformation. For α=0.1, p=0.9, we obtain G=0.576 from the EMT and G$\simeq$0.56 from numerical simulations, while the b=2 RG predicts G=0.73 and the b=3 RG predicts G=0.69. Thus, the larger cell, which has a higher fraction of conductors pointing in the y-direction, gives an answer closer to the truth, although neither cell is very accurate.

It is tempting to try to find cells which deal with anisotropy more accurately. One could use cells in which the top row of conductors is not cut off, but this only increases the number of vertical conductors to 6 out of 18 (from 4 out of 13) for a b=3 cell. This also sacrifices the self dual symmetry of the cells, so that the wrong value of p_c is predicted. Other procedures, such as weighting the vertical conductors more heavily in the average, could probably be made to work, but suffer from being arbitrary.

In spite of the inaccuracies described above, the RG is a useful tool for studying the critical region. The method gives answers which are at least qualitatively reasonable, if not quantitively correct, and it is quite simple computationally. This last advantage is critical close to the percolation threshold, where the EMT breaks down, and numerical methods encounter serious difficulties as convergence slows down and sample to sample variations become large. Thus, the RG is the only choice presently available arbitrarily close to the percolation threshold. Hopefully, information obtained by it will be at least qualitatively correct.

For $0<\alpha<\infty$, it has been rigorously shown that, in the limit as p approaches p_c, the same critical exponent t characterizes systems which differ only in their anisotropy (Halperin 1979, Smith and Lobb 1979). This is true because the bulk conductance as a function of p is bounded above and below by the conductance of isotropic lattices where the non-zero conductances are either all 1 or all α (see figure 5.8). There is also some evidence for the stronger conjecture that the lattice conductance becomes isotropic as p approaches p_c (Shklovskii 1978). The renormalization group agrees with both of these results, predicting A approaches 1 as p approaches p_c. This is true because the sequence $\alpha^{(1)}, \alpha^{(2)}, \ldots, \alpha^{(n)}$ is found to approach 1 for α not equal to zero at $p=p_c=1/2$.

There are, however, significant differences between anisotropic and isotropic lattices, even near p_c. Figure 5.9 shows an effective critical exponent $\hat{t}(p)$, defined as $\partial \log(G_{approx.})/\partial \log(p-p_c)$ (Bernasconi 1978). As p approaches p_c, this approaches t, as can be

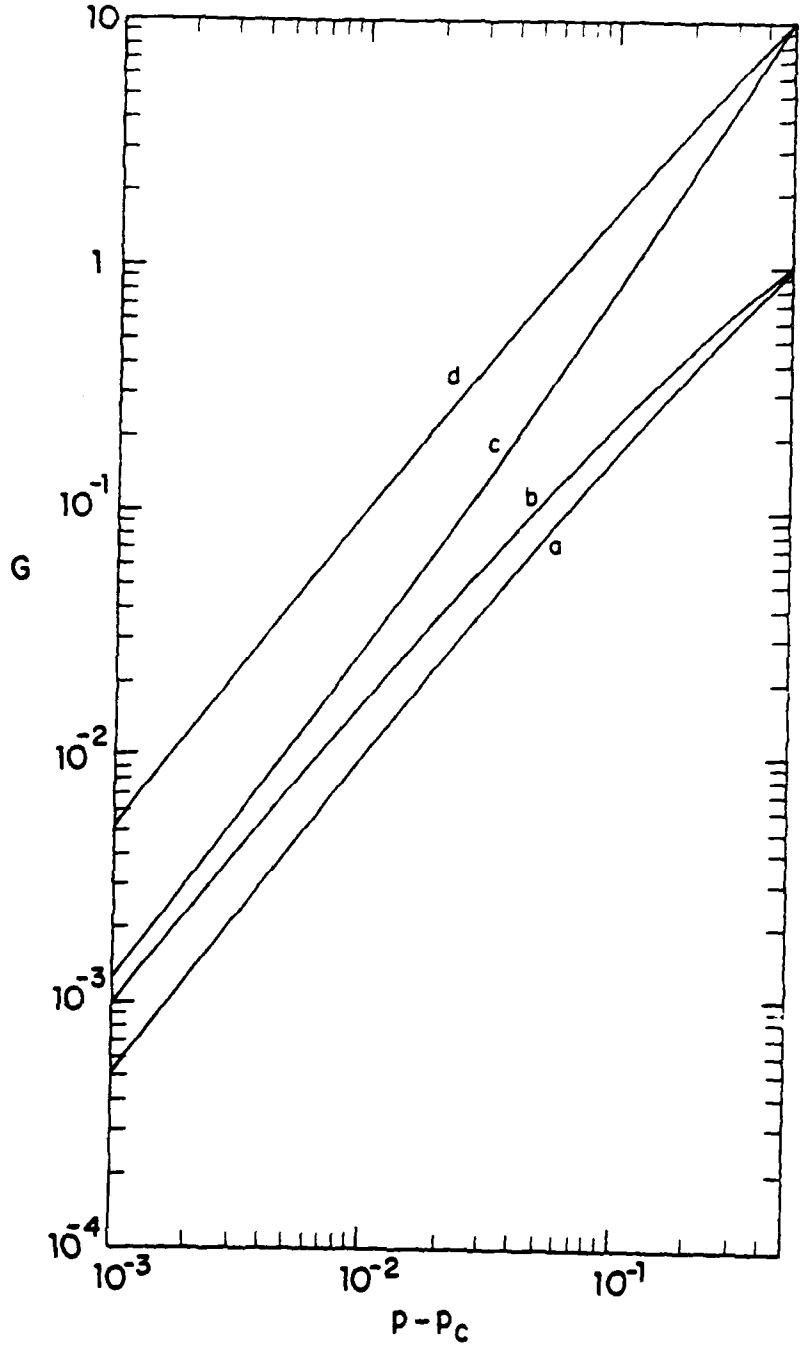

Figure 5.8 Conductance in the x-direction vs. concentration as calculated by the RG. (g_x, g_y) = (1,1), (1,10), (10,1), (10,10) for curves a-d.

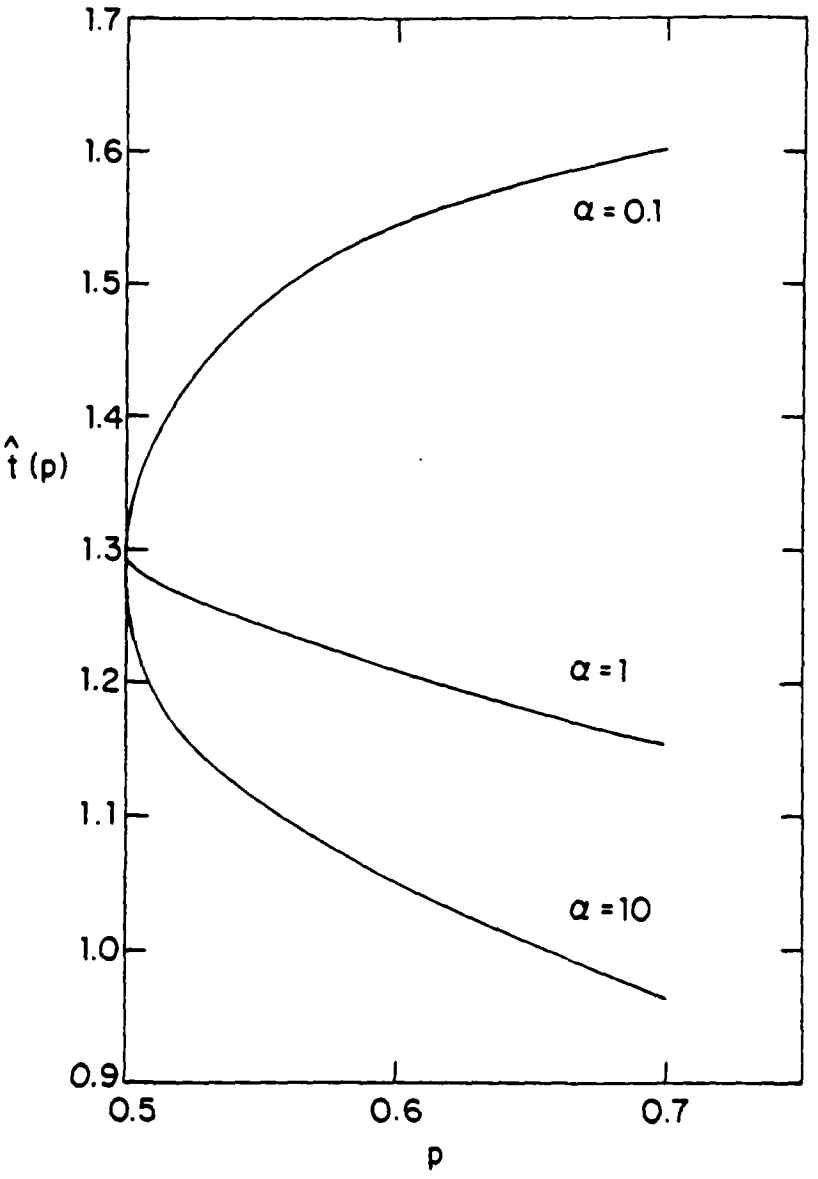

Figure 5.9 Effective exponent $\hat{t}$ (p) vs. p for various anisotropies α.

seen from (5.9). This quantity converges to t much faster as p approaches p_c for the isotropic lattice than for highly anisotropic ones. Thus, if we operationally define the critical region as the range of p over which $\hat{t}(p)$ is within a given percentage of t, the critical region shrinks as a result of anisotropy. Experimentally, this means that one needs to be closer to p_c to extract a good value of t from data on a highly anisotropic system than from data on an isotropic system.

We can use figure 5.8 to obtain a bound on the uncertainty in t. Since the conductance is bounded above and below, its logarithmic derivative $\hat{t}(p)$ can vary from t by roughly $\log(\alpha^{1/2})/\log(p-p_c)$. In fact, the data in figure 5.9 is well approximated by $\hat{t}(p)=1.29+0.4\log(\alpha^{1/2})/\log(p-p_c)$ for $\alpha=0.1$ and 10. For $\hat{t}(p)$ to be within 0.01 of t, this says that $(p-p_c)<\alpha^{\pm 20}$ (+ for $\alpha<1$, - for $\alpha>1$), which is a very stringent requirement.

D. Other Renormalization Schemes

A number of different lattice renormalization schemes have been used. Most of them differ from the one used here in that they calculate the conductance between two points in a lattice (Stinchcombe and Watson 1976) (see figure 5.10). Cells with equipotential boundaries, such as we use here, correctly predict that $A=\alpha$ at $p=1$. In contrast, the cell in figure 5.10 predicts $\alpha' = \alpha(\alpha+3)/(3\alpha+1)$ after one iteration at $p=1$, which incorrectly implies that $A=\alpha$ only for $\alpha=0,1$, or ∞ when $p=1$.

AD-A088 196 HARVARD UNIV CAMBRIDGE MA DIV OF APPLIED SCIENCES F/G 20/3
PERCOLATION AND ELECTRICAL CONDUCTION IN SUPERCONDUCTING COMPOS--ETC(U)
AUG 80 C J LOBB N00014-77-C-0085
UNCLASSIFIED TR-16 NL

2 OF 2
AD
A088196

END
DATE FILMED
9-80
DTIC

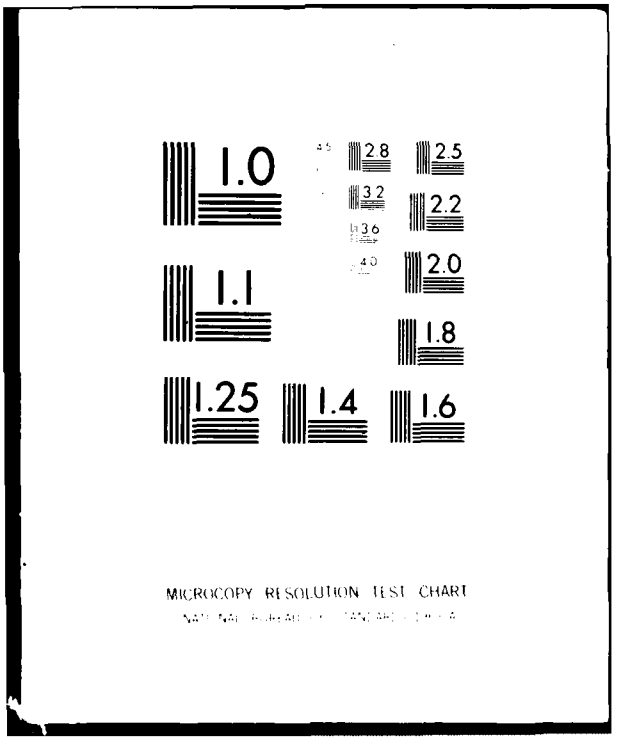
1.0
2.8
2.5
3.2
2.2
3.6
4.0
2.0
1.1
1.8
1.25
1.4
1.6
MICROCOPY RESOLUTION TEST CHART

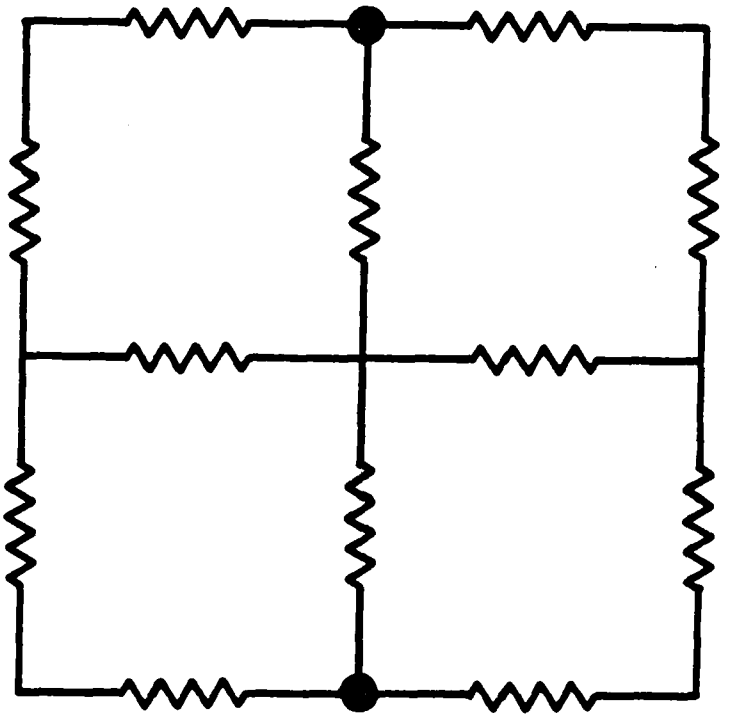

Figure 5.10 Alternative cell for RG calculations. The rescaled conductance is calculated between two points instead of between two equipotential lines.

E. Comparison with Experiments

If we apply the qualitative result summed up in figure 5.9 for a continuum superconductor-normal composite, we would expect $\hat{s}$, the measured value of s, to be larger than the isotropic value when the superconducting filaments are elongated. This agrees qualitatively with the results reported in chapter three (Lobb et al. 1978). Quantitative comparison is not possible, since we cannot convert from temperature to probability with any accuracy.

A system to which our model calculations apply more directly has recently been reported (Smith and Lobb 1979). The conductivities of percolative networks produced photolithographically from laser speckle patterns were measured. These results are shown in figure 5.11 for various aspect ratios of metal islands. The results of numerical simulations on a fifty by fifty site lattice for the corresponding α's are shown in the inset. The qualitative agreement is striking, demonstrating that the model outlined in section 5.1A is quite good. The experimental data is consistent with figure 5.9, in that the measured exponent depends on anisotropy if the critical region is assumed to be the same for all anisotropies. Fitting the speckle pattern data to 15% above the percolation threshold yields t= 0.85, 1.75, and 2.3 for α=25, 0.16 and 0.0016. Using t=1.3 and $\hat{t}(p)=t+0.4\log(\alpha^{1/2})/\log(f-f_c)$ as implied by the lattice model gives $\hat{t}(p)$=0.95, 1.48 and 1.97. The agreement is quite good considering the approximations made.

Figure 5.11 Normalized conductance vs. area fraction for anisotropic metal islands on an insulating substrate. The solid lines are to guide the eye. Inset contains numerical simulations on 50 by 50 site lattices with the cooresponding anisotropies. The aspect ratio of the islands L_x/L_y is equal to $\alpha^{1/2}$, as can be seen from (5.5). We note that the metal islands have an f_c of about 0.4, while the lattices have a p_c of 0.5.

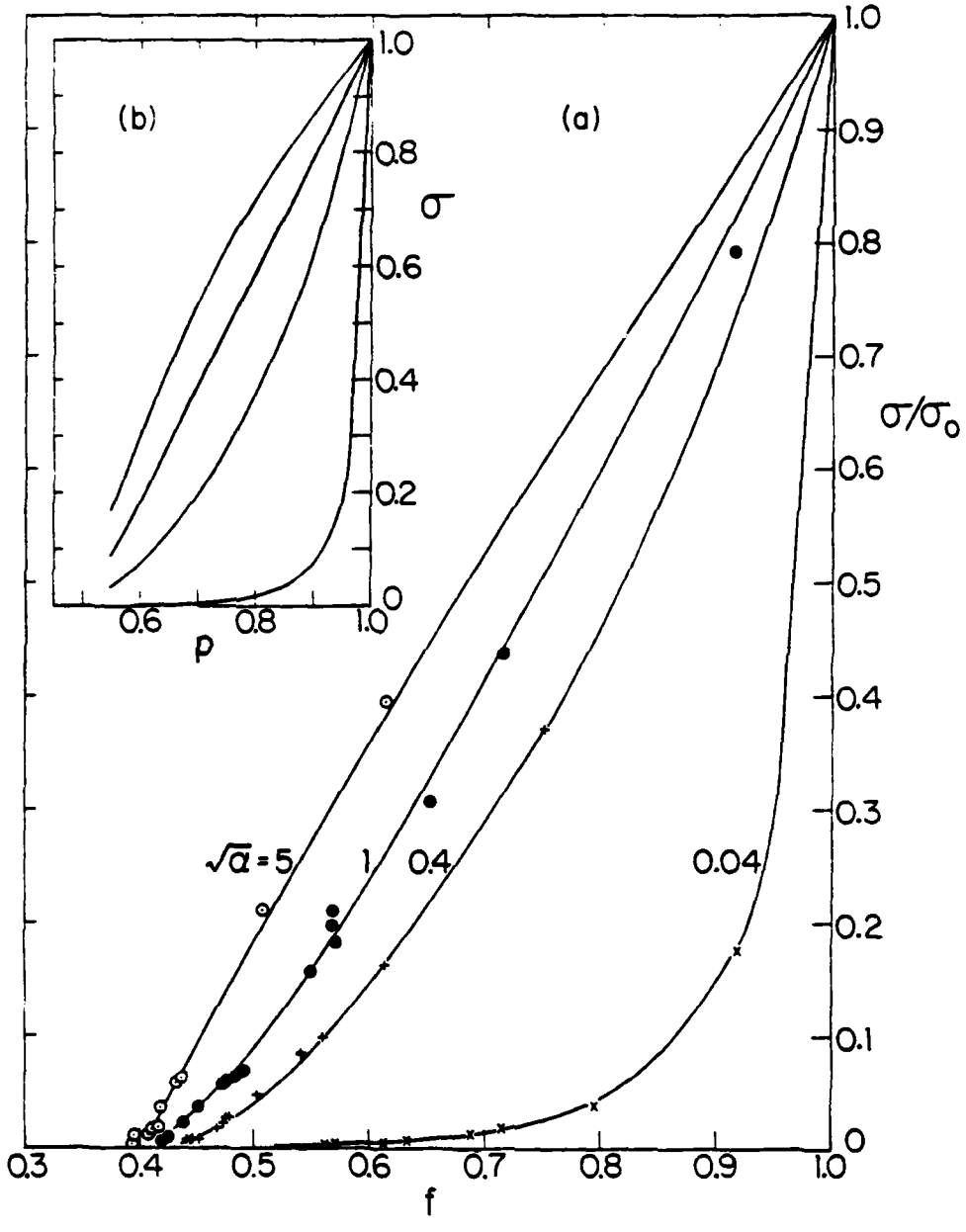
(b)
(a)
σ
p
σ/σ₀
f
√α = 5
1
0.4
0.04
0.3
0.4
0.5
0.6
0.7
0.8
0.9
1.0
0
0.2
0.4
0.6
0.8
1.0

The isotropic speckle pattern samples have roughly 450,000 units which are either conducting or non-conducting. This is much larger than any percolative system previously studied. We obtained $t \simeq 1.3$ for the isotropic samples, a result in good agreement with our calculations in the next section, but in poor agreement with earlier numerical results (Kirkpatrick 1973, Straley 1977).

5.4 Large Cell Renormalization Group Calculations of Critical Exponents

In the remaining sections of this chapter, we calculate the exponents ζ, s, and t (see (5.6) through (5.8)), and also calculate the critical exponent ν which characterizes the critical current behavior near the percolation threshold (Lobb and Frank 1979, 1980, Lobb and Karasek 1980).

The cluster size exponent ζ is known to within a few percent in two dimensions (Reynolds et al. 1978, 1980). We use the large cell approach first employed by Reynolds et al. (1978) on the site-diluted lattice to calculate ζ for the bond-diluted lattice. Our results agree with the results of Reynolds et al. (1978), supporting the notion of universality.

Earlier estimates for transport exponents s,t,and ν vary widely, falling in the range 1 (de Gennes 1976) to 1.43 (Fisch and Harris 1978). By studying lattice rescalings for various b's, we obtain more reliable estimates, concluding that the transport exponents equal ζ ($\simeq 1.35$) to within a few percent in two dimensions.

A. The Critical Exponent ν

In this section we apply a large cell renormalization group scheme to the bond percolation problem on a square lattice. This method was recently developed and applied to site percolation in two dimensions, where it yielded highly accurate results (Reynolds et al. 1978,1980). Generalizing the b=2 cell proposed by Reynolds et al. (1977) for bond percolation, we find the convergence in the bond problem to be much faster than in the site problem.

When a fraction of bonds p are present in an infinite lattice, we expect the mean cluster size to vary as$(p-p_c)^{-\nu}$, as in (5.6), where p_c =1/2 for the square lattice (Sykes and Essam 1964). If R(b,p) is the probability that a finite lattice with b bonds on a side is connected, Reynolds et al. (1978) have argued that

$$\log(\lambda(b)) = (1/\nu)\log(b)+\text{constant} \qquad (5.23)$$

where $\lambda(b)= \partial R(b,p)/\partial p\big|_{p^*}$, p* is defined by R(b,p*)=p* and R(b,p) is the probability of getting across the cell from left to right. Equation (5.23) is asymptotically true for large b. We note that, except for the additive constant, (5.23) is identical to (5.13a). The inclusion of the constant is suggested by arguments that (5.13a) should apply only for large b (Reynolds et al. 1978, 1980).

A cell of the type used here is shown in figure 5.1. It can be

shown by duality that $p^*=1/2$ independently of b for this type of cell (Bernasconi 1978). Thus, equation (5.23) and calculations on finite cells can be used to estimate ν.

R(b,p) has been calculated analytically and differentiated to give $\lambda(b)$ for b=2,3 (Reynolds et al. 1977, Bernasconi 1978). We have computed $\lambda(b)$ for b up to 95 using Monte Carlo methods, as follows.

The probability that a lattice of size b is connected is given by

$$R(b,p) = \sum_i p^n (1-p)^m \qquad (5.24)$$

where the sum is over all connected configurations and n_i and m_i are the number of bonds present and absent, respectively, in the i^{th} configuration. Differentiating this with respect to p, we obtain

$$\partial R/\partial p = \sum_i p^{n_i} (1-p)^{m_i} (n_i/p - m_i/(1-p)) \quad . \qquad (5.25a)$$

At p=1/2, this becomes

$$\lambda(b) = (1/2^N) \sum_i 2(n_i-m_i) \qquad (5.25b)$$

where $N=n_i+m_i$. If 2M Monte Carlo realizations are studied, M will be connected (within statistical uncertainties) at $p=p^*$, so that (5.25b) is approximated by

$$\lambda(b) = (1/M) \sum_{i=1}^{M} (n_i - m_i) \qquad (5.26)$$

where the sum is over the connected configurations.

The calculations were done on a DEC LSI-11/2, a small computer with 32k of core. Lattices were generated and studied using the cluster multi-labeling technique of Hoshen and Kopleman (1976), modified to fit the limited memory of our machine. Since we were concerned only with whether a given realization was connected, it was possible to re-number the clusters after a column was completed, dropping those clusters which had died out. Thus, the program requires only two arrays of size 2b and one of size b to be stored. Since $p^*=1/2$ is known exactly for these cells, it was not necessary to determine it numerically, which resulted in a further saving of computer time.

We can gain some understanding of when b is large enough for (5.23) to be valid by examining "one-shot" estimates of ζ,

$$\nu(b)_{\text{1-shot}} = \log(b)/\log(\lambda(b)) \quad . \qquad (5.27)$$

These numbers approach each other for b sufficiently large. Table 5.1 shows these estimates, the number of realizations considered, and the statistical uncertainty in each case. (The uncertainty represents one standard deviation from the mean of $\lambda(b)$.) These data demonstrate the quick convergence of the method. Within the statistical errors given, the values obtained are indistinguishable from one another for $b \geq 4$. This implies that (5.23) is valid even for small b in this problem, and that the additive constant in (5.23) is small. We believe that this rapid convergence is a result of the self-dual symmetry property of these cells, which they share with the lattice itself. For example, Reynolds *et al.* (1978) obtain $\nu(b)_{\text{1-shot}} = 1.47$ for the site problem when b=5, although their answers extrapolate to lower values.

We can improve on the one-shot approach by fitting all of the data to equation (5.23). As can be seen from the log(λ(b)) vs. log(b) plot of figure 5.12, the deviation from the expected straight line is small, even for small b. The fit yields

$$\nu = 1.343 \pm 0.017 \quad . \qquad (5.28)$$

Equation (5.23) is only true asymptotically. Therefore, in addition to statistical uncertainty, the quoted error spans values

b	$\nu_{1\text{-shot}}$	$\delta\nu_{1\text{-shot}}$	N
2	1.428	0	all
3	1.380	0	all
4	1.353	0.013	160,000
5	1.352	0.011	175,000
6	1.354	0.015	82,000
10	1.358	0.011	43,000
15	1.354	0.019	42,000
20	1.343	0.013	76,000
30	1.323	0.017	60,000
50	1.370	0.039	23,000
70	1.366	0.028	34,000
95	1.341	0.012	81,000

Table 5.1 "One-shot" values of ν for different length rescalings b. The uncertainty represents one RMS deviation from the mean, and N is the total number of configurations studied for each value of b.

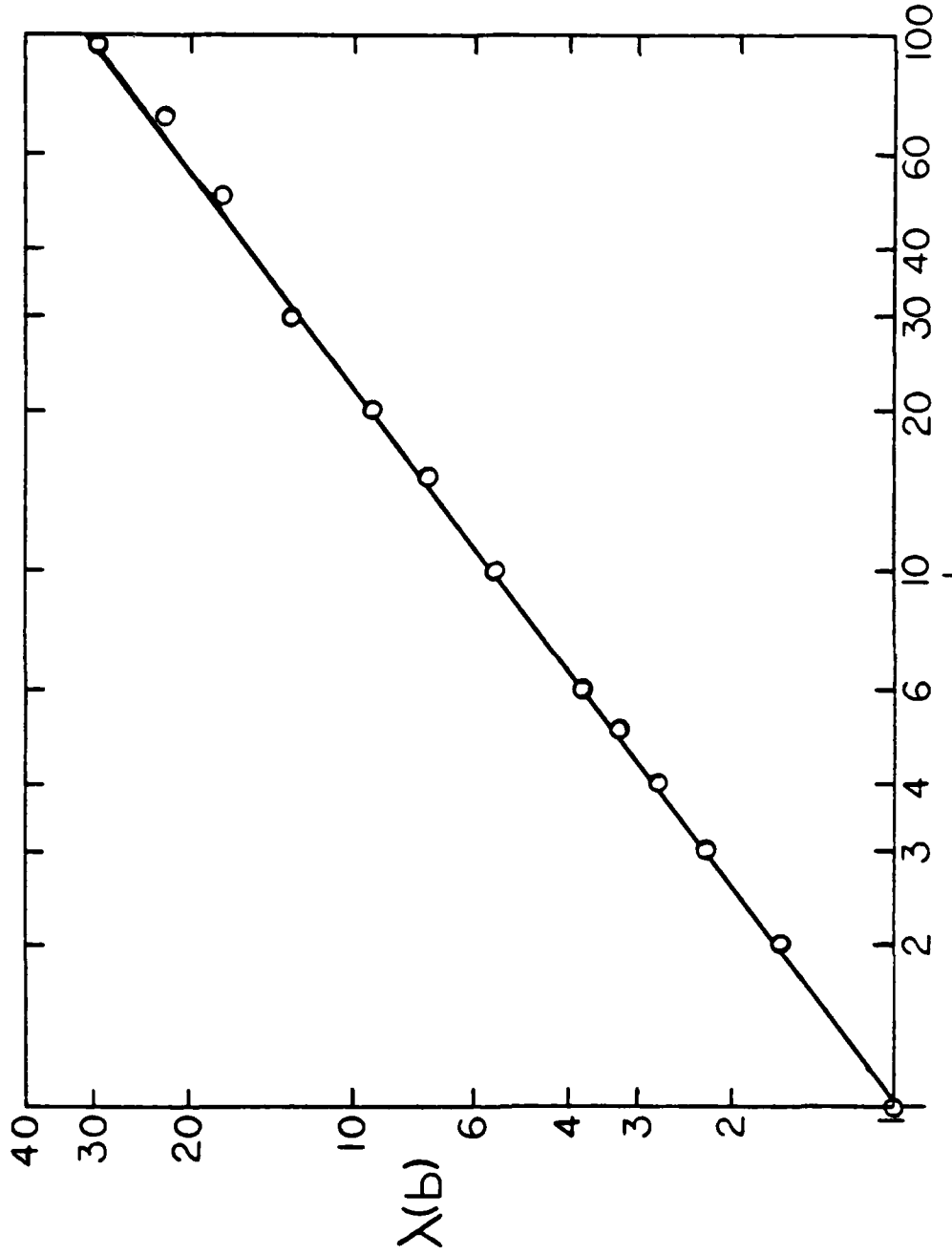

Figure 5.12 λ(b) vs. b on a log-log plot. The slope of this line is an estimate of 1/ν.

obtained by including or excluding some of the smaller points in the fit. This value for ν is slightly smaller than, but in good agreement with, the site percolation result $\nu=1.354\pm0.015$ (Reynolds et al. 1980). It is also in fair agreement with the value $\nu=1.365\pm0.015$ obtained by Kirkpatrick (1979) using large cells which were not self-dual.

B. The Critical Exponents s, t, and v

In this section, we use finite size scaling arguments to find how transport properties scale with sample size near the percolation threshold. We then estimate the critical exponents t and v for the bulk conductance and critical supercurrent density in a percolating square lattice.

Consider a square lattice of size L, with lattice spacing ℓ. Links are present with probability p. For calculating conductance properties, these links are taken to have unit resistance. To calculate critical current properties, the links are assigned a unit critical supercurrent.

The average conductance, $\langle G \rangle$, of a finite lattice is

$$\langle G \rangle = f(\epsilon, 1/b) \qquad (5.29)$$

where $\epsilon = p - p_c$ and average means any power-like mean, such as the n^{th}

root of the n^{th} power. We assume that f is a homogenous function of its variables (Straley 1977b)

$$f(\varepsilon, 1/b) = \beta f(\beta^{-x}\varepsilon, \beta^{-y}/b) \quad . \qquad (5.30)$$

(Phenomenologically, this assumption can be justified as follows. As a critical point is approached by varying a given parameter (such as $p-p_c$), measured properties (such as $\langle G \rangle$) often vary as a power of the parameter. As different parameters are varied, different power laws are observed. A homogeneous function approaches the origin with different powers along different axes. It is thus reasonable to represent $\langle G \rangle$ as a homogeneous function of $p-p_c$ and $1/b$, since critical behavior is expected for infinite samples as p approaches p_c.)

We wish to determine x and y. Letting $\varepsilon\beta^{-x}=1$ and taking b to infinity, we obtain

$$\langle G \rangle = \varepsilon^{1/x} f(1,0)\{1+ \mathcal{O}(\varepsilon^{-y/x}/b)) \quad . \qquad (5.31)$$

By letting $b=\infty$ and comparing this to (5.7), we see that $1/x=t$. Since $\xi \propto \varepsilon^{-\nu}$ is the only important length in this problem, we also identify $y/x=\nu$. Thus we see that

$$\langle G \rangle = \varepsilon^{t} f(1,0)(1+\mathcal{O}(\xi/L)) \qquad (5.32)$$

for large b and small ε.

Similarly, for $\beta^{-y}/b=1$ and ε approaching 0,

$$\langle G \rangle = b^{-t/\nu} f(0,1)(1+ (b^{1/\nu}\varepsilon)) \qquad (5.33)$$

so that the average conductance at $\varepsilon=0$ varies as $b^{-t/\nu}$ for large b.

To summarize,

$$G \sim (p-p_c)^{t} \qquad \text{(infinite sample)} \qquad (5.34a)$$

$$\langle G \rangle \sim b^{-t/\nu} \qquad \text{(when } p=p^*\text{)} \qquad (5.34b)$$

Similarly, the critical current density varies as

$$J_c \sim (p-p_c)^{\nu} \qquad \text{(infinite sample)} \qquad (5.35a)$$

which defines v, and

$$\langle J_c \rangle \sim b^{-v/\nu} \qquad \text{(when } p=p^*\text{)} \qquad (5.35b)$$

We can re-write (5.34b) and (5.35b) as

$$\log(1/\langle G \rangle) = (t/\nu)\log(b)+\text{constant} \qquad (5.36a)$$

$$\log(1/\langle J_c \rangle) = (v/\nu)\log(b)+\text{constant} \qquad (5.36b)$$

We can thus calculate the infinite sample exponents t and v by looking at the average behavior of large samples. We note the similarity between (5.36a) and (5.13b). As in the last section, we have gained an additive constant.

For b=2,3, we calculated arithmetic, geometric and harmonic means exactly, by going through all of the possible configurations. For larger cells, realizations were generated randomly and studied with the aid of a program designed to calculate the conductance of larger lattices exactly. To calculate the conductance of a given realization, this program removed dangling ends, reduced simple series and simple parallel combinations, and used the Y-Δ transformation (see figure 5.13a) until the cell was reduced to a single conductance. In the

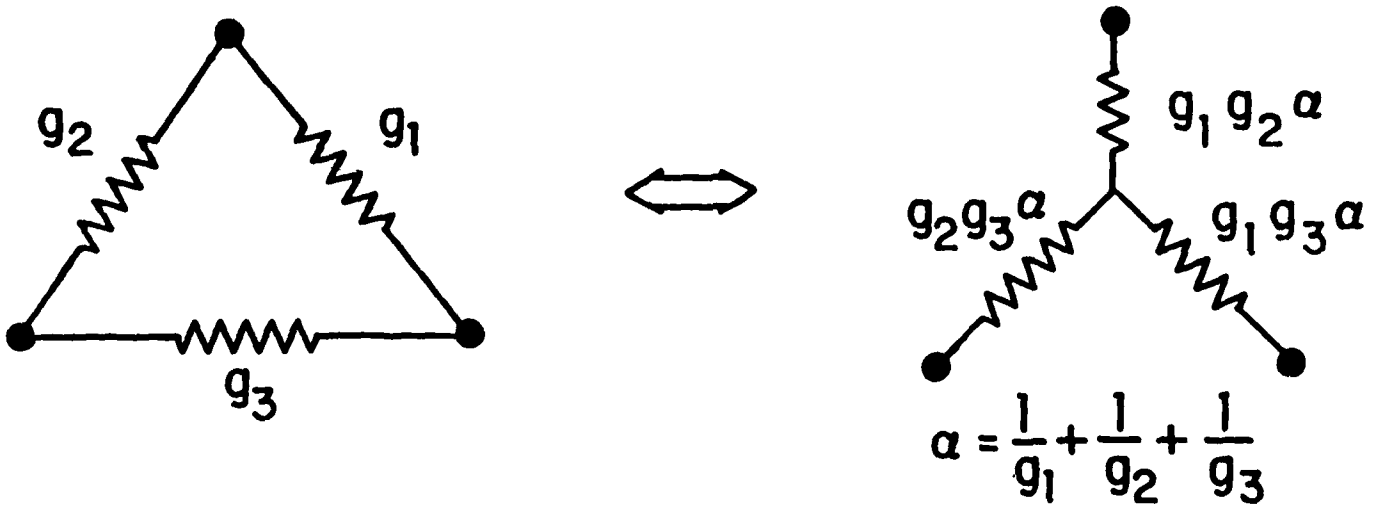

Figure 5.13a The y-Δ transformation for conductances.

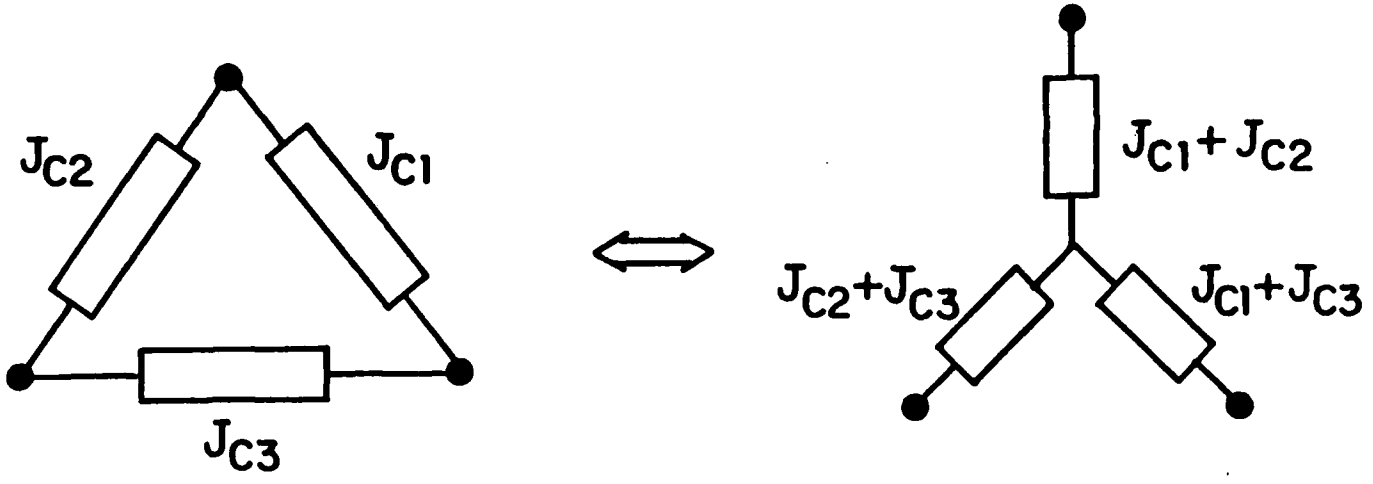

Figure 5.13b The Y-Δ transformation for critical currents.

largest cells considered, where b=14, the program failed to reduce only 0.5% of the 30,000 cases studied. This introduces a small known uncertainty into the estimate of <G> (Lobb and Frank 1979).

To calculate the critical current of a cell, we proceed in the same way, employing a rather simplified model. We assume that the critical current of a parallel arrangement is the sum of the individual critical currents, that the weakest link gives the critical current of a series arrangment, and hence Y-Δ transformations can be made as in figure 5.13b. Using this model, we have studied up to b=20, where only 28 out of 40,000 cases failed to reduce. In all cases, we calculated arithmetic, geometric and harmonic means of conductance and critical current density, as well as standard deviations, which give distribution widths.

Figures 5.14 and 5.15 are log-log plots of $1/\langle G\rangle$ and $1/\langle J_c\rangle$ vs. b, for various means. As (5.34b) and (5.35b) predict, the points on each graph fall onto straight parallel lines. The slopes of these lines imply that

$$t/\mathcal{J} = 0.996\pm0.01 \qquad (5.37a)$$

$$v/\mathcal{J} = 0.990\pm0.005 \qquad (5.37b)$$

The error bars include statistical uncertainties, as well as subjective estimates of error due to the differences between various

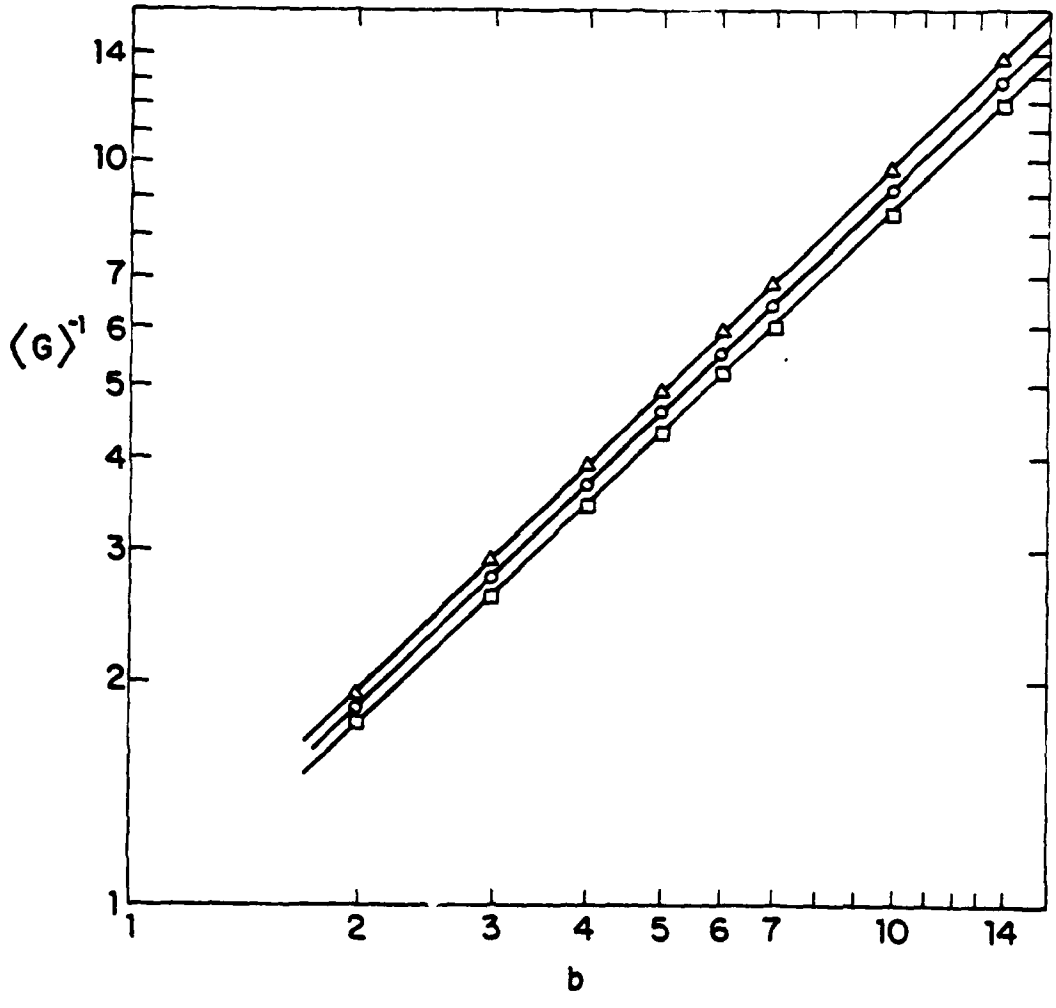

Figure 5.14 $\langle G \rangle^{-1}$ vs. b on a log-log plot. The slope of this line is an estimate of t/ν.

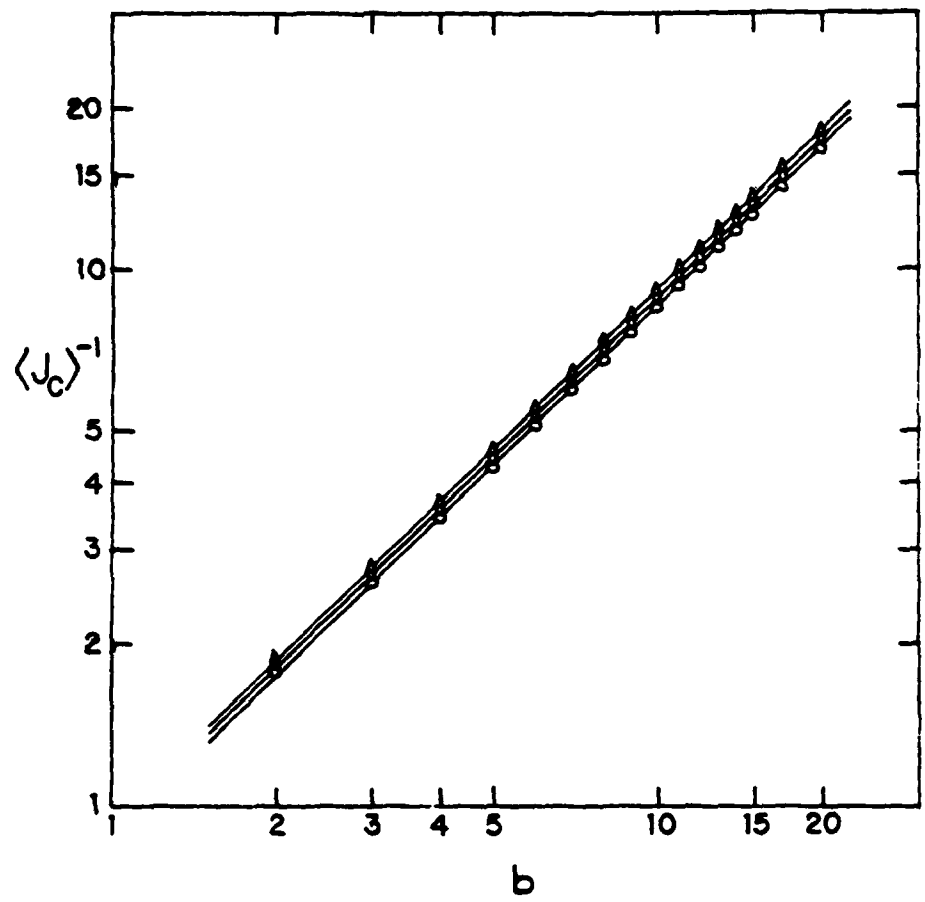

Figure 5.15 $< J_c >^{-1}$ vs. b on a log-log plot. The slope of this line is an estimate for ν/ν.

means and the effects of including or not including data for small b in the fit. We believe that these results are consistent with the hypothesis $t=\nu=\nu$ (Shklovskii 1978), as larger cells of this type tend to give higher estimates of t/ν (Bernasconi 1978, Lobb and Frank 1979) and ν/ν. Using the value $\nu=1.356\pm0.015$ (Reynolds et al. 1978), we obtain $t=1.35\pm0.02$ and $\nu=1.343\pm0.016$.

These results are applicable to different problems through the use of duality relations (Straley, 1977a). The dual of (5.34a) implies that $s=1.35$ in two dimensions. Similarly, the dielectric breakdown voltage of a metal-dielectric composite, which is dual to the critical current problem considered here, should also vary as $(p-p_c)^{1.35}$.

Alternate approaches to these problems have suggested that either $t=\nu=\nu$ (Shklovskii 1978) or that $t=\nu=1$ (de Gennes 1976, Huse and Guyer 1979). Our data are difficult to reconcile with the latter predictions, which imply that the slope of figures 5.14 and 5.15 should be $1/\nu=0.74$ instead of 1. Numerical simulations which seem to suggest $t=1.1$ (Straley 1977, Kirkpatrick 1973, 1979) have depended on varying p while keeping L fixed at a large value, as suggested by (5.34a). This method has the disadvantage of requiring increasingly larger lattices as p approaches p_c to keep fluctuations and the first order term in (5.32) small. As demonstrated by table 5.1 , our method converges to a good value for ν for fairly small b. This suggests that our results for t and v are trustworthy, even though we used cells only up to b=20.

As mentioned earlier in this chapter, the largest experimental system studied to date (Smith and Lobb 1979) gives $t\simeq1.3$, in reasonable agreement with our calculation. In addition, Deutscher and Rappaport

(1979) have measured ν for Pb-Ge films, obtaining $\nu=1.3\pm0.1$. This answer is in better agreement with our result than with the prediction $\nu=1$ (Huse and Guyer 1979).

CHAPTER SIX: SUMMARY AND CONCLUSIONS

In the preceding chapters, we have discussed a number of different research projects on the physics of inhomogeneous superconductors. These studies have ranged from measurements of the practical properties of superconducting *in situ* composite wires to theoretical work on random resistor lattices. In this final chapter we will review our results for each of the projects in turn and make suggestions for further work in each area.

Our work on Cu-V_3Ga *in situ* composites led to significant improvements in their properties. We were able to produce samples with T_c=15.5K and H_{C2}=22.4T (at 4.2K) comparable to bulk V_3Ga. Our critical current densities were also quite high, being $2x10^5 A/cm^2$ at 4T and $10^4 A/cm^2$ at 18T at 4.2K.

The *in situ* technique has not been optimized for V_3Ga. Variation of such parameters as annealing time and temperature, degree of reduction, and superconducting volume fraction should lead to further improvement. It would also be useful to add fourth elements to *in situ* composites, as additional elements sometimes raise the T_c of A-15 compounds.

In addition to being potentially useful, *in situ* composites are interesting in their own right. By observing the superconducting transition in a number of samples in which both the concentration of superconductor and the electron mean free path in the normal metal were varied, we helped to settle the early controversy over the conduction mechanism in these materials. Geometrical percolation and the proximity effect are *both* necessary to understand the superconductivity

of these composites. In general, the proximity effect is more important in lower concentration samples with clean matrices, with geometrical percolation being important when the proximity effect is weak.

Our simple model for the temperature dependence of the superconducting to normal transition, while being incorrect in detail, did correctly recognize that a phase transition occurs as the proximity effect reduces the overall resistance of a sample to zero. Quantitative comparison of our data to more rigorous models for the transition has been difficult because of the geometrical anisotropy of the samples. Work on isotropic composites with simpler phase diagrams such as Ge-Pb and Cu-Pb should lead to improved understanding while making quantitive comparison with theory possible.

Theoretical models for the phase transition predict a number of interesting effects in two-dimensional samples. This led us to prepare thin films consisting of PbBi islands coated with a thin layer of CuAl. Our measurements on systems with the PbBi near the percolation threshold have shown behavior qualitively similar to three dimensional samples.

Future work should exploit the fact that the interisland superconducting phase coupling can be varied by changing the thickness of the PbBi and CuAl layers. It is also possible to make regular arrays of weakly coupled superconductors in two dimensions. Comparisons between regular arrays and naturally occuring random systems should prove interesting, and should help to sort out the effects of geometrical randomness.

The behavior of classical mixtures of conductors, and the very weakly coupled limit of superconductor-normal composites, is explained by percolation theory. We did numerical simulations and renormalization group calculations on square random resistor lattices to study the effects of conductance anisotropy. This work was suggested by the geometrical anisotropy of in situ composite wires which can be shown to be equivalent to conductance anisotropy in a geometrically isotropic system. We found that although the renormalization group underestimated the effects of anisotropy, it was qualitatively correct, and yielded information about the critical region behavior which is presently unobtainable by other means.

Looking at isotropic lattices, we calculated the coherence length exponent ν for the bond problem by a large-cell renormalization group technique which had previously been applied to the site problem. Our result supported the notion of site-bond universality. By extending this method, we calculated the conductance exponent t and found it to be essentially equal to ν. This calculation represented a significant improvement over earlier estimates. We also developed a simple model for percolative superconducting mixtures and showed that the critical current density exponent v is also essentially equal to ν in two dimensions.

Our methods can be applied to a number of additional problems. More detailed knowledge of the conductance distribution as a function of lattice size could be used to check the scaling hypothesis. In addition, non-ohmic circuit elements (the simple critical current element being one example) can be studied. Finally, all of our

techniques can be applied in three dimensions, where they could presumably improve the accuracy with which critical exponents and the percolation threshold are known.

REFERENCES

Abeles, B., H. L. Pinch and J. I. Gittleman, 1975, Phys. Rev. Lett. 35, 247.

Allen, J. F., 1933, Phil. Mag. 16, 1005.

Bernasconi, J., 1974, Phys. Rev. B9, 4575.

Bernasconi, J., 1978, Phys. Rev. B18, 2185.

Bernasconi, J., W. R. Schneider and H. J. Weismann, 1977, Phys. Rev. B16, 5250.

Bevk, J., F.. Habbal, C. J. Lobb and James P. Harbison, 1979a, Appl. Phys. Lett. 35, 93.

Bevk, J., F. Habbal, C. J. Lobb and G. Dublon, 1979b, Proc. of the Third International Conference on Cryogenic Engineering, Vol. 25, to be published.

Bevk J., J. P. Harbison and J. L. Bell, 1978, J. Appl. Phys. 49, 6031.

Bevk J., James P. Harbison, F. Habbal, G. R. Wagner and A. I. Braginski, 1980, Appl. Phys. Lett. 36, 85.

Bevk J. and Karasek K. R., 1979, in New Developments and Applications in Composites, Doris Kuhlmann-Wilsdorf and William C. Harrigan, Jr., ed., (AIME),Warrendale, Pennsylvania, 101.

Bruggeman, D. A. G., 1935, Ann. Phys. (Leipz.) 24, 636.

Callaghan, Timothy J. and Louis E. Toth, 1975, J. Appl. Phys. 46, 4013.

Chambers, R. G., 1952, Proc. Roy. Soc. A215, 481.

Chen, W. Y. K. and C. C. Tsuei, 1976, J. Appl. Phys. 47, 715.

Das, B. N., J. E. Cox, R. W. Huber and R. A. Meussner, 1977, Metall. Trans. A8, 541.

Davidson, A., 1975, PhD. thesis, Harvard University (unpublished).

Davidson, A., M. R. Beasley and M. Tinkham, 1975, IEEE Trans. Mag., MAG-11, 276.

Davidson, A. and M. Tinkham, 1976, Phys. Rev. B13, 3261.

deGennes, P. G., 1966, Superconductivity in Metals and Alloys, (W. A. Benjamin, Inc.), New York

deGennes, P. G., 1976, J. Physique Lett. 37, L-1.

Deutscher, G. and P. G. deGennes, 1969, in Superconductivity, R. D. Parks, ed., (Marcel Dekker), New York, 1005.

Deutscher, G. and L. Rappaport, 1979, J. Physique Lett. 40, L-219.

Dew-Hughes, D., 1975, Cryogenics 15, 435.

Finnemore, D. K., J. D. Verhoeven, J. E. Ostenson, E. D. Gibson and H. H. Sample, 1979, J. Appl. Phys. 50, 2867.

Fisch, R. and A. B. Harris, 1978, Phys. Rev. B18, 416.

Fihey, J. L., M. Neff, R. Roberge, M. C. Flemings, S. Foner and B. B. Schwartz, 1979, Appl. Phys. Lett. 35, 715.

Giovannini, B. and L. Weiss, 1978, Sol. St. Comm. 27, 1005.

Halperin, B. I., 1979, private communication.

Halperin, B. I. and David R. Nelson, 1979, J. Low Temp. Phys. 36, 599.

Hansen, Max and Kurt Anderko, 1958, Constitution of Binary Alloys, (McGraw-Hill), New York.

Harbison, James Prescott, 1977, PhD. thesis, Harvard University (unpublished).

Harbison, James P. and J. Bevk, 1977, J. Appl. Phys. 48, 5180.

Holland, L., 1958, Vacuum Deposition of Thin Films, (John Wiley and Sons), New York.

Hoshen, J. and R. Kopelman, 1976, Phys. Rev. B14, 3348.

Huse, D. A. and R. A. Guyer, 1979, Phys. Rev. Lett. 43, 1163.

Imry, Y., 1980, in Inhomogeneous Superconductors, D. U. Gubser, T. L. Francavilla, J. R. Leibowitz and S. A. Wolf, ed., AIP Conference Proc. 58, (American Institute of Physics), New York, 1980.

Karasek, Keith R. and J. Bevk, 1979, Scripta MET 13, 259.

Kirkpatrick, S., 1973, Rev. Mod. Phys. 45, 574.

Kirkpatrick, S., 1979, in Proceeding of the Les Houches Summer School on Ill Condensed Matter, (North Holland), to be published.

Klapwijk, T. M., 1980, private communication.

Kosterlitz, J. M., 1974, J. Phys. C: Sol. St. Phys. 7, 1046.

Labbe, J. and J. Friedel, 1966, Le J. de Phys. 27, 153.

Landauer, Rolf, 1952, J. Appl.Phys. 23, 779.

Landauer, Rolf, 1978, in Electrical Transport and Optical Properties of Inhomogeneous Media, J. C. Garland and D. B. Tanner, ed., AIP Conf. Proc. 40, (American Institute of Physics), New York, 2.

Levinshtein, M. E., M. S. Shur and A. L. Efros, 1975, Sov. Phys. JETP 42, 1120.

Liang, N. T., Y. Shan and S. Wang, 1976, Phys. Rev. Lett. 37, 526.

Lobb, C. J. and D. J. Frank, 1979, J. Phys. C: Sol. St. Phys. 12, L827.

Lobb, C. J. and D. J. Frank, 1980, in Inhomogeneous Superconductors, D. U. Gubser, T. L. Francavilla, J. R. Leibowitz and S. A. Wolf, ed., AIP Conf. Proc. 58, (American Institute of Physics), New York, 308.

Lobb, C. J. and Keith R. Karasek, 1980, J. Phys. C: Sol St. Phys., to be published.

Lobb, C. J., Tinkham M. and Skocpol W. J., 1978, Sol. St. Comm. 27, 1273.

Ma, Shang-Keng, 1976, Modern Theory of Critical Phenomena, (W. A. Benjamin, Inc.), Reading, Massachusetts.

Matthiessen, A., 1860, Pogg. Ann. 110, 190.

Maxwell, J. C., 1892, A Treatise on Electricity and Magnetism, Vol. 1, (Clarendon Press), Oxford.

Morris, J. E. and T. J. Coutts, 1977, Thin Solid Films 47, 3.

Patton, B. R., W. Lamb and D. Stroud, 1980, in Inhomogeneous Superconductors, D. U. Gubser, T. L. Francavilla, J. R. Leibowitz and S. A. Wolf, ed., AIP Conf. Proc. 58, (American Institute of Physics), New York, 13.

Redner, S. and H. E. Stanley, 1979, J. Phys. A: Math. Gen. 12, 1267.

Reynolds, P. J., W. Klein and H. E. Stanley, 1977, J. Phys. C: Sol. St. Phys. 10, L167.

Reynolds, Peter J., H. Eugene Stanley and W. Klein, 1978, J. Phys. A: Math. Gen. 11, L199.

Reynolds, Peter J., H. Eugene Stanley and W. Klein, 1980, Phys. Rev. B21, 1223.

Roberge, R., J. L. Fihey and B. Schwartz, 1978, J. de Physique C6, C6-695.

Roberts, B. W., 1969, Superconductive Materials and Some of Their Properties, NBS Technical Note 482, U.S. Govt. Printing Office.

Rosman, R. and B. Shapiro, 1977, Phys. Rev. B16, 5117.

Shante, V. K. S. and S. Kirkpatrick, 1971, Adv. Phys. 20, 325.

Sher, H. and R. Zallen, 1970, J. Chem. Phys. 53, 3759.

Shklovskii, B. I., 1978, Phys. Stat. Sol. (b) 85, K111.

Smith, L. N. and C. J. Lobb, 1979, Phys. Rev. B20, 3653.

Stinchcombe, R. B. and B. P. Watson, 1976, J. Phys. C: Sol. St. Phys. 9, 3221.

Straley, Joseph P., 1977a, Phys. Rev. B15, 5773.

Straley, Joseph P., 1977b, J. Phys. C: Sol. St. Phys. 10, 1903.

Sykes, M. F. and J. W. Essam, 1964, J. Math. Phys. 5, 1117.

Tinkham, Michael, 1975, Introduction to Superconductivity, (McGraw-Hill), New York.

Tinkham, M., 1977, in Electrical Transport and Optical Properties of Inhomogeneous Media, J. C. Garland and D. B. Tanner, ed., AIP Conf. Proc. 40, (American Institute of Physics), New York, 130.

Tsuei, C. C., 1973, Science 180, 57.

Tsuei, C. C., 1974, J. Appl. Phys. 45, 1385.

Tsuei, C. C. and L. R. Newkirk, 1973, J. Mat. Sci. 8, 1307.

van der Pol, B. and H. Bremmer, 1950, Operational Calculus, (Cambridge Univ. Press), Cambridge, 371.

Webman, Itzhak, Joshua Jortner and Morrel H. Cohen, 1975, Phys. Rev. B11, 2885.

Wolf, S. A., D. U. Gubser and Y. Imry, 1979, Phys. Rev. Lett. 42, 324.

Yoshida, Y., K. Tachikawa and Y. Iwasa, 1975, Appl. Phys. Lett. 27, 632.

Young, A. P. and Stinchcombe R. B., 1975, J. Phys. C: Sol. St. Phys. 8, L535.

DISTRIBUTION LIST FOR ONR ELECTRONIC AND SOLID STATE SCIENCES

Director
Advanced Research Projects Agency
Attn: Technical Library
1400 Wilson Boulevard
Arlington, Virginia 22209

Office of Naval Research
Electronics Program Office (Code 427)
800 North Quincy Street
Arlington, Virginia 22217

Office of Naval Research
Code 105
800 North Quincy Street
Arlington, Virginia 22217

Director
Naval Research Laboratory
4555 Overlook Avenue, S.W.
Washington, D.C. 20375
Attn: Technical Library (6 cps)
Code 5200 (1 copy)
5210 (1 copy)
5270 (1 copy)
6400 (1 copy)

Office of the Director of Defense
Research and Engineering
Office of the Assistant Director
Electronics & Physical Sciences
The Pentagon, Room 3D1079
Washington, DC 20301

Defense Documentation Center (12 cps)
Cameron Station
Alexandria, Virginia 22314

Commanding Officer
Office of Naval Research Branch Office
536 South Clark Street
Chicago, Illinois 60605

San Francisco Area Office
Office of Naval Research
50 Fell Street
San Francisco, California 94102

Commanding Officer
Office of Naval Research Branch Office
1030 East Green Street
Pasadena, California 91101

Commanding Officer
Office of Naval Research Branch Office
495 Summer Street
Boston, Massachusetts 02210

New York Area Office
Office of Naval Research
115 Broadway 5th Floor
New York, New York 10003

ODDR&E Advisory Group on Electron Devices
201 Varick Street
New York, New York 10014

Naval Air Development Center
Attn: Technical Library
Johnsville
Warminster, Pennsylvania 18974

Naval Weapons Center
China Lake, California 93555
Attn: Technical Library (1 copy)
Code 6010 (1 copy)

Naval Research Laboratory
Underwater Sound Reference Division
Technical Library
P.O. Box 8337
Orlando, Florida 32806

Navy Underwater Sound Laboratory
Technical Library
Fort Trumbull
New London, Connecticut 06320

Commandant, Marine Corps
Scientific Advisor (Code AX)
Washington, D.C. 20380

Naval Ordnance Station
Technical Library
Indian Head, Maryland 20640

Naval Postgraduate School
Monterey, California 93940
Attn: Technical Library (1 copy)
Elect. Engin. Depart. (1 copy)

Naval Missile Center
Technical Library (Code 5632.2)
Point Mugu, California 93010

Naval Electronics Laboratory Center
San Diego, California
Attn: Technical Library (1 copy)
Code 2300 (1 copy)
2600 (1 copy)
4800 (1 copy)

Naval Undersea Center
Technical Library
San Diego, California 92132

Naval Weapons Laboratory
Technical Library
Dahlgren, Virginia 22448

Naval Ship Research and Development Center
Central Library (Codes L42 and L43)
Washington, D.C. 20007

Naval Surface Weapons Center
White Oak Laboratory
Silver Spring, Maryland 20910
Attn: Technical Library (1 copy)
Code 200 (1 copy)
212 (1 copy)

Deputy Chief of Naval Operations
(Development)
Technical Analysis and Advisory Group
(Code NOP-077D)
Washington, D.C. 20350

Commander
Naval Air Systems Command
Washington, D.C.
ATTN: Code 310 (1 copy)
360 (1 copy)

Commander
Naval Electronics Systems Command
Washington, D.C. 20360
Attn: Code 304 (1 copy)
310 (1 copy)

Commander
Naval Sea Systems Command
Washington, D.C. 20360

Naval Surface Weapons Center
Attn: Library
Dahlgren, Virginia 22448

Air Force Office of Scientific Research
Attn: Electronic and Solid State
Sciences Division
Department of the Air Force
Washington, D.C. 20333

Air Force Weapon Laboratory
Technical Library
Kirtland Air Force Base
Albuquerque, New Mexico 87117

Air Force Avionics Laboratory
Air Force Systems Command
Technical Library
Wright-Patterson Air Force Base
Dayton, Ohio 45433

Air Force Cambridge Research Laboratory
L.G. Hanscom Field
Technical Library
Cambridge, Massachusetts 02138

Harry Diamond Laboratories
Technical Library
Connecticut Avenue at Van Ness, N.W.
Washington, D.C. 20438

U.S. Army Research Office
Box CM, Duke Station
Durham, North Carolina 27706

Director
U.S. Army Engineering Research
and Development Laboratories
Fort Belvoir, Virginia 22060
Attn: Technical Documents Center

Director National Bureau of Standards
Attn: Technical Library
Washington, D.C. 20234

Naval Research Laboratory
4555 Overlook Avenue, S.W.
Washington, D.C. 20375
Attn: Code 5300 (1 copy)
7100 (1 copy)
7900 (1 copy)

Naval Electronics Laboratory Center
San Diego, California 92152
Attn: Code 2100 (1 copy)
2200 (1 copy)

C.C. Klick
Superintendent
Materials Sciences Division
Naval Research Laboratory
4555 Overlook Avenue, S.W.
Washington, D.C. 20375

Naval Research Laboratory
4555 Oberlook Avenue, S.W.
Washington, D.C. 20375
Attn: Code 5220 (1 copy)
5230 (1 copy)
5250 (1 copy)
5260 (1 copy)
5270 (1 copy)
5500 (1 copy)

Naval Electronics Laboratory Center
San Diego, California 92152
Attn: Code 2500 (1 copy)
4000 (1 copy)

Office of Naval Research (2 cps)
800 N. Quincy Street
Arlington, Virginia 22217
Attn: Code 430 (2 copies)

Naval Research Laboratory
4555 Overlook Avenue, S.W.
Washington, D.C. 20375
Attn: Code 5400

Naval Electronics Laboratory Center
San Diego, California 92152
Attn: Code 3000 (1 copy)
5000 (1 copy)
5600 (1 copy)

Air Force Office of Scientific Research
Mathematical and Information Sciences
Directorate
1400 Wilson Blvd.
Washington, D.C. 20333

JSEP REPORTS DISTRIBUTION LIST

ANNUAL REPORTS

DEPARTMENT OF DEFENSE

Director
National Security Agency
ATTN: Dr. T. J. Beahn, R-5
Fort George G. Meade, MD 20755

Defense Documentation Center (12 copies)
ATTN: DDC-DDA
Cameron Station
Alexandria, VA 22314

Dr. George Gamota
Assistant for Research
Deputy Under Secretary of Defense for Research
and Engineering (Research & Advanced Technology)
Room 3D1067, The Pentagon
Washington, DC 20301

Defense Advanced Research Projects Agency
ATTN: (Dr. R. Reynolds)
1400 Wilson Boulevard
Arlington, VA 22209

DEPARTMENT OF THE ARMY

Commander
US Army Armament R&D Command
ATTN: DRDAR-RD
Dover, NJ 07801

Commander
US Army Ballistics Research Laboratory
ATTN: DRDAR-BAD
Aberdeen Proving Ground
Aberdeen, MD 21005

Commander
US Army Communication Command
ATTN: CC-OPS-PT
Fort Huachuca, AZ 85613

Commander
US Army Materials and Mechanics Research Center
ATTN: Chief, Applied Sciences Division
Watertown, MA 02172

Commander
US Army Material Development
and Readiness Command
ATTN: Technical Library, Rm. 7S 35
5001 Eisenhower Avenue
Alexandria, VA 22333

Commander
US Army Missile R&D Command
ATTN: Chief, Document Section
Redstone Arsenal, AL 35809

Commander
US Army Satellite Communications Agency
Fort Monmouth, NJ 07703

Commander
US Army Atmospheric Sciences Laboratory
ATTN: DELAS-DM-A (Tech Writing Sec.)
White Sands Missile Range, NM 88002

Commander
US Army Communications R&D Command
ATTN: DRDCO-COM-D-4 (Mr. John Walker)
Fort Monmouth, NJ 07703

Director
TRI-TAC
ATTN: TT-AD (Mrs. Briller)
Fort Monmouth, NJ 07703

Commander
US Army Electronics R&D Command
Night Vision & Electro-Optics Labs
ATTN: DELNV (Dr. Rudolf G. Buser)
Fort Monmouth, NJ 07703

Director
US Army Electronics R&D Command
ATTN: DELEW-D (Electronic Warfare Laboratory)
White Sands Missile Range, NM 88002

Executive Secretary, TCC/JSEP
US Army Research Office
P. O. Box 12211
Research Triangle Park, NC 27709

Commander
Harry Diamond Laboratories
ATTN: Mr. John E. Rosenberg
2800 Powder Mill Road
Adelphi, MD 20783

HQDA (DAMA-ARZ-A)
Washington, DC 20310

Director
US Army Electronics Technology & Devices Lab
ATTN: DELET-E (Dr. Jack A. Kohn)
Fort Monmouth, NJ 07703

Director
US Army Electronics Technology & Devices Lab
ATTN: DELET-ER (Dr. S. Kronenberg)
Fort Monmouth, NJ 07703

Director
US Army Electronics R&D Command
Night Vision & Electro-Optics Labs
ATTN: Dr. Ray Balcerak
Fort Belvoir, VA 22060

Commander
US Army Research Office
ATTN: DRXRO-PH (Dr. Paul Boggs)
P. O. Box 12211
Research Triangle Park, NC 27709

Commander
US Army Missile R&D Command
Research Directorate
ATTN: DRDMI-TRD (Dr. Charles Bowden)
Redstone Arsenal, AL 35809

Commander
US Army Missile R&D Command
Advanced Sensors Directorate
ATTN: DRDMI-TER (Dr. Don Burlage)
Redstone Arsenal, AL 35809

Director
US Army Electronics R&D Command
Night Vision & Electro-Optics Labs
ATTN: Mr. John Dehne
Fort Belvoir, VA 22060

Director
US Army Electronics R&D Command
Night Vision & Electro-Optics Labs
ATTN: Dr. William Ealy
Fort Belvoir, VA 22060

Commander
US Army Missile R&D Command
Physical Sciences Directorate
ATTN: DRDMI-TER (Dr. Michael D. Fahey)
Redstone Arsenal, AL 35809

Commander
US Army Missile R&D Command
Physical Sciences Directorate
ATTN: DRDMI-TRO (Dr. William L. Gamble)
Redstone Arsenal, AL 35809

Commander
White Sands Missile Range
ATTN: STEWS-ID-FR (Dr. Al L. Gilbert)
White Sands Missile Range, NM 88002

Commander
US Army Communications R&D Command
ATTN: DRDCO-TCS-BP (Mr. David Haratz)
Fort Monmouth, NJ 07703

Commander
US Army Communications R&D Command
ATTN: DRDCO-COM-RF (Mr. R. A. Kulinyi)
Fort Monmouth, NJ 07703

Commander
US Army Communications R&D Command
ATTN: DRDCO-TCS-BG (Dr. E. Lieblein)
Fort Monmouth, NJ 07703

Director
US Army Electronics Technology and Devices Lab
ATTN: DELET-M (Mr. V. Gelnovatch)
Fort Monmouth, NJ 07703

Commander
US Army Electronics R&D Command
ATTN: DRDEL-CT (Dr. W. S. McAfee)
2800 Powder Mill Road
Adelphi, MD 20783

Director
US Army Electronics R&D Command
Night Vision and Electro-Optics Labs
ATTN: DELNV
Fort Belvoir, VA 22060

Senior Standardization Representative
US Army Standardization Group, Canada
National Defense Headquarters
Ottawa, Ontario, Canada K1A 0K2

Commander
US Army Communications R&D Command
ATTN: DRDCO-COM-RM-4 (Dr. Felix Schwering)
Fort Monmouth, NJ 07703

Director
US Army Electronics R&D Command
Night Vision & Electro-Optics Labs
ATTN: Dr. Randy Longshore
Fort Belvoir, VA 22060

Director
US Army Electronics Technology and Devices Lab
ATTN: DELET-I (Dr. C. G. Thornton)
Fort Monmouth, NJ 07703

Commander
US Army Research Office
ATTN: DRXRO-EL (Dr. James Mink)
P. O. Box 12211
Research Triangle Park, NC 27709

Commander
Harry Diamond Laboratories
ATTN: DELHD-R (Mr. H. Sommer)
2800 Powder Mill Road
Adelphi, MD 20783

Director
US Army Electronics R&D Command
Night Vision & Electro-Optics Labs
ATTN: DELNV-RD (Dr. John Pollard)
Fort Belvoir, VA 22060

Commander
US Army Research Office
ATTN: DRXRO-EL (Dr. William A. Sander)
P. O. Box 12211
Research Triangle Park, NC 27709

Director
Division of Neuropsychiatry
Walter Reed Army Institute of Research
Washington, DC 20012

Commander
USA ARRADCOM
ATTN: DRDAR-SCF-CC (Dr. N. Coleman)
Dover, NJ 07801

Director
US Army Signals Warfare Lab
ATTN: DELSW-OS
Vint Hill Farms Station
Warrenton, VA 22186

Director
U.S. Army Electronics Technology and Devices Lab
ATTN: DELET-ED (Dr. E. H. Poindexter)
Fort Monmouth, NJ 07703

Director
US Army Electronics Technology & Devices Lab
ATTN: DELET-ES (Dr. F. Rothwarf)
Fort Monmouth, NJ 07703

U.S. Army Research Office (3 copies)
ATTN: Library
P. O. Box 12211
Research Triangle Park, NC 27709

Commander
U.S. Army Communications R&D Command
ATTN: DRDCO-TCS-BG (Mr. J. Fullback)
Fort Monmouth, NJ 07703

Dr. Sidney Ross
RCA R&D Engineering
Cherry Hill, NJ 08358

DEPARTMENT OF THE AIR FORCE

Mr. Robert Barrett
RADC/ES
Hanscom AFB, MA 01731

Dr. Carl E. Baum
AFWL (ES)
Kirtland AFB, NM 87117

Dr. E. Champagne
AFAL/DH
Wright-Patterson AFB, OH 45433

Dr. R. P. Dolan
RADC/ESR
Hanscom AFB, MA 01731

Mr. W. Edwards
AFAL/DH
Wright-Patterson AFB, OH 45433

Professor R. E. Fontana
Head Dept. of Electrical Eng
AFIT/ENG
Wright-Patterson AFB, OH 45433

Dr. Alan Garscadden
AFAPL/POD
Wright-Patterson AFB, OH 45433

USAF European Office of Aerospace Research & Development
ATTN: Captain A. E. Mardiguian
Box 14, FPO, New York 09510

Mr. Murray Kesselman (ISCA)
Rome Air Development Center
Griffiss AFB, NY 13441

Col. R. V. Gomez
Air Force Member, TCC
Air Force Office of Scientific Research
(AFSC) AFOSR/NE
Bolling Air Force Base, DC 20332

Chief, Electronic Research Branch
AFAL/DHR
Wright-Patterson AFB, OH 45433

Dr. Edward Altshuler
RADC/EEP
Hanscom AFB, MA 01731

Mr. John Mott-Smith (TOIT)
HQ ESD (AFSC), Stop 36
Hanscom AFB, MA 01731

Dr. Richard Picard
RADC/ETSL
Hanscom AFB, MA 01731

Dr. J. Ryles
Chief Scientist
AFAL/CA
Wright-Patterson AFB, OH 45433

Dr. Allan Schell
RADC/EE
Hanscom AFB, MA 01731

[illegible]
Rome Air Development Center
Griffiss AFB, NY 13441

Dr. Howard Schlossberg
Air Force Office of Scientific Research
(AFSC) AFOSR/NP
Bolling Air Force Base, DC 20332

LTC [illegible]
Air Force Office of Scientific Research
(AFSC) AFOSR/NP
Bolling Air Force Base, DC 20332

Major [illegible]
Air Force Office of Scientific Research
(AFSC) AFOSR/NE
Bolling Air Force Base, DC 20332

DEPARTMENT OF THE NAVY

Office of Naval Research
800 North Quincy Street
Arlington, VA 22217
Attn: [illegible]
427
432

Commanding Officer
Naval Research Laboratory
Washington, DC 20375
ATTN: Codes 2615 - Dr. A. Tertier
2627 - Mrs. D. Folen
5200 - A. Brodzinsky
5210 - J. E. Davey
5270 - B. D. McCombe
[illegible] - [illegible] Sheats
5530 - J. B. Swann
5560 - W. L. Faust
6805 - S. G. Brown

Director
Office of Naval Research Branch Office
666 Summer Street
Boston, MA 02210

Director
Office of Naval Research
New York Area Office
715 Broadway, 5th Floor
New York, NY [illegible]

Director
Office of Naval Research Branch Office
536 South Clark Street
Chicago, IL 60605

Director
Office of Naval Research Branch Office
1030 East Green Street
Pasadena, CA 91106

Naval Surface Weapons Center
ATTN: Technical Library
Code DX-21
Dahlgren, VA 22448

Dr. J. H. Mills, Jr.
Naval Surface Weapons Center
Code DF
Dahlgren, VA 22448

Naval Air Development Center
Warminster, PA 18974
ATTN: Codes 301 [illegible]
Technical Library

Dr. Gernot M. R. Winkler
Director, Time Service
U. S. Naval Observatory
Mass. Avenue at 34th Street, NW
Washington, DC 20390

[illegible]
Technical Director
Naval Coastal Systems Center
Panama City, FL 32407

Technical Director
Naval Underwater Systems Center
New London, CT 06320

Naval Research Laboratory
Underwater Sound Reference Detachment
Technical Library
P. O. Box 8337
Orlando, FL 32856

Naval Ocean Systems Center
San Diego, CA 92152
ATTN: Codes 015 - P. C. Fletcher
4112 - M. J. Onyko
422 - W. M. Wieder
[illegible] - J. H. Richter

Naval Weapons Center
China Lake, CA 93555
ATTN: Codes 601 - F. C. Essig
5515 - M. H. Ritchie

Donald E. Kirk
Professor & Chairman, Electronic Engineering
Sp-304
Naval Postgraduate School
Monterey, CA 93940

Mr. [illegible] Frazer
National Bureau of Standards
Electronics Technology Division
Washington, DC [illegible]

[illegible]
Office of Research, Development, Test & Evaluation
NOP-987
The Pentagon, Room 5D760
Washington, DC 20350

Dr. A. L. Slafkosky
Code RD-1
Headquarters, U. S. Marine Corps
Washington, DC 20380

Dr. [illegible] Mueller
Naval Air Systems Command
AIR-310
Washington, DC 20360

Mr. Moore E. Peterson
Naval Electronics Systems Command
Code 03R
NC #1
2511 Jefferson Davis Hwy
Arlington, VA 20360

Naval Sea Systems Command
NC #3
2531 Jefferson Davis Hwy
Washington, DC 20362
ATTN: Code 03C - J. H. Huth

David Taylor Naval Ship Research & Development Center
Bethesda, MD 20084
ATTN: Code 522.1 - Technical Library
Code [illegible] - [illegible]

Naval Surface Weapons Center
White Oak
Silver Spring, MD 20910
ATTN: Codes WX-40-Technical Library
[illegible] - [illegible] Allgaier

Dr. Edward S. Eby
Code 101E
Naval Underwater Systems Center
New London Laboratory
New London, CT 06320

Dr. Martin Mandelberg
Code 34
Naval Underwater Systems Center
New London Laboratory
New London, CT 06320

Dr. [illegible]
Code 34
Naval Underwater Systems Center
New London Laboratory
New London, CT 06320

OTHER GOVERNMENT AGENCIES

Dr. Herbert S. Bennett
Director
Division of Materials Research
National Science Foundation
1800 G Street
Washington, DC 20550

[illegible]
Program Director
Devices and Waves Program
National Science Foundation
1800 G Street
Washington, DC 20550

Los Alamos Scientific Laboratory
ATTN: Main Library
P. O. Box 1663
Los Alamos, NM 87545

Dr. Jagan Mehtaali
Program Director, Solid-State Physics
Division of Materials Research
National Science Foundation
1800 G Street
Washington, DC 20550

M. Zane Thornton
Deputy Director, Institute for
Computer Sciences & Technology
National Bureau of Standards
Washington, DC 20234

Head, Electrical Sciences & Analysis Section
National Science Foundation
1800 G Street, NW
Washington, DC 20550

Deputy Director for Research
Research and Technology Division
Office of Aeronautics and Space Tech
NASA
Washington, DC 20546

Judson C. French, Director
Center for Electronics and Electrical Engineering
A361 Technology Bldg
National Bureau of Standards
Washington, DC 20234

Dr. Ray Ruker
Chief, Sensing & Detection
Electronics Division, Code RE
NASA HQ
600 Independence Avenue, SW
Washington, DC 20546

Mr. Herbert Ernst
Manager, Data Management Program, Code RSI-5
NASA HQ
600 Independence Avenue, SW
Washington, DC 20546

Mr. John Sos
Assistant Chief, Information Processing Division
Code 560
Goddard Space Flight Center
Greenbelt, MD 20771

Mr. Charles Husson
Aerospace Technologist
Langley Research Center
Hampton, VA 23665

Mr. John Gould
Chief, Design Techniques Branch
George C. Marshall Space Flight Center
Marshall Space Flight Center, AL 35812

NON-GOVERNMENT AGENCIES

Director
Columbia Radiation Laboratory
Columbia University
538 West 120th Street
New York, NY 10027

Director
Coordinated Science Laboratory
University of Illinois
Urbana, IL 61801

Director
Division of Applied Sciences
Harvard University
Pierce Hall
Cambridge, MA 02138

Director
Electronics Research Center
The University of Texas
P. O. Box 7728
Austin, TX 78712

Director
Electronics Research Laboratory
University of California
Berkeley, CA 94720

Director
Electronics Sciences Laboratory
University of Southern California
Los Angeles, CA 90007

Director
Microwave Research Institute
Polytechnic Institute of New York
333 Jay Street
Brooklyn, NY 11201

Director
Research Laboratory of Electronics
Massachusetts Institute of Technology
Cambridge, MA 02139

Director
Stanford Electronics Laboratory
Stanford University
Stanford, CA 94305

Director
Edward L. Ginzton Laboratory
Stanford University
Stanford, CA 94305

Dr. Lester Eastman
School of Electrical Engineering
Cornell University
316 Phillips Hall
Ithaca, NY 14850

Dr. Carlton Walter
ElectroScience Laboratory
The Ohio State University
Columbus, OH 43212

Dr. Richard Saeks
Department of Electrical Engineering
Texas Tech University
Lubbock, TX 79409

Dr. Roy Gould
Executive Officer for Applied Physics
California Institute of Technology
Pasadena, CA 91125

Director
School of Electrical Engineering
Georgia Institute of Technology
Atlanta, GA 30332

Prof. J. F. Walkup
Department of Electrical Engineering
Texas Tech University
Lubbock, TX 79409